QCD thermodynamics with 2+1 quark flavours in lattice simulations

Dissertation

zur Erlangung des Doktorgrades
der Fakultät für Physik
der Universität Bielefeld

vorgelegt von
Andreas Peikert

Mai 2000

Contents

List of Figures

List of Tables

Introduction

The fundamental theory for strongly interacting quarks and gluons is Quantum Chromodynamics (QCD). It is formulated as a non-Abelian $SU(3)$ gauge theory with the gluons as the gauge bosons. Up to now six quark species are known which are labelled by their flavour (up, down, strange, charm, bottom, top). All of them carry additional internal colour degrees of freedom. The coupling between quarks and gluons is realized through colour. The experimental test of perturbative QCD is restricted to deep inelastic scattering where the momentum transfer is large. In this regime quarks act as asymptotically free particles, the strong coupling constant α_s is small and a perturbative description meaningful. For larger distances or smaller momentum transfers the coupling strength increases and thus perturbative calculations break down. This is also reflected in the observation that quarks are confined to colour neutral bound states, the baryons and mesons. To explore the non-perturbative properties of QCD an alternative approach has been proposed by Wilson [1]. He suggested a discretisation of the Euclidean path integral formulation of QCD by introducing a four dimensional space-time lattice to regularise the theory. This so-called $SU(3)$ lattice gauge theory can be calculated by means of Monte-Carlo simulations. The results obtained on the discrete lattice, which are expressed in terms of the finite lattice spacing a, are not free of discretisation errors. They have to be extrapolated to the continuum $a \to 0$. It turned out that the cut-off effects induced by a straight-forward discretisation of the action is quite large for most observables. During the last years it has become clear that improved discretisation schemes provide a solution to this problem. The aim of these improved actions is to reduce the cut-off distortions such that the results are more continuum-like already at finite lattice spacing .

One of the most fascinating predictions of non-perturbative QCD on the lattice is the existence of a phase transition from a confined low temperature phase with broken chiral symmetry to a deconfined and chirally symmetric high temperature phase of liberated quarks and gluons, a so-called quark gluon plasma. In heavy ion experiments at the CERN SPS (Super Proton Synchrotron) evidence from several signatures has been found that such a new state of matter exists [2]. In future experiments at RHIC (Relativistic Heavy Ion Collider) in Brookhaven and at LHC (Large Hadron Collider) at CERN the collision energy of the nuclei will be sufficiently high to produce a nearly baryon-free fireball. This corresponds to the system investigated in finite temperature lattice simulations such that also quantitative comparisons between lattice and experimental data might become possible.

Lattice results also have consequences for evolution scenarios of the early universe. There the nature of the QCD phase transition very much determines if persisting inhomogeneities in the universe might have been produced during the QCD transition which occured shortly after the big bang.

During the last years the investigation of QCD at finite temperature on the lattice has lead to quantitative predictions for the critical temperature at which the phase transition takes place, the order of the transition and the equation of state. Due to limited computer resources the first simulations were restricted to the quenched approximation of QCD, where the quark degrees of freedom are neglected in the dynamics of the system. Different discretisation schemes lead a transition tem-

perature of 265 MeV to 273 MeV in the continuum limit. A further success and consistency check of the lattice formulation is the continuum extrapolation of the pressure which also agrees within a few percent for unimproved and improved discretisations. Additionally it has been shown that the use of improved actions allows the extraction of continuum physics at much larger lattice spacing and consequently with smaller computer resources.
In finite temperature simulations of full QCD the results have not reached the same level of precision. Both widely used fermion formulations, Wilson and staggered fermions, respectively, suffer from severe cut-off effects. This is the starting point of this work. A highly improved staggered fermion action will be used to investigate the nature of the finite temperature phase transition. For three degenerate quark flavours the mass parameter will be varied from quite heavy to relatively light quarks to analyse how the transition changes from a confinement-deconfinement transition to a chiral phase transition in the limit $m_q \to 0$. For three flavour QCD universality arguments predict Ising critical exponents at the second order endpoints of the first order chiral and deconfinement regions. These predictions will be tested.
In thermodynamic calculations heavy quarks with mass $m_q a$ are suppressed with $\exp(-m_q/T)$, where at the phase transition the critical temperature T is about 180 MeV. Since this is close to the strange quark mass a systematic study of the influence of a third quark flavour in addition to the two light ones has been performed. The effect on thermodynamic quantities like the transition temperature, pressure and energy density has been analysed. A first continuum estimate will be possible with this action based on the analysis of remaining cut-off effects.

This work is organized as follows:
In the first chapter the formulation of finite temperature QCD on the lattice will be presented. Especially the properties of staggered fermions are described in some detail. All physical observables which are discussed in the following chapters are introduced and a brief description of the simulation algorithm is given.
Chapter 2 deals with the improvement of gluonic and staggered fermion actions. The basic principles of improvement in pure gauge theory and their benefit in finite temperature lattice calculations will be discussed. For staggered fermions the main focus in this chapter lies on the presentation of actions which improve the flavour and rotational symmetry. The expected improvement has been tested in perturbative and lattice calculations. In a final section the computational costs of simulations with improved actions will be presented.
The topic of the third chapter is the finite temperature phase transition in QCD. For the regime of heavy quarks the confinement-deconfinement transition is discussed for three quark flavours with improved staggered fermions. In the opposite limit of QCD with three light quarks the chiral transition has been investigated. In both cases the numerical results are compared to predictions from effective models, the Potts model with an external field and the $SU(3) \otimes SU(3)$ σ-model, respectively. Additionally also results for two light and two light plus one heavier quark flavour are summarized.
In chapter 4 QCD thermodynamic calculations with improved staggered fermions are presented. The critical temperature and the equation of state are analysed for two, two plus one and three quark flavours. Additionally the reduction of cut-off effects for improved actions has been investigated.
In the appendix the Dirac γ matrices in Euclidean metric, the generators of the group $SU(N)$ and the force computation in the Hybrid R algorithm for p4 and fat link staggered fermion actions is given. In the third part of the appendix the results for the string tension extracted from the static quark potential in full QCD are presented.

Chapter 1

Finite temperature QCD on the lattice

In this chapter the formulation of a $SU(N)$ gauge theory interacting with n_f quark flavours at finite temperature will be presented. The non-perturbative regime of such a theory, in this case especially QCD, has been quite successfully explored using the lattice formulation. It will be discussed how the QCD action can be discretized and in which way continuum results can be extracted from lattice QCD. All observables and thermodynamic quantities measured and referred to in this work are presented. Finally the numerical methods of the lattice simulation are explained. A general introduction to lattice gauge theories can be found in the recent books of Rothe [3] or Montvay and Münster [4], the treatment of phase transitions in QCD is discussed in an review article by Meyer-Ortmanns [5]. The starting point of this chapter is the continuum QCD Lagrangian.

The QCD Lagrangian in the continuum

For n_f quark flavours with mass m_f and the gauge group $SU(N)$ the Lagrangian consists of a gluonic and a fermionic part

$$\mathcal{L}_{\mathrm{QCD}}(x) = \mathcal{L}_{\mathrm{gluon}} + \mathcal{L}_{\mathrm{fermion}} \tag{1.1}$$

$$\mathcal{L}_{\mathrm{gluon}}(x) = -\frac{1}{4} F^a_{\mu\nu}(x) F_a^{\mu\nu}(x) \tag{1.2}$$

$$\mathcal{L}_{\mathrm{fermion}}(x) = \sum_{f=1}^{n_f} \overline{\psi}^{\alpha}_f(x) \; (\not{D}_{\alpha\beta} - m_f \delta_{\alpha\beta}) \psi^{\beta}_f(x) \tag{1.3}$$

with the covariant derivative $\not{D}$ and the field strength tensor $F^a_{\mu\nu}$. The index f denotes the flavours while Greek letters will be used as Dirac indices in this chapter.

$$\not{D} \equiv i(\partial_\mu + ig\frac{\lambda^a}{2} A^a_\mu)\gamma^\mu \tag{1.4}$$

$$F^a_{\mu\nu} \equiv \partial_\mu A^a_\nu - \partial_\nu A^a_\mu - g f_{abc} A^b_\mu A^c_\nu \tag{1.5}$$

A^a_μ denote the continuum gauge fields, $\psi^\alpha_f(x)$ and $\overline{\psi}^\alpha_f(x)$ are the quark fields. λ^a are the generators of $SU(N)$ and f_{abc} are the corresponding structure constants.

QCD at finite temperature

The partition function of QCD in the Euclidean path-integral formulation is given by

$$Z(T,V) = \int \mathcal{D}A_\mu \mathcal{D}\overline{\psi}\mathcal{D}\psi \exp(-S^E_{\rm QCD}[T,V,A_\mu,\overline{\psi},\psi,g,m_f]) \quad , \tag{1.6}$$

where the action depends on two parameters, the gauge coupling g and the quark mass m_f. A possible additional chemical potential is set to zero. The Euclidean action reads

$$S^{\rm E}_{\rm QCD}[T,V,...] = \int_0^{1/T} dt \int_V d^3x \mathcal{L}^E_{QCD}[A_\mu,\overline{\psi},\psi,g,m_f] \quad , \tag{1.7}$$

where the Euclidean Lagrangian is obtained from 1.1 by going from Minkowskian to Euclidean metric, thus substituting $x_0 \to -ix_4$, and by using the Euclidean γ matrices

$$\begin{aligned} \mathcal{L}^{\rm E}_{\rm QCD}(x) &= \mathcal{L}^E_{\rm gluon} + \mathcal{L}^E_{\rm fermion} \\ &= \frac{1}{4}F^a_{\mu\nu}(x)F^{\mu\nu}_a(x) \; + \; \sum_{f=1}^{n_f} \overline{\psi}^\alpha_f(x) \; (\not{D}^E_{\alpha\beta} + m_f\delta_{\alpha\beta})\psi^\beta_f(x) \quad . \end{aligned} \tag{1.8}$$

The Euclidean covariant derivative is defined as $\not{D}^E = (\partial_\mu + ig\frac{\lambda_a}{2}A^a_\mu)\gamma^E_\mu$, where the γ^E_μ and λ_a are the Euclidean Dirac matrices and $SU(N)$ generators given in the appendix A.
Thermal expectation values of physical observables are now defined as

$$\langle \mathcal{O} \rangle = \frac{\int \mathcal{D}A_\mu \mathcal{D}\overline{\psi}\mathcal{D}\psi \mathcal{O} \exp(-S^{\rm E}_{\rm QCD})}{\int \mathcal{D}A_\mu \mathcal{D}\overline{\psi}\mathcal{D}\psi \exp(-S^{\rm E}_{\rm QCD})} \quad . \tag{1.9}$$

In the following only quantities defined in the Euclidean metric are used and the additional subscript is omitted.

1.1 The lattice as a regulator of QCD

The functional integral in the expression for the partition function 1.6 is not well defined. One possible approximation to the partition function is the formulation of QCD on a four-dimensional hyper-cubic lattice [1]. The integral over the space-time continuum $T^{-1}V$ is replaced by a finite sum over a hyper-cubic lattice where the number of points in the spatial and temporal directions are N_σ and N_τ, respectively. The sites on the lattice are labeled by $x = (x_1, x_2, x_3, x_4)$ and are related to the continuum coordinate by $x_{\rm cont} = x \cdot a$, where a is the lattice spacing.

1.1.1 The gauge action on the lattice

The gluonic fields are represented by elements of the colour gauge group $SU(3)$ which are denoted by $U_\mu(x)$. This so-called link variable connects a point at site x to a point at site $x + \hat{\mu}$, where $\hat{\mu}$ is a unit vector in μ direction. The relation to the gauge fields is achieved defining the gauge link as a parallel transporter

$$U_\mu(x) = \exp\left(iga \int_{xa}^{(x+\hat{\mu})a} dy A_\mu(y) \right) \quad . \tag{1.10}$$

The simplest gauge invariant object which can be constructed from the link variable is a plaquette. It is defined as the product of links around the shortest closed loop

$$U_{\mu,\nu}(x) \equiv U_\mu(x) U_\nu(x+\hat{\mu}) U_\mu^\dagger(x+\hat{\nu}) U_\nu^\dagger(x) \quad , \tag{1.11}$$

The gluonic action can then be defined as

$$\begin{aligned} S_{\text{gluon}} = \beta\, S_{\text{G}}(\{U\}) &= \beta \sum_{x,\mu<\nu} \left(1 - \frac{1}{N}\text{ReTr} U_{\mu,\nu}(x)\right) \\ &= \beta \sum_{x,\mu<\nu} \left(1 - \frac{1}{N}\text{ReTr} \quad \right) \quad , \end{aligned} \tag{1.12}$$

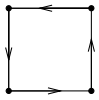

where β is related to the gauge coupling by $\beta = 2N/g^2$. To reproduce the continuum action an expansion in powers of the lattice spacing a and the coupling g has to be performed. Using the Baker-Hausdorff formula $e^A e^B = e^{A+B+1/2[A,B]+\cdots}$ and a Taylor expansion of the gauge fields A_μ around the center of the plaquette, $U_{\mu,\nu}$ becomes

$$U_{\mu,\nu}(x) = \exp\left\{iga^2\left(\partial_\mu A_\nu(xa) - \partial_\nu A_\mu(xa) + ig\left[A_\mu(xa), A_\nu(xa)\right]\right) + \mathcal{O}(a^3)\right\} \tag{1.13}$$

Inserting this into the action leads to an expression with corrections starting at $\mathcal{O}(a^2)$ in $\mathcal{O}(g^0)$.

$$\begin{aligned} S_{\text{gluon}} &= \frac{a^4}{4} \sum_{n,\mu<\nu} \left[\text{Tr}\; F_{\mu\nu}F_{\mu\nu} + \mathcal{O}(a^2)\right] + \mathcal{O}(g^2a^2) \\ &\underset{a\to 0}{\longrightarrow} \frac{1}{4}\int_V d^3x \int_0^{1/T} dx_4\; \text{Tr}\; F_{\mu\nu}F_{\mu\nu} + \mathcal{O}(g^2) \quad , \end{aligned} \tag{1.14}$$

where $F_{\mu\nu}$ is the field-strength tensor

$$F_{\mu\nu}(x) = \partial_\mu A_\nu(x) - \partial_\nu A_\mu(x) - ig[A_\mu(x), A_\nu(x)] \quad . \tag{1.15}$$

1.1.2 The fermion action on the lattice

Naive fermion formulation

The Grassmanian fields ψ on the lattice obey periodic boundary conditions in space and antiperiodic boundary conditions in time in order to realize the commutation relations. The derivative in the continuum will be replaced by a finite difference scheme. The local gauge invariance is realized by inserting gauge links to connect the fermion fields. This ensures the correct transformation properties according to the gauge group $SU(3)$. The action then reads

$$S_{\text{fermion}}^{\text{naive}} = \sum_{f=1}^{n_f} \sum_{x,y} \overline{\psi}_\alpha^f(x) M_f^{\alpha\beta}(x,y) \psi_\beta^f(y) \quad , \tag{1.16}$$

where the fermion matrix is defined as

$$\begin{aligned} M_f^{\alpha\beta}(x,y) &= m_f\; \delta^{\alpha\beta}\delta(x,y) \\ &\quad + \frac{1}{2a}\sum_\mu (\gamma_\mu)^{\alpha\beta}\left[U_\mu(x)\delta(x+\hat{\mu},y) - U_\mu^\dagger(x-\hat{\mu})\delta(x-\hat{\mu},y)\right] \quad . \end{aligned} \tag{1.17}$$

In the limit $a \to 0$ this action reproduces the continuum action and respects the global chiral $U(n_f) \otimes U(n_f)$ symmetry of QCD. To see this one has to expand the action in powers of the lattice spacing a. For a gauge link this expansion reads

$$U_\mu(x) = \mathbb{1} + iga\left[A_\mu(xa) + \frac{1}{2}a\partial_\mu A_\mu(xa) + \frac{1}{6}a^2\partial_\mu^2 A_\mu(xa) + \mathcal{O}(a^3)\right] + \mathcal{O}(a^2 g^2) \quad . \tag{1.18}$$

When this expression is plugged into the lattice action 1.17, the continuum fermion action is reproduced

$$\begin{aligned} S_{\text{fermion}}^{\text{naive}} \quad &= \quad a^4 \sum_x \sum_f \Bigg[\sum_\mu \gamma_\mu^{\alpha\beta} \overline{\psi}_\alpha^f(xa) \frac{1}{2a} \Bigg(\psi_\beta^f((x+\hat{\mu})a) - \psi_\beta^f((x-\hat{\mu})a) \\ &\quad + iga\Big(A_\mu((x+\hat{\mu})a)\psi_\beta^f((x+\hat{\mu})a) + A_\mu((x+\hat{\mu})a)\psi_\beta^f((x-\hat{\mu})a)\Big)\Bigg)\Bigg] \\ &\quad + m_f \ \overline{\psi}_\alpha^f(xa)\psi_\beta^f(xa)\delta^{\alpha\beta} + \mathcal{O}(a^5) \\ &\underset{a\to 0}{\longrightarrow} \quad \int dx \ \sum_f \left[\sum_\mu \gamma_\mu^{\alpha\beta} \overline{\psi}_\alpha^f(x)\Big(\partial^\mu + igA^\mu(x)\Big)\psi_\beta^f(x)\right] + m_f \ \overline{\psi}_\alpha^f(x)\psi_\beta^f(x)\delta^{\alpha\beta} \quad . \end{aligned} \tag{1.19}$$

Fermion Doublers

Unfortunately the naive lattice fermions suffer from severe problems related to the number of degenerate fermions which are realized by this formulation. In momentum space the free action for one flavour reads

$$S_{\text{fermion}}^{\text{naive}} = \int_{-\pi/a}^{\pi/a} \frac{d^4p}{(2\pi)^4} \overline{\psi}(p) \left[\sum_\mu i\gamma_\mu \frac{1}{a} \sin(p_\mu a) + m \right] \psi(p) \quad . \tag{1.20}$$

Thus the free propagator in momentum space has the form

$$\left\langle \overline{\psi}_\alpha(p)\psi_\beta(q) \right\rangle_0 \quad = \quad \frac{\left(i\sum_\mu \gamma_\mu \tilde{p}_\mu - m\right)_{\alpha,\beta}}{\sum_\mu \tilde{p}_\mu^2(p) + m^2} \ \delta_{p,q} \quad , \tag{1.21}$$

where $\tilde{p}_\mu = 1/a \sin(p_\mu a)$. This propagator does not only have a pole at $p = (0,0,0,0)$, but 15 further ones at the border of the Brillouin zone. To each additional pole there corresponds an unwanted particle state which is referred to as doubler. Thus n_f naive flavours in d dimensions correspond to $2^d \cdot n_f$ physical quarks.

There are different solutions to reduce the fermion doublers which will be discussed in the following sections. In the Wilson fermion formulation there are no doublers, but the chiral symmetry is explicitely broken even for $m \to 0$. The chiral limit is defined as the vanishing of the pion mass at a certain set of bare parameters. But it has been argued that these Goldstone bosons might not be related to the spontaneous breakdown of the chiral but instead the parity-flavour symmetry. Only in the continuum limit the chiral symmetry is expected to be restored. Staggered fermions on the other hand retain an exact $U(1) \otimes U(1)$ remnant of the continuum $U(n_f) \otimes U(n_f)$ chiral symmetry. Thus the advantage of this formulation is the fact that taking the quark mass to zero corresponds to the chiral limit. Unfortunately staggered fermions describe four flavours of degenerate quarks and

the flavour symmetry is broken which is evident from the fact that only one of the $(n_f^2 - 1)$ pseudo scalar mesons has its continuum Goldstone character. The connection between doublers and chiral symmetry is stated in the No-Go theorem by Nielsen and Ninomiya [7]. Finally a new approach, formulated in five dimensions, circumvents the No-Go theorem and leads to lattice fermions which have no doublers and an exact chiral and flavour symmetry. The drawback in this formulation is the increase of computational costs as will be discussed below.

1.1.3 Staggered fermions

Free staggered or Kogut-Susskind fermions

The staggered fermion formulation is based on the idea by Kogut and Susskind [8] to reduce the fermion degrees of freedom by a spin diagonalisation of the action. This can be achieved by applying a local transformation $\Lambda(x)$ to the fermion fields

$$\begin{aligned} \psi(x) &\rightarrow \Lambda(x)\psi(x) \\ \overline{\psi}(x) &\rightarrow \overline{\psi}(x)\Lambda^\dagger(x) \end{aligned} \tag{1.22}$$

such that the Dirac γ matrix is transformed to a diagonal form

$$\Lambda^\dagger(x)\gamma_\mu\Lambda(x+\hat{\mu}) = \eta_\mu(x) \quad \mathbb{1} \quad . \tag{1.23}$$

A possible choice is $\Lambda(x) = \gamma_1^{x_1}\gamma_2^{x_2}\gamma_3^{x_3}\gamma_4^{x_4}$ which leads to the following staggered phases $\eta_\mu(x) = (-1)^{x_1+\ldots+x_\mu-1}$.
The resulting fermion action is diagonal in the Dirac components, they just act as flavour components

$$S_{\text{fermion}} = \frac{1}{2}a^4 \sum_{x,\mu,\alpha} \eta_\mu(x)\frac{1}{a}\overline{\psi}_\alpha(x)\left(\psi_\alpha(x+\hat{\mu}) - \psi_\alpha(x-\hat{\mu})\right) + m\ a^4 \sum_{x,\alpha} \overline{\psi}_\alpha(x)\psi_\alpha(x) \quad . \tag{1.24}$$

The number of degenerate flavours can now be reduced by taking into account only one of the Dirac components. Then the staggered fermion action will be written in terms of one-component staggered fermion fields χ

$$S_{\text{KS}} = a^4 \sum_{x,\mu} \eta_\mu(x)\frac{1}{2a}\overline{\chi}(x)\left(\chi(x+\hat{\mu}) - \chi(x-\hat{\mu})\right) + m\ a^4 \sum_{x} \overline{\chi}(x)\chi(x) \quad . \tag{1.25}$$

Flavour content of staggered fermions

The connection between staggered and continuum flavours has been established by H. Kluberg-Stern *et al.* [9] in 1983. Their idea is based on the interpretation of the 16 staggered fields on the corners of a 2^4 hypercube as 4 Dirac quark fields each carrying 4 Dirac indices. For this purpose one has to introduce coordinates which label the hypercubes, $y = (y_1, y_2, y_3, y_4)$, where the y_i can take the values $0, 2, 4, \ldots, N_\sigma - 1$ or $N_\tau - 1$ respectively. Within the hypercube the 2^4 points are labeled by $\xi = (\xi_1, \xi_2, \xi_3, \xi_4)$ with $\xi_i = 0, 1$. The coordinates on the hyper-cubic lattice are then related to the ordinary ones by $x = y + \xi$. Now it is possible to reconstruct quark fields

living on the hyper-cubic lattice which have a Dirac and a flavour component labeled by α and f, respectively. They are defined as

$$\begin{aligned} q^f_\alpha(y) &\equiv \frac{1}{2}\sum_\xi \left(\gamma^\xi\right)_{\alpha f}\chi_\xi(y) \\ \overline{q}^f_\alpha(y) &\equiv \frac{1}{2}\sum_\xi \overline{\chi}_\xi(y)\left(\gamma^{\xi^\dagger}\right)_{f\alpha} \quad , \end{aligned} \tag{1.26}$$

with $\gamma^\xi \equiv \gamma_1^{\xi_1}\gamma_2^{\xi_2}\gamma_3^{\xi_3}\gamma_4^{\xi_4}$ and the fermion fields $\chi_\xi(y) \equiv 1/4\chi(y+\xi)$. Using these fermion fields the staggered action can be transformed to the following form

$$S_{\rm KS} = \sum_y (2a)^4 \overline{q}(y)\left[\sum_\mu \left[(\gamma_\mu \otimes 1\!\!1)\partial_\mu + a(\gamma_5 \otimes t_{\mu 5})\,\Box_\mu\right] + m(1\!\!1 \otimes 1\!\!1)\right] q(y) \quad , \tag{1.27}$$

where the first operator in the tensor product acts on the Dirac and the second operator on the flavour components. Since the new fields $q(y)$ live on the hyper-cubic lattice also the differential operators are defined on it,

$$\begin{aligned} \partial_\mu q(y) &\equiv \frac{1}{4a}\left(q(y+2\hat{\mu}) - q(y-2\hat{\mu})\right) \\ \Box_\mu q(y) &\equiv \frac{1}{4a^2}\left(q(y+2\hat{\mu}) - 2q(y) + q(y-2\hat{\mu})\right) \quad . \end{aligned} \tag{1.28}$$

The corresponding relations hold for $\overline{q}(y)$. The matrices t are defined as the transposed of the γ matrices, $t_{\mu 5} \equiv t_\mu t_5 \equiv \gamma_\mu^{\rm t}\gamma_5^{\rm t}$.
Obviously the action 1.27 corresponds to 4 degenerate quark flavours and a lattice spacing that is doubled compared to that of the original staggered action 1.25. There is a corrections to the continuum action at $\mathcal{O}(a)$ when the new quark fields are defined as in 1.26.

Staggered fermions with gauge interactions

The coupling of the gauge fields to the fermions can be realized in the same way as for naive fermions

$$S_{\rm KS} = a^4 \sum_{x,\mu} \eta_\mu(x)\overline{\chi}(x)\frac{1}{2a}\left[U_\mu(x)\chi(x+\hat{\mu}) - U^\dagger_\mu(x-\hat{\mu})\chi(x-\hat{\mu})\right] + \; m\; a^4 \sum_x \overline{\chi}(x)\chi(x) \tag{1.29}$$

where the fermion fields now have a colour component. Also for this gauge invariant staggered fermion formulation fields living on the hyper-cubic lattice can be constructed.

$$\begin{aligned} q^f_\alpha(y) &\equiv \frac{1}{2}\sum_\xi \left(\gamma^\xi\right)_{\alpha f}\tilde{U}_\xi(y)\chi_\xi(y) \\ \overline{q}^f_\alpha(y) &\equiv \frac{1}{2}\sum_\xi \overline{\chi}_\xi(y)\tilde{U}^\dagger_\xi(y)\left(\gamma^{\xi^\dagger}\right)_{f\alpha} \quad , \end{aligned} \tag{1.30}$$

where

$$\tilde{U}_\xi(y) \equiv [U_1(y)]^{\xi_1}[U_2(y+\xi_1)]^{\xi_2}\cdot\ldots\cdot[U_4(y+\xi_1+\ldots+\xi_3)]^{\xi_4} \quad , \tag{1.31}$$

is defined as the product of links that connects points in the hypercube.

Naive continuum limit

Using the expansion of the gauge link 1.18 and the fermion fields 1.30 the staggered action after some calculations reads

$$\begin{aligned} S_{\mathrm{KS}} &= \sum_{y,\mu} (2a)^4 \, \overline{q}(y) \Big\{ (\mathbb{1} \otimes \mathbb{1}) m + (\gamma_\mu \otimes \mathbb{1}) \boldsymbol{D}_\mu \\ &+ a(\gamma_5 \otimes t_{\mu 5}) \boldsymbol{D}_\mu^2 - \frac{1}{4} iga \sum_\nu T_{[\mu,\nu]} F_{\mu,\nu}(y) \Big\} q(y) + \mathcal{O}(a^2) \end{aligned} \tag{1.32}$$

with the covariant derivative

$$\boldsymbol{D}_\mu(x) \equiv \partial_\mu + igA_\mu(x) \tag{1.33}$$

and the antisymmetric tensor T

$$T_{[\mu,\nu]} \equiv (\gamma_\mu - \gamma_\nu) \otimes \mathbb{1} + \frac{1}{2} \gamma_5^\dagger [\gamma_\mu, \gamma_\nu] \otimes (t_\mu + t_\nu)^\dagger t_5^\dagger \quad . \tag{1.34}$$

Thus the correct continuum action is reproduced in leading order. The corrections start at $\mathcal{O}(a)$ with a contribution that is not diagonal in flavour space and is therefore responsible for the breaking of flavour symmetry. In a work by Luo [10] it has been shown that the action is in fact already correct up to orders a^2 since no operators of $\mathcal{O}(g^{2n}a)$ can be added to the staggered fermion action which respect the staggered symmetries. This also becomes obvious when writing the action in terms of improved fermion fields as it is done in the next section when the flavour symmetry is discussed.

1.1.4 Symmetries of the staggered fermion formulation

In this section the different symmetries realised by the continuum Lagrangian are discussed. The Poincaré invariance of the continuum is only realized as a discrete subgroup in the staggered formulation. The details are important for the identification of lattice particle states and their relation to the continuum particles. An elaboration on it can be found in [11] but will not be discussed in this work. The local $SU(3)$ gauge invariance is realised by construction, the global $U_V(1) \otimes SU_V(n_f) \otimes U_A(1) \otimes SU_A(n_f)$ chiral symmetry of the continuum action in the case of massless quarks is broken down to a subgroup as will be shown in this section. The $U_V(1)$ is responsible for the baryon number conservation which is realised also in the case of massive non-degenerate quark flavours, the $SU_V(n_f)$ is the generalized Iso spin symmetry for mass degenerate flavours. It is responsible for the mass degeneracy of particle states in the $n_f^2 - 1$ multiplet. The $U_A(1)$ flavour-singlet symmetry is broken by quantum effects already in the continuum and the axial $SU_A(n_f)$* in the case of massless quarks leads to a mass degeneracy of parity partners. In nature this degeneracy is not observed and therefore this symmetry is expected to be broken spontaneously. Finally the flavour symmetry which is realised in the continuum but broken by the staggered formulation will be discussed.

*Quite often this symmetry alone is referred to as the chiral symmetry

Chiral symmetry

Since the coupling of gauge fields to the fermions does not change the chiral properties of the action, it is sufficient to investigate the chiral symmetry for free fermions. Applying transformations $U_o, U_e \in U(1)$ to the staggered fields χ and $\overline{\chi}$ gives

$$\begin{array}{rcl} \chi(x) & \longrightarrow & \chi'(x) = U_o\chi(x), \quad \overline{\chi}(x) \longrightarrow \overline{\chi}'(x) = U_o^\dagger\overline{\chi}(x), \quad x \text{ even} \\ \chi(x) & \longrightarrow & \chi'(x) = U_e\chi(x), \quad \overline{\chi}(x) \longrightarrow \overline{\chi}'(x) = U_e^\dagger\overline{\chi}(x), \quad x \text{ odd} \end{array} , \tag{1.35}$$

where points are denoted as even or odd when $|x| = \sum_{i=1}^{4} x_i$ is even or odd. The kinetic part of the action is invariant under these transformations. For the mass term this is only true for $U_o = U_e$.

$$\begin{array}{rcl} \overline{\chi}(x)\left(\chi(x+\hat{\mu}) - \chi(x-\hat{\mu})\right) & \longrightarrow & \overline{\chi}(x)U_e^\dagger\left(U_e\chi(x+\hat{\mu}) - U_e\chi(x-\hat{\mu})\right) \\ & = & \overline{\chi}(x)\left(\chi(x+\hat{\mu}) - \chi(x-\hat{\mu})\right) \\ m\,\overline{\chi}(x)U_e^\dagger U_o\chi(x) & \longrightarrow & m\,\overline{\chi}(x)U_e^\dagger U_o\chi(x) \end{array} \tag{1.36}$$

Thus in the massless case staggered fermions have a $U(1) \otimes U(1)$ chiral symmetry which for non-zero mass is reduced to the diagonal subgroup.
The relation between the full chiral symmetry of massless QCD and the staggered remnant $U(1) \otimes U(1)$ can be analysed when looking at the transformation properties of the new quark fields q and $\bar{q}$.

$$\begin{array}{rcl} q(x) & \longrightarrow & q'(x) = \left(U_oP_o + U_eP_e\right)q(x) \\ & = & \frac{1}{2}U_o(1\!\!1 \otimes 1\!\!1 - \gamma_5 \otimes t_5) + \frac{1}{2}U_e(1\!\!1 \otimes 1\!\!1 + \gamma_5 \otimes t_5)q(x) \\ & = & \frac{1}{2}(U_e + U_o)(1\!\!1 \otimes 1\!\!1) + \frac{1}{2}(U_e - U_o)(\gamma_5 \otimes t_5)q(x) \\ \overline{q}(x) & \longrightarrow & \overline{q'}(x) = \overline{q}(x)\left(P_oU_e^\dagger + P_eU_o^\dagger\right) \\ & = & \frac{1}{2}\overline{q}(x)(1\!\!1 \otimes 1\!\!1 - \gamma_5 \otimes t_5)U_e^\dagger + \frac{1}{2}\overline{q}(x)(1\!\!1 \otimes 1\!\!1 + \gamma_5 \otimes t_5)U_o^\dagger \\ & = & \frac{1}{2}\overline{q}(x)(1\!\!1 \otimes 1\!\!1)(U_e^\dagger + U_o^\dagger) + \frac{1}{2}\overline{q}(x)(\gamma_5 \otimes t_5)(U_o^\dagger - U_e^\dagger) \end{array} \tag{1.37}$$

where $P_e = 1/2(1\!\!1 \otimes 1\!\!1 + \gamma_5 \otimes t_5)$ and $P_o = 1/2(1\!\!1 \otimes 1\!\!1 - \gamma_5 \otimes t_5)$ are operators which project on even and odd lattice sites, respectively.
The action is invariant under this transformation for $U_o = U_e$ and for $U_o = -U_e$. In the first case the transformation reduces to the operator $1\!\!1 \otimes 1\!\!1$. It leaves the kinetic and mass term of the action invariant and is thus connected to the continuum $U_V(1)$ which is responsible for baryon number conservation. The second choice leads to a transformation with the operator $\gamma_5 \otimes t_5$ which anti-commutes with the operators in the kinetic part of the action. Thus only this part is invariant under these transformations, the mass term is not. Since in addition $\gamma_5 \otimes t_5$ is traceless in flavour space it cannot be connected to the axial $U_A(1)$ but is a subgroup of the axial $SU_A(4)$. Thus, when the $U(1)$ on the lattice is spontaneously broken, the associated Goldstone boson is a flavour non-singlet, like the pion in the continuum. This property of staggered fermions make them especially interesting for the investigation of chiral symmetry breaking and its restoration at high temperatures. On the other hand since only the $U(1)$ is spontaneously broken on the lattice all but one of the $n_f^2 - 1$ flavour non-singlet states do not have Goldstone character.

Flavour symmetry

In the previous section a term proportional to $a(\gamma_5 \otimes t_{\mu 5})$ in the staggered action 1.32 has been identified to break the flavour symmetry of continuum QCD. In fact, when using the improved

fermion fields proposed by Luo [10]

$$\begin{aligned} q^{\mathrm{I}}_{\xi}(y) &= \exp\Big(-a\sum_{\lambda} A_\lambda \overline{D}_\lambda\Big)\ \tilde{U}_\xi(y)\chi_\xi(y) \quad , \\ \bar{q}^{\mathrm{I}}_{\xi}(y) &= \bar{\chi}_\xi(y)\tilde{U}^{\dagger}_{\xi}(y)\ \exp\Big(-a\sum_{\lambda} A_\lambda \overleftarrow{\overline{D}}_\lambda\Big) \quad , \end{aligned} \tag{1.38}$$

with $\overleftarrow{D}_\lambda = \overleftarrow{\partial}_\lambda - igA_\lambda$, the free staggered quark action can be written as

$$\begin{aligned} S_{\mathrm{KS}} &= \int_y \sum_{\xi\xi'} \bar{q}_\xi(y)\Big\{\sum_{\mu} \overline{(\gamma_\mu \otimes I)}_{\xi\xi'}[D_\mu + \frac{a^2}{6}D^3_\mu] + m\ \overline{(I\otimes I)}_{\xi\xi'}\Big\} q_{\xi'}(y) \\ &\quad + \mathcal{O}(a^3) + \mathcal{O}(g^{2n}a^2) \quad . \end{aligned} \tag{1.39}$$

In tree level the corrections thus start at $\mathcal{O}(a^2)$ with a term that is flavour symmetric and is not responsible for flavour symmetry breaking. One therefore can conclude that tree level corrections to the flavour symmetry at most start at $\mathcal{O}(a^3)$.
The effect of flavour symmetry breaking should be visible in a twofold way in lattice simulation. First of all the mass degeneracy of the particle states in the $n_f^2 - 1$ multiplet should not be present and second the spontaneously broken axial $SU_A(n_f)$ is not realised and thus only one of the expected $n_f^2 - 1$ Goldstone bosons really has the Goldstone character as was already pointed out in this section.

1.1.5 Wilson fermions

Wilson's idea [1] how to deal with the doublers was to add an additional term to the naive action which lifts all doublers such that only the pole at $(0,0,0,0)$ survives in the continuum limit.

$$\begin{aligned} S_{\mathrm{Wilson}} &= S^{\mathrm{naive}}_{\mathrm{fermion}} + r/2 \sum_{x,y} \overline{\psi}(x)\ \Box(x,y)\psi(y), \\ \Box(x,y) &= \sum_{\mu} \delta(x+\hat{\mu},y) + \delta(x-\hat{\mu},y) - 2\delta(x,y) \end{aligned} \tag{1.40}$$

Wilson fermions then describe only one quark flavour but the additional term breaks chiral symmetry at $\mathcal{O}(a)$. The scaling violations are also $\mathcal{O}(a)$. Both lattice artifacts can be reduced with the so-called Clover action [12]. The mass term is altered such that the scaling and chiral symmetry violations are of $\mathcal{O}(a^2)$. The flavour symmetry is realized for Wilson and Clover fermions.
At finite lattice spacing the vanishing of the pseudo-scalar mass can be interpreted as the chiral limit since the PCAC relation is telling that the expression $m_{\mathrm{PS}} \propto m_q^2 + \mathcal{O}(a)$ holds. On the other hand Aoki [13] pointed out that the symmetry, which is restored as the pseudo-scalar meson gets massless, is not the chiral symmetry but the parity flavour symmetry. Only in the continuum limit the correct chiral symmetry will be restored. For this reason Wilson fermion simulations are problematic when the finite temperature chiral phase transition is under investigation.

1.1.6 Domain wall fermions, Overlap fermions

Domain wall fermions and the overlap formalism provide an alternative approach to lattice fermions. With both formulations it is in principle possible to realize exact chiral symmetry on the lattice.

The main point is that the effective Dirac operator of domain wall and overlap fermions satisfy the Ginsparg-Wilson relation [14], which implies an exact chiral symmetry.
Domain wall (DW) fermions are defined in a space-time with an extra fifth dimension. The massive Wilson fermion fields are five-dimensional whereas the gauge fields are as usual four-dimensional. In the fifth dimension they are set to unity. When boundary conditions along the fifth dimension are free, the two chiralities are localized at different boundary walls. The mixing of the chiralities is exponentially suppressed with the length of the fifth dimension L_s. For $L_s = \infty$ no mixing occurs and the theory is chirally symmetric already at finite lattice spacing a for zero quark mass. The pole mass for free DW fermions is given by $m_{\text{pole}} = M(2-M)[m_f + (1-M)^{L_s}]$, $(0 < M < 2)$, where M is the domain wall height and m_f the coupling of the boundaries, which turns out to be proportional to the 4-dimensional bare quark mass. The pole mass vanishes in the limit $L_s \to \infty$ and $m_f \to 0$, thus chiral symmetry is realised. This behaviour is very much desired in thermodynamic studies when the finite temperature chiral phase transition and the strength of the axial $U_A(1)$ symmetry breaking is investigated. The latter will have an influence on the order of the chiral phase transition depending on whether the axial $U_A(1)$ is effectively restored already at the chiral transition or not.
Numerical studies with DW fermions show that in full QCD the lattice spacing has to be quite small to ensure the restoration of chiral symmetry [15]. At an inverse lattice spacing of $1/a = 1\text{GeV}$ the pion mass does not approach zero as L_s is sent to infinity and m_f to zero. Only at $1/a = 2\text{GeV}$ and $L_s = 10-20$ this is realized, meaning that finite temperature simulations have to be performed with a temporal size as large as $N_\tau = 11$ to meet this requirement[†]. The increase of computational costs with N_τ will be discussed in the next chapter. Compared to ordinary fermion simulations the computational costs grow linearly with the additional factor L_s.
At present only the first exploratory calculations on modest lattices are under way at the largest parallel machines available. In the future it will be very interesting to see whether quantities related to the chiral symmetry of QCD come out the same for domain wall fermions as for staggered and Wilson fermions in the continuum limit where the chiral symmetry should also be restored.
Details on domain wall fermions can be found in [16, 17] and references therein. The overlap formalism which will not be the topic of this work is discussed for example in [18].

1.2 From the lattice to the continuum

The fields and observables are defined on the lattice in terms of the lattice spacing a in such a way that only dimensionless quantities occur. The physical scale is introduced by either calculating ratios of physical quantities or determining the lattice spacing a by interpreting lattice results as physical. There are several ways to fix the scale of QCD. They are e.g. realised by measuring the rho meson mass $m_\rho a$ or the string tension σa^2.

$$a = \frac{m_\rho a}{770}\text{MeV}^{-1} \qquad a = \frac{\sqrt{\sigma} a}{420}\text{MeV}^{-1} \tag{1.41}$$

The physical interpretation is only justified, for example in case of the ρ meson mass, if the bare quark masses considered are sufficiently small such that the lattice result can be interpreted physically. Since the inverse rho meson mass is identified with the rho meson correlation length $\xi = 1/m_\rho a$, it follows that $a = 1/(\xi \cdot 770)\text{MeV}^{-1} = 1/\xi$ 0.26fm and the limit $a \to 0$ is realised at $\xi \to \infty$.
For some value of the coupling parameters for lattice theories the limit $\xi \to \infty$ is achieved at a second order point. Thus physical behaviour connected to the IR modes of the theory can be

[†]It is assumed that the critical temperature for full QCD is about 180 MeV. From this N_τ can be deduced by using $T_c = 1/N_\tau a \Rightarrow N_\tau$=2GeV/180MeV

described by critical phenomena. A main property exhibited by critical phenomena is universality, i.e. they do not depend on the details of the microscopic theory. For lattice theories this means that in the continuum limit the results do no longer depend on the details of the discretisation. As a consequence also the symmetries broken by the discretisation are being recovered in the continuum limit.
In QCD the limit $\xi \to \infty$ is realised at $\beta \to \infty$ ($g \to 0$) due to asymptotic freedom. Since this is the weak coupling limit the functional dependence between the lattice spacing and the coupling can be computed perturbatively. The result can be written as

$$a\frac{dg}{da} = b_0 g^3 + b_1 g^5 + \mathcal{O}(g^7) \quad , \tag{1.42}$$

where the first two coefficients b_0 and b_1 are universal in the sense that they are the same for different discretisation schemes and also for continuum QCD.

$$b_0 = \frac{1}{16\pi^2}\left(\frac{11N}{3} - \frac{2n_f}{3}\right) \tag{1.43}$$

$$b_1 = \left(\frac{1}{16\pi^2}\right)^2 \left(\frac{34N^2}{3} - \left(\frac{10N}{3} + \frac{N^2-1}{N}\right) n_f\right) \tag{1.44}$$

Equation 1.42 after integration leads to

$$a\Lambda_L \equiv R(\beta) = \left(\frac{2Nb_0}{\beta}\right)^{\frac{-b_1}{2b_0^2}} \exp\left\{-\frac{\beta}{4Nb_0}\right\} \tag{1.45}$$

where Λ_L is the so-called Λ parameter of the theory. In principle if lattice results at finite a show the behaviour of 1.45 a reliable continuum extrapolation is possible.

1.3 Observables at finite temperature

In this section it is convenient to formulate lattice QCD on an anisotropic lattice with a temporal lattice spacing a_τ and a spatial lattice spacing a. They are related via the anisotropy parameter ξ, $\xi = a/a_\tau$. In this formulation the temperature and volume are independent quantities

$$1/T = N_\tau \; a_\tau \qquad V^{1/3} = N_\sigma \; a \quad . \tag{1.46}$$

Since the lattice spacing enters in the action only indirectly through the bare couplings one has to introduce different couplings for the spatial and temporal parts of the action.

$$\begin{aligned} \beta_\sigma S_{\mathrm{G},\sigma} &+ \beta_\tau S_{\mathrm{G},\tau} \\ &= \beta_\sigma \sum_{x;\mu<\nu<4} \left(1 - \frac{1}{N}\mathrm{ReTr}U_{\mu,\nu}(x)\right) + \beta_\tau \sum_{x;\mu=1,2,3} \left(1 - \frac{1}{N}\mathrm{ReTr}U_{\mu,4}(x)\right) \end{aligned} \tag{1.47}$$

$$\begin{aligned} S_{\mathrm{KS}} &= \sum_x \Big\{ m_q a \; \overline{\chi}(x)\chi(x) \\ &+ \frac{1}{2}\sum_{\mu=1,2,3} \eta_\mu(x) \left[\overline{\chi}(x)U_\mu(x)\chi(x+\hat{\mu}) - \overline{\chi}(x)U_\mu^\dagger(x-\hat{\mu})\chi(x-\hat{\mu})\right] \\ &+ \frac{\gamma_F}{2}\eta_4(x)\left[\overline{\chi}(x)U_4(x)\chi(x+\hat{4}) - \overline{\chi}(x)U_4^\dagger(x-\hat{4})\chi(x-\hat{4})\right]\Big\} \\ &= \sum_{x,y}\overline{\chi}(x)\left[\sum_{\mu=1,2,3} D_{(x,y);\mu} + \gamma_F D_{(x,y);4} + m_q a \; \delta_{xy}\right]\chi(y) \end{aligned} \tag{1.48}$$

The couplings are conveniently defined as $\beta_\sigma = 2N/g_\sigma^2\xi$, $\beta_\tau = 2N\xi/g_\tau^2$ and $\gamma_F = \xi$ such that the anisotropic action reduces to the correct classical action in the naive limit. In lattice perturbation theory the anisotropic couplings can be related to the anisotropy ξ and the bare coupling on the isotropic lattice. The relations are given by

$$\begin{aligned} \beta_\sigma &= \beta\ \xi^{-1}\ \left[1 + c_\sigma(\xi) g^2 + \mathcal{O}(g^4)\right] \\ \beta_\tau &= \beta\ \xi\ \left[1 + c_\tau(\xi) g^2 + \mathcal{O}(g^4)\right] \qquad (1.49) \\ \gamma_F &= \xi\ \left[1 + c_F(\xi) g^2 + \mathcal{O}(g^4)\right] \end{aligned}$$

(1.50)

The quantum corrections have been calculated in pure gauge theory [19] and for full QCD [20] in the limit of $\xi = 1$.

1.3.1 Energy density and pressure

In thermodynamics the energy density and the pressure are fundamental quantities describing the system. They are defined as the derivative of $\ln Z$ with respect to the inverse temperature T^{-1} and the volume V.

$$\epsilon = -\frac{1}{V}\left(\frac{\partial \ln Z}{\partial\,(1/T)}\right)_V \qquad (1.51)$$

$$p = T\left(\frac{\partial \ln Z}{\partial V}\right)_T \qquad (1.52)$$

These formula show that it is necessary to vary the temporal and spatial lattice spacing independently in order to perform the corresponding derivatives. For a fixed volume $N_\sigma^3 \times N_\tau$ the energy density is

$$\begin{aligned} \frac{\epsilon}{T^4} &= \frac{(\epsilon_{\rm G} + \epsilon_{\rm F})}{T^4} \\ &= \left(\frac{N_\tau}{\xi N_\sigma}\right)^3 \left(\xi \frac{\partial \ln Z}{\partial \xi}\right)\Bigg|_{\xi=1} \quad . \qquad (1.53) \end{aligned}$$

The gluonic and the fermionic contributions are given by

$$\begin{aligned} \frac{\epsilon_{\rm G}}{T^4} &= \left(\frac{N_\tau}{N_\sigma}\right)^3 \beta \Bigg(\left(\overline{\langle S_{{\rm G},\sigma}\rangle} - \overline{\langle S_{{\rm G},\tau}\rangle}\right) \\ &\quad + g^2 \left(\left(\frac{dc_\sigma(\xi)}{d\xi}\right)\Bigg|_{\xi=1} \overline{\langle S_{{\rm G},\sigma}\rangle} + \left(\frac{dc_\tau(\xi)}{d\xi}\right)\Bigg|_{\xi=1} \overline{\langle S_{{\rm G},\tau}\rangle} \right) \Bigg) \quad , \qquad (1.54) \end{aligned}$$

$$\frac{\epsilon_{\rm F}}{T^4} = \left(\frac{N_\tau}{N_\sigma}\right)^3 \frac{n_f}{4} \left(\frac{d\gamma_F}{d\xi}\Bigg|_{\xi=1} \overline{\langle {\rm Tr}\ \ D_4\ M^{-1}\rangle} - \left(a\frac{dm_q a}{da}\right)_\beta \overline{\langle {\rm Tr}\ \ M^{-1}\rangle} \right) \quad . \qquad (1.55)$$

It has been made use of a notation where the vacuum contributions are already subtracted to normalize the thermodynamic quantities to zero at $T = 0$.

$$\begin{aligned} \overline{\langle \mathcal{O}\rangle} &= \langle \mathcal{O}\rangle_{(N_\tau < N_\sigma)} - \langle \mathcal{O}\rangle_{(N_\tau = N_\sigma)} \\ &= \langle \mathcal{O}\rangle_T - \langle \mathcal{O}\rangle_0 \qquad (1.56) \end{aligned}$$

The pressure is related to the energy density via $\epsilon - 3p$.

$$\frac{\epsilon - 3p}{T^4} = \left(\frac{N_\tau}{N_\sigma}\right)^3 \left(\left(a\frac{d\beta}{da} \right)_{am_q} \left(\overline{\langle S_{\mathrm{G},\sigma} \rangle} - \overline{\langle S_{\mathrm{G},\tau} \rangle} \right) + \frac{n_f}{4} \left(a\frac{dm_q a}{da} \right)_\beta \overline{\langle \mathrm{Tr}\ M^{-1} \rangle} \right) \quad (1.57)$$

with the β-functions $R_\beta = a\,(d\beta/a)\,|_{am_q}$ and $R_{m_q a} = a\,(dm_q a/da)\,|_\beta$. $\epsilon - 3p$ is also referred to as the interaction measure, indicating the deviations of the QCD equation of state to the ideal gas, where this quantity vanishes.
For all thermodynamic quantities discussed so far it is necessary to calculate in addition to simple gluonic and fermionic expectation values also the β-functions and derivatives of the anisotropic couplings with respect to the anisotropy. A non-perturbative determination is in principle possible for all these quantities but relatively simple only for R_β. The use of perturbative values lead to problems like a negative pressure at the critical point.
Fortunately there exists an alternative prescription to calculate the pressure which allows a completely non-perturbative determination. It is based on the simple observation that for a homogeneous statistical system the free energy is proportional to the pressure.

$$p = -f = \frac{T}{V} \ln Z \quad (1.58)$$

The derivative of equation 1.58 gives

$$\frac{1}{T^4}\ \frac{dp}{d\beta} = -\left(\frac{N_\tau}{N_\sigma}\right)^3 \langle S_G \rangle \quad . \quad (1.59)$$

Thus the pressure can be calculated by integrating 1.59 and subtracting the zero temperature contributions

$$\frac{p}{T^4}\Big|_{\beta_0}^{\beta} = \left(\frac{N_\tau}{N_\sigma}\right)^3 \int_{\beta_0}^{\beta} d\beta'\ (\langle S_G \rangle_0 - \langle S_G \rangle_T) \quad . \quad (1.60)$$

The calculation of the pressure is now reduced to the calculation of the action at zero and finite temperature and the determination of the point β_0 where the action difference vanishes within errors.

1.3.2 The Polyakov loop and the chiral condensate

In statistical mechanics phase transitions are generally related to spontaneous symmetry breaking. In pure gauge theory this symmetry is the $Z(3)$ center symmetry of the pure gluonic action which is related to deconfinement. The symmetry transformation is defined on all temporal links of a timeslice

$$U_4(\vec{x}, x_4) \to z U_4(\vec{x}, x_4) \quad , z \in Z(3), \quad \forall \vec{x},\ x_4 \text{ fixed} \quad . \quad (1.61)$$

Since the elements of $Z(3)$ commute with elements of $SU(3)$, the action remains unchanged under this transformation whereas the Polyakov loop $L(\vec{x})$ does transform non-trivially

$$L(\vec{x}) \equiv \frac{1}{N} \mathrm{Tr} \prod_{x_4=1}^{N_\tau} U_4(\vec{x}, x_4) \quad , \quad (1.62)$$

$$L(\vec{x}) \to z L(\vec{x}) \quad , z \in Z(3) \quad . \quad (1.63)$$

When the $Z(3)$ symmetry of the action is preserved the expectation value of the Polyakov loop $\langle L \rangle = \langle 1/N_\sigma^3 \, |\sum_{\vec{x}} L(\vec{x})| \rangle$ will vanish in the infinite volume limit. Otherwise it will have a non-zero value.
On the other hand the Polyakov loop is connected to the change of the free energy due to the insertion of a fermionic test charge into a gluonic medium,

$$\langle L \rangle \propto e^{-f_q(T)/T} \tag{1.64}$$

In the confined phase a single coloured charge cannot be screened, the free energy is infinite and the Polyakov loop expectation value is zero. This is no longer true in the deconfinement phase where the free energy is finite and the Polyakov loop non-zero.
The maximum of the Polyakov loop susceptibility χ_L can be used to define a pseudo-critical coupling β_c

$$\chi_L \equiv N_\sigma^3 \left(\left\langle |L|^2 \right\rangle - \langle L \rangle^2 \right) \quad . \tag{1.65}$$

In the limit of zero quark mass QCD has a global chiral symmetry $U(n_f) \otimes U(n_f)$, which for staggered fermions is reduced to a $U(1) \otimes U(1)$ symmetry. The chiral condensate which is defined as the derivative of $\ln Z$ with respect to the bare mass $m_q a$ serves as an order parameter. Different from the infinite mass limit it can directly be derived from the QCD partition function.

$$\begin{aligned} \langle \overline{\psi}\psi \rangle &= \frac{1}{N_\tau N_\sigma^3} \frac{n_f}{4} \frac{\partial}{\partial m_q a} \ln Z \\ &= \frac{1}{N_\tau N_\sigma^3} \frac{n_f}{4} \left\langle \mathrm{Tr}\ M^{-1} \right\rangle \end{aligned} \tag{1.66}$$

where the factor $n_f/4$ corrects for the number of flavours. The chiral symmetry is spontaneously broken at low temperatures and therefore one obtains a non-vanishing chiral condensate. At high temperature one expects the symmetry to be restored.
The chiral susceptibility is defined as the derivative of $\langle \overline{\psi}\psi \rangle$ with respect to the mass $m_q a$

$$\begin{aligned} \chi_{\langle \overline{\psi}\psi \rangle} &= \frac{1}{N_\tau N_\sigma^3} \frac{n_f}{4} \frac{\partial^2}{\partial (m_q a)^2} \ln Z \\ &= \frac{1}{N_\tau N_\sigma^3} \frac{n_f}{16} \left(\left\langle \left(\mathrm{Tr}\ M^{-1} \right)^2 \right\rangle - \left\langle \mathrm{Tr}\ M^{-1} \right\rangle^2 \right) \\ &\quad - \frac{n_f}{4} \sum_x \left\langle M^{-1}(x,0) M^{-1}(0,x) \right\rangle \quad , \end{aligned} \tag{1.67}$$

where the last line corresponds to the connected part of the chiral condensate which is omitted in this work since it has no effect on the quantities considered. To calculate the disconnected part 25 random vectors have been used on each configuration to obtain a noisy estimator for $\left\langle \left(\mathrm{Tr}\ M^{-1} \right)^2 \right\rangle$.
In the case where the quark mass is neither zero nor infinite the chiral condensate or the Polyakov loop show a rapid change at the transition point. The maximum of the susceptibility of both quantities still can be used to define the pseudo-critical coupling. As it turned out they agree within errors for all calculations performed up to now. The case of intermediate quark masses will be discussed in some detail later.

1.4 Observables at zero temperature

In this work different observables at zero temperature are considered. They are used to set the scale of the finite temperature calculations. For calculations of the equation of state the temperature

scale can be defined with the string tension σ which is extracted from the heavy quark potential. The effective physical quark mass can be determined from the ratio of the pseudo-scalar to vector meson mass, $(m_{\mathrm{PS}}/m_{\mathrm{V}})^2 \propto m_{\mathrm{phys}}$. Thus the extraction of meson masses from correlation functions will be discussed.

1.4.1 The heavy quark potential

The potential between a static quark anti-quark pair can be calculated from the temporal Wilson loop

$$W(R,L) \equiv \left\langle \mathrm{Tr} \prod_{l \in \mathcal{C}} U_l \right\rangle \quad , \tag{1.68}$$

which is the trace of an ordered product of links U_l along a path $\mathcal{C}$ with a space- and time-like extension R and L, respectively.
For large temporal size it is connected to the potential between static quarks via

$$W(R,L) = \lim_{L\to\infty} F(R) \exp(V_{q\bar{q}}(R)L) \quad , \tag{1.69}$$

where $F(R)$ is the amplitude which characterizes the overlap of the Wilson loop operator with the ground state of the system. The ansatz

$$V_{q\bar{q}}(R) = V_0 + \frac{\alpha}{R} + \sigma R \quad , \tag{1.70}$$

has proven quite successful for the description of the potential behaviour. The coulombic term correctly describes the short-range behaviour and ensures asymptotic freedom, the linear term with the string tension σ accounts for the confinement property of QCD. In the presence of light quarks in the full theory one would expect the formation of a heavy light meson pair, if the static quark anti-quark pair is sufficiently separated. When the potential is extracted from Wilson loops in zero temperature lattice simulations of QCD this string breaking phenomenon has however not been observed for distances up to 2fm. Only at nonzero temperature this effect has been found in the confining phase [21]. In that case the potential is determined from Polyakov loop correlations.
Since the potential is not dependent on the actual path in the Wilson loop it can be optimized to obtain a maximal overlap of the Wilson loop with the ground state. The APE group [22] proposed the so-called smearing procedure in which iteratively a spatial staple is added to the link

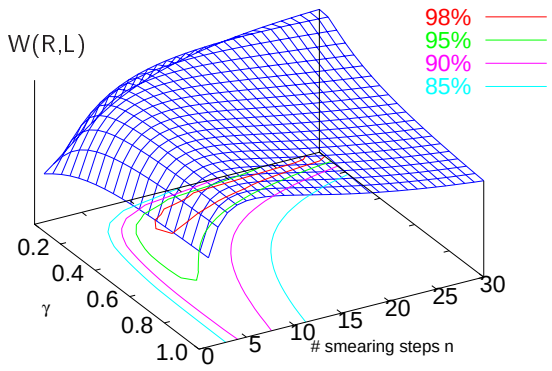

Figure 1.1: Smeared Wilson loop as a function of γ and the number of smearing steps n. The lines show the different level of signal enhancement.

$$U_\mu \to U_\mu + \gamma \sum_{\nu-\mu} (1 \times 1 - \mathrm{staples})_\nu \quad , \tag{1.71}$$

where the factor γ together with the number of smearing steps n are the parameters which are used for tuning. In general a Wilson loop of a certain size will be chosen to test the smearing. In figure 1.1 the relative value of the Wilson loop depending on the factor γ and the number of smear steps is plotted. Obviously after only a few steps the signal can be much improved. For the Wilson loop operator $W(N_\sigma/2, 1)$ an enhancement of the signal by more than a factor of 6 has been achieved in pure gauge theory as well as in full QCD.

1.4.2 Meson correlation functions

In this section the procedure how to measure meson masses from meson correlation functions for staggered fermions will be summarized. The lattice states have to be identified with the corresponding continuum states. This is achieved by analysing the irreducible representations of the discrete transformations of staggered fermions which lie within a discrete subgroup of the Poincaré group. The different symmetries of the lattice group are identified with those of the continuum and by this the lattice states are matched to the appropriate continuum states. A complete analysis of meson operators in the staggered formulation can be found in a work by Goltermann and Smit [11] which is summarized in [23].
The correlation function is defined as

$$C_{M-M'}(t) = \left\langle O_M(t) O^\dagger_{M'}(t) \right\rangle \quad , \tag{1.72}$$

where $O_M(t)$ is the staggered meson operator which is given in terms of the physical q fields as defined in 1.30

$$O_M(t) \quad \equiv \quad \sum_y \bar{q}(y)(\Sigma_A \otimes \Sigma_B) q(y) \quad . \tag{1.73}$$

The operators Σ_A and Σ_B act on the Dirac and flavour indices, respectively, and determine the quantum number of the meson operator. In terms of the staggered fields the local zero momentum meson operator is given by

$$O_{\mathrm{local}}(t) \quad \equiv \quad \sum_{\vec{x}} \phi(\vec{x}) \overline{\chi}(\vec{x}, t) \chi(\vec{x}, t) \quad . \tag{1.74}$$

The meson phases $\phi(x)$ determine the corresponding quantum number of the meson.
An alternative zero momentum operator is constructed using a so-called wall-source. Correlation functions built from local meson operators are usually contaminated by exited states such that large temporal extensions of the lattice are necessary to determine the ground state reliably. The idea now is to construct operators which have an improved overlap with the lightest particle state. It turned out that operators constructed from wall sources achieve this requirement for staggered fermions [23]

$$O_{\mathrm{wall}}(t) \quad \equiv \quad \frac{1}{V_8^2} \sum_{\vec{x}, \vec{e}, \vec{e'}} \phi(\vec{x}) \overline{\chi}(\vec{x} + \vec{e}, t) \chi(\vec{x} + \vec{e'}, t) \quad , \tag{1.75}$$

where $V_8 = N_\sigma^3/8$. The sum is taken in addition to the strictly local operator also over all even points in each direction denoted by $\vec{e}$ and $\vec{e'}$. The operator has been made gauge invariant by fixing the Coloumb gauge on the time slice t.
Both operators, $O_{\mathrm{local}}(t)$ and $O_{\mathrm{wall}}(t)$, project onto states with the same quantum number. The ones measured in this work are given in table 1.4.2. The phases are $\zeta_\mu = (-1)^{x_{\mu+1}+\ldots+x_4}$, $\epsilon(x) =$

$(-1)^{x_1+\ldots+x_4}$ and the usual staggered phases $\eta_\mu(x)$
Two correlation functions have been analysed, the local-local and local-wall correlations

$$\begin{aligned} C_{\mathrm{local-local}}(t) &= \left\langle O_{\mathrm{local}}(t) O^\dagger_{\mathrm{local}}(0) \right\rangle \\ &= -(-1)^t N_\sigma^3 \sum_{\vec{x}} \phi(x)\eta_4(\vec{x}) \left\langle |G(\vec{x},t;\vec{x},0)|^2 \right\rangle \\ C_{\mathrm{local-wall}}(t) &= \left\langle O_{\mathrm{local}}(t) O^\dagger_{\mathrm{wall}}(0) \right\rangle \\ &= -(-1)^t N_\sigma^3 \sum_{\vec{x}} \phi(x)\eta_4(\vec{x}) \left\langle \left| \frac{1}{V_8} \sum_{\vec{e}} G(\vec{x},t;\vec{e},0) \right|^2 \right\rangle \quad , \end{aligned} \tag{1.76}$$

where G is the quark propagator.
On the lattice the masses can thus be calculated by measuring the quark propagators and constructing the correlation functions. They are related to the masses of the particle states in the following way

$$\begin{aligned} C_{M-M'}(t) &= A\left(e^{-m_A t} + e^{-m_A(T-t)}\right) \\ &+ (-1)^t B\left(e^{-m_B t} + e^{-m_B(T-t)}\right), \end{aligned} \tag{1.77}$$

where A and B are the amplitudes and m_A and m_B the masses of the corresponding meson states. A fit to the ansatz 1.77 yields the masses. When reducing the fitting range by leaving out data points at small temporal distances the mass parameters should approach a constant value. This is especially true for the wall source correlations since there the exited states are suppressed.

operator	state A	state B
$\overline{\chi}\chi$	π	f_0
$\eta_4\zeta_4\overline{\chi}\chi$	π	-
$\eta_i\epsilon\zeta_i\overline{\chi}\chi$	ρ	b_1
$\eta_4\zeta_4\eta_i\epsilon\zeta_i\overline{\chi}\chi$	ρ	a_1

Table 1.1: Local meson operators and their corresponding continuum particle states.

The two different correlation functions have been used to check the consistency of the results. The values quoted in this work are extracted from wall sources.

1.5 The numerical simulation

In this section the numerical methods to perform a simulation of lattice gauge theory with dynamical quarks will be discussed. The general aim in simulations of statistical systems is to produce a Markov chain which provides micro states $\mathcal{C}$ of the system which allow the calculation of an ensemble average. This is especially true when the configurations $\mathcal{C}$ are distributed according to the Boltzmann factor $\exp(-S)$ of the system under consideration. Then the expectation value of an observable $\mathcal{O}$ can be approximated by

$$\langle O \rangle \approx \frac{\sum_{\mathcal{C}} \mathcal{O}(C)}{\#\mathcal{C}} \quad , \tag{1.78}$$

where $\#\mathcal{C}$ denotes the number of configuration in the ensemble. The detailed balance condition ensures that the system converges towards the equilibrium distribution

$$e^{-S(\mathcal{C})} P(\mathcal{C},\mathcal{C}') = e^{-S(\mathcal{C}')} P(\mathcal{C}',\mathcal{C}) \quad , \tag{1.79}$$

where $P(\mathcal{C},\mathcal{C}')$ is a non-zero transition probability from one configuration to another.
In pure gauge theory generally heat-bath [24] and overrelaxation [25] algorithms are used. They

are local updates which alter the degrees of freedom by going successively through the lattice. When the fermion degrees of freedom are added to the system the locality of the action is lost due to the fermion determinant in the action which results from integrating out the Grassmann fields. Gottlieb and Toussaint [26] proposed two global algorithms which are based on hybrid molecular dynamics methods. The so-called Hybrid Monte Carlo algorithm uses pseudo-fermion fields to describe the fermion determinant and can be made exact by a final Metropolis accept-reject step. The evolution of the system is based on the molecular dynamics method where the main numerical task consists of the inversion of the fermion matrix which is performed with the conjugate gradient method for staggered fermions. The algorithm is only applicable to two Wilson flavours and four staggered flavours. An alternative algorithm for an arbitrary number of flavours is the Hybrid R which will be discussed in the following. It has been used in staggered simulations in this work with two, two plus one and three flavours.

1.5.1 The Hybrid R algorithm

The partition function of QCD for n_f Wilson or staggered flavours can be written as

$$\begin{aligned} Z &= \int \mathcal{D}U\mathcal{D}H \exp(-\frac{1}{2}\mathrm{tr}\ H^2 - S_\mathrm{G}) \det(M^\dagger M)^{n_f/N_M} \\ &= \int \mathcal{D}U\mathcal{D}H \exp(-\frac{1}{2}\mathrm{tr}\ H^2 - S_\mathrm{G} + \frac{n_f}{N_M}\mathrm{tr}\ \ln(M^\dagger(U)M(U))) \\ &= \int \mathcal{D}U\mathcal{D}H \exp(-\mathcal{H}) \end{aligned} \tag{1.80}$$

where $N_M = 2$ for Wilson and $N_M = 4$ for staggered fermions, respectively. H is defined as the conjugate momentum to the gauge link U and can be introduced into the partition function without changing expectation values of physical quantities depending on U. The equations of motion then have the form

$$\begin{aligned} \dot{U}_\mu(x) &= iH_\mu(x)U_\mu(x) \quad , \quad H \text{ is traceless Hermitian} \\ 0 &= \sum_{x,\mu} \mathrm{tr}\ H_\mu(x)\dot{H}_\mu(x) + \frac{d}{d\tau}S_\mathrm{G} - \frac{n_f}{N_M}\mathrm{tr}\ \frac{1}{M^\dagger(U)M(U)}\frac{d}{d\tau}\left(M^\dagger(U)M(U)\right) \quad , \end{aligned} \tag{1.81}$$

where the derivatives $\dot{U}$ and $\dot{H}$ are taken with respect to the molecular dynamics time. The second equation implicitly defines $\dot{H}_\mu(x)$ using the requirement that the Hamiltonian is constant in molecular dynamics time, $\dot{\mathcal{H}} = 0$. The explicit form will be derived in the appendix B.
The idea of the algorithm now consists of alternately update the H field using a heat-bath method and update the H fields and gauge links U simultaneously with the molecular dynamics method while keeping the effective Hamiltonian $\mathcal{H}$ fixed. Since the equations of motion cannot be solved using an exact numerical method the crucial part, the inverse of $(M^\dagger(U)M(U))$, has to be approximated by a noisy estimator

$$0 = \sum_{x,\mu} \mathrm{tr}\ H_\mu(x)\dot{H}_\mu(x) + \frac{d}{d\tau}S_\mathrm{G} - \frac{n_f}{N_M}\mathrm{tr}\ X^*\frac{d}{d\tau}\left(M^\dagger(U)M(U)\right)X \quad , \tag{1.82}$$

where $X = 1/(M^\dagger(U)M(U))\ M(U)\ R$ with the Gaussian noise vector R. These equations of motion are now integrated by replacing the derivatives by a difference scheme such that the error in observables is of the order of $\delta\tau^2$, where τ is the molecular dynamics time. To achieve this a modified leapfrog scheme has to be applied. The molecular dynamics evolution of the system from time τ to $\tau + \delta\tau$ is summarised starting from a newly refreshed field $H_\mu(x)[\tau]$:

1. Start with an intermediate U:

$$U_\mu(x)\left[\tau+\delta\tau\left(\frac{1}{2}-\frac{n_f}{2N_M}\right)\right]=\exp\left(i\delta\tau\left(\frac{1}{2}-\frac{n_f}{2N_M}\right)H_\mu(x)[\tau]\right)U_\mu(x)\,[\tau]$$

2. Generate an intermediate vector Φ:

$$\Phi=M^\dagger\left[\tau+\delta\tau\left(\frac{1}{2}-\frac{n_f}{2N_M}\right)\right]\;R$$

3. Compute U at $\tau+1/2\;\delta\tau$:

$$U_\mu(x)\left[\tau+\frac{1}{2}\delta\tau\right]=\exp\left(i\delta\tau\left(\frac{n_f}{2N_M}\right)H_\mu(x)[\tau]\right)\cdot U_\mu(x)\left[\tau+\delta\tau\left(\frac{1}{2}-\frac{n_f}{2N_M}\right)\right]$$

4. Calculate X using the conjugate gradient method:

$$X=\frac{1}{M^\dagger(U)\left[\tau+\frac{1}{2}\delta\tau\right]M(U)\left[\tau+\frac{1}{2}\delta\tau\right]}\;\Phi$$

5. Compute the momentum derivative $\dot{H}_\mu(x)\left[\tau+\frac{1}{2}\delta\tau\right]$ as given in the appendix B.

6. Compute $H_\mu(x)\,[\tau+\delta\tau]$:

$$H_\mu(x)\,[\tau+\delta\tau]=H_\mu(x)\,[\tau]+\delta\tau\dot{H}_\mu(x)\left[\tau+\frac{1}{2}\delta\tau\right]$$

7. Unless this is the last time step, compute the next U:

$$U_\mu(x)\left[\tau+\delta\tau\left(\frac{1}{2}-\frac{n_f}{2N_M}\right)+\delta\tau\right]=$$
$$\exp\left(i\delta\tau\left(1-\frac{n_f}{2N_M}\right)H_\mu(x)[\tau+\delta\tau]\right)U_\mu(x)\left[\tau+\frac{1}{2}\delta\tau\right]$$

8. Repeat the steps 2 to 7 N times. In the last iteration omit step 7 and compute the final U:

$$U_\mu(x)\,[\tau+N\delta\tau]=\exp\left(i\frac{\delta\tau}{2}H_\mu(x)[\tau+N\delta\tau]\right)U_\mu(x)\left[\tau+\left(N-\frac{1}{2}\right)\delta\tau\right]$$

The computation of the time derivative of H will be discussed in the appendix B for different staggered fermion actions.

Step size dependence in the Hybrid R algorithm

As already mentioned in the previous section the leapfrog steps are chosen such that the error of observables induced by the Hybrid R algorithm is proportional to $\delta\tau^2$. In general simulations at different step-sizes have to be performed and then extrapolated to zero step-size. Instead it should be sufficient to perform a simulation at one step size which leads to a result that agrees within statistical errors with the extrapolation to zero step-size. In this section a general criterion to choose an appropriate $\delta\tau$ will be defined. The JLQCD collaboration [27] examined the dependence of the critical coupling and the maximum of the chiral susceptibility on the step size.

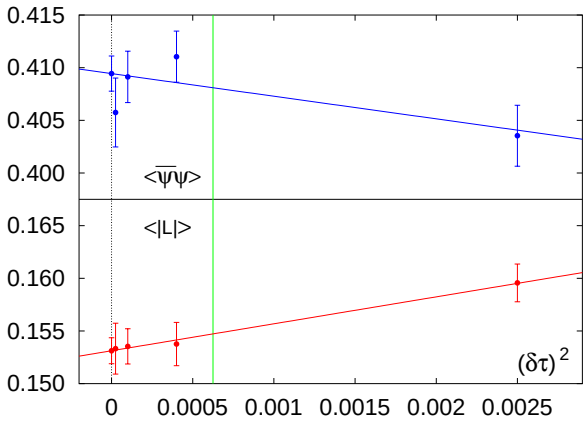

Figure 1.2: The Polyakov loop and the chiral condensate for different values of the step size $\delta\tau$. The straight line is a fit to the data in $\delta\tau^2$.

On an $8^3 \times 4$ lattice with a quark mass of $m_q a = 0.02$ they determined these two quantities for different $\delta\tau$ and found that the relation $\delta\tau \approx \frac{m_q a}{2}$ should hold to ensure that the error is acceptable. In a different study [60] the equation of state has been investigated with the staggered fermion action on an $12^3 \times 6$ and 12^4 lattice. There the step size effects in the plaquette are crucial for the correct determination of the pressure. Their general statement is that the $T = 0$ results show a stronger step size effect than the $T \neq 0$ results which is probably due to the larger volume which accumulates the error.

In this work the step size effect using an improved[‡] staggered fermion action has been investigated. The Polyakov loop and the chiral condensate have been calculated on an $8^3 \times 4$ lattice at a quark mass of $m_q a = 0.05$ for different $\delta\tau$. The results together with an extrapolation to zero step size are plotted in figure 1.2. The green vertical line indicates where the condition $\delta\tau = m_q a/2$ is realised. The data at this step size reasonably well agree with the value at zero step size. To improve the agreement throughout this work a value of $\delta\tau = m_q a/2.5$ has been applied if not stated otherwise.

The step size effects in the equation of state will be discussed in chapter 4.

[‡]The improvement of lattice actions is the topic of the next chapter

Chapter 2

Improved gluon and staggered fermion actions

As discussed in the previous chapter straight forward discretisation of the QCD action leads to expressions which at finite lattice spacing a have corrections to the continuum action in some order of a. Therefore observables which are sensitive to the ultraviolet cut-off show a strong a dependence and one is forced to perform simulations at quite small lattice spacing to be able to extract continuum results or to extrapolate to the continuum limit reliably. Unfortunately this increases the computational effort dramatically.
In this chapter it will be discussed how the situation can be improved by using improved actions. The general aim is to minimize the cut-off effects for finite lattice spacing. One strategy which will be the main topic of the next section is to reduce the a corrections on the level of the lattice action. This procedure turns out to be successful only in tree-level, in one loop order the $\mathcal{O}(a^2)$ dependence of physical quantities has to be analyzed and then removed by an appropriate choice of the coefficients in the action. These approaches base on a perturbative expansion of the action or a physical observables in orders of the coupling g and should give the best results when the coupling is small. Since simulations are in general performed at intermediate couplings, Lepage and Mackenzie [30] introduced the concept of mean-field or tadpole improvement. Based on the observation that lattice perturbation theory converges badly in terms of the bare coupling g, but much better when a renormalized coupling is used, they suggested the replacement of a single link U_μ in the action by $U_\mu/\langle U\rangle$. This should bring the lattice action closer to the continuum one already at intermediate couplings.
A different approach concentrates on renormalisation group arguments. Hasenfratz and Niedermayer [31] suggested to construct actions which are classically perfect in the sense that at $g = 0$ there are no cut-off effects at $\mathcal{O}(a^n)$. For another class of actions the parameters are chosen such that the action stays close to the renormalized trajectory after one or two block-spin transformations. All these improvement schemes have been used in pure gauge simulations during the last years. The results will be discussed in section 2.2 focussing on observables which are relevant for finite temperature QCD.
The improvement of the fermionic sector for staggered fermions will be the topic of section 2.3. In addition to the improvement schemes discussed above, Heller *et al.* [32] used the reduction of rotational symmetry violations as a guideline to construct improved actions. This will be explained in section 2.3.1 together with the properties these actions have.
It was already pointed out in the previous chapter that staggered fermions break flavour symmetry at order $\mathcal{O}(a^3)$. In section 2.3.5 it will be shown that this problem can be reduced by introducing

a so-called fat-link [33] , the sum of a link and the corresponding staple, into the fermionic action. This chapter is completed by an analysis of the computational cost of simulation with improved staggered actions and a discussion of full QCD actions suitable for QCD thermodynamics.

2.1 Improvement of the gluonic sector of QCD

2.1.1 Symanzik improved actions

For the Wilson gauge action one finds cut-off effects which start at $\mathcal{O}(a^2)$ as pointed out in the previous chapter. Since it is not the only possible discretization of the continuum SU(3) gauge action one can add other operators than the plaquette to the lattice action and tune the coefficients such that it reproduces the correct continuum limit, but also removes the deviations from the continuum action at a certain order of $g^n a^{2k}$. This procedure of improving the action order by order in the perturbative expansion was suggested by Symanzik [29] in 1983 for the ϕ^4 theory.
In SU(3) lattice gauge theory Weisz and Wohlert [34] used an ansatz for the action taking into account all operators of length 4 and 6 to construct an action which is free of $\mathcal{O}(a^2)$ corrections in tree-level and one loop order.

$$
\begin{aligned}
S^{\mathrm{imp}}_{\mathrm{gluon}} \;=\; \beta \Bigg[& \; c_0(g^2) \sum_{x,\mu<\nu} \Big(1 - \frac{1}{N}\mathrm{ReTr} \quad (x)\Big) \\
& + \; c_1(g^2) \sum_{x,\mu<\nu} \Big(1 - \frac{1}{N}\mathrm{ReTr} \quad (x)\Big) \\
& + \; c_2(g^2) \sum_{x,\mu<\nu<\rho} \Big(1 - \frac{1}{N}\mathrm{ReTr} \quad (x)\Big) \\
& + \; c_3(g^2) \sum_{x,\mu<\nu<\rho} \Big(1 - \frac{1}{N}\mathrm{ReTr} \quad (x)\Big) \Bigg]
\end{aligned}
\tag{2.1}
$$

where the coefficients c_i are of the from $c_i(g^2) = g^0 c_i^{(0)} + g^2 c_i^{(2)} + \mathcal{O}(g^4)$ with the normalization relation $c_0(g^2) + 4c_1(g^2) + 2c_2(g^2) + 4/3c_3(g^2) = 1$. The graphical representation of the loops stands for all loops of that shape which are based at the point x and have the first link pointing to the positive μ direction. These operators span a basis of dimension 6 operators and are therefore suitable to construct an $\mathcal{O}(g^n a^2)$ improved action.
At tree-level it is sufficient to regard the expansion of the action and to choose the coefficients such that the corrections in $\mathcal{O}(g^0 a^2)$ are removed. The unique solution is

$$
c_0^{(0)} = 5/3 \quad c_1^{(0)} = -1/6 \quad c_2^{(0)} = c_3^{(0)} = 0 \quad c_i^{(k)}(g^2) = 0, \quad k = 2, 4, \ldots \; . \tag{2.2}
$$

In one-loop order one has to take into account the expansion of physical or on-shell quantities in order to avoid to impose unphysical conditions on the coefficients $c_i(g^2)$. Lüscher and Weisz [35] used a meson mass and a scattering amplitude to numerically fix the coefficients up to order $\mathcal{O}(g^2 a^2)$. In principle this procedure could be followed up to every order $g^n a^2$ if the expansion of

these quantities was known to n-th order. The tree-level coefficients remain unchanged, in one-loop they are

$$c_0^{(2)} = 0.2370 \quad c_1^{(2)} = -0.05042 \quad c_2^{(2)} = -0.01764 \quad c_3^{(2)} = 0 \quad c_i^{(k)}(g^2) = 0, \quad k = 4, 6, \ldots \quad . \tag{2.3}$$

Additionally to this perturbative improvement the link variables in the action can be redefined in order to make them more continuum-like. Lepage and MacKenzie [30] suggested the replacement $U_\mu(x) \rightarrow U_\mu(x)/\langle U \rangle$ at every point of the lattice, where $\langle U \rangle$ is the gauge link expectation value. In tree-level the link variable remains unchanged but one expects that higher order corrections to the continuum action are reduced by this redefinition. $\langle U \rangle$ is not a gauge invariant quantity and has to be calculated in a fixed gauge. Therefore in practice the fourth root of the plaquette is used as an approximation to the expectation value of the link variable.
In this work results with the so-called tree-level and tadpole improved 1×2 gluon actions are discussed, which only contain the plaquette and the 1×2 loop.

$$S^{1\times 2}_{\text{gluon}} = \beta \sum_{x,\nu>\mu} \left(\frac{5}{3}\frac{1}{N}\text{ReTr} \right.$$

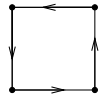

$$(x)$$

$$- \frac{1}{12u_0^2}\frac{1}{N}\text{ReTr} \left(\right.$$

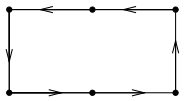

$$(x) +$$

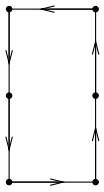

$$\left. (x) \right) \Bigg) \quad , \tag{2.4}$$

where $u_0 = 1$ for the tree-level action and $u_0 = \langle U_{\text{plaq}} \rangle^{1/4}$ for the tadpole improved action.

2.1.2 Renormalisation group improved actions

A different strategy of improving an action can be derived from renormalisation group theory. Applying block transformations to a lattice action induces many additional interactions in the effective action. If this blocking is repeated a renormalisation group flow in the infinite dimensional coupling space of effective actions is defined. All actions which lie in the scaling region are expected to approach the renormalised trajectory after sufficiently many blocking steps. The renormalised trajectory is thought of as a RG flow which starts from an infra-red fixed point S_{FP} in the critical surface. This fixed point S_{FP} defines the continuum limit of the theory. All actions on the renormalised trajectory are connected to the continuum by infinitely many renormalisation group transformations and therefore show continuum properties. They are referred to as perfect actions.
Since infinitely many operators cannot be handled in lattice simulations Hasenfratz and Niedermayer [31] proposed to use an approximation to the classical perfect action S_{FP}. At weak coupling an integral equation can be found for S_{FP} which can be solved numerically with a proper finite-dimensional ansatz for the effective action. One type of approximate classically perfect fixed point actions is FPIII which will be discussed in the following section.
In an alternative approach, first followed by Iwasaki [36], the number of operators has been restricted to two, the plaquette and the 1×2 loop. The general procedure is to choose a set of parameters that minimizes the distance to the renormalized trajectory after a few blocking transformations. In Iwasaki's so-called RG action the coefficients are fixed to

$$c_0^{(0)} = 1 - 8c_1^{(0)} \quad c_1^{(0)} = -0.331 \quad , \tag{2.5}$$

in order to achieve a minimal distance to the RG trajectory after one block transformation. This action has been widely used in finite temperature simulation in pure SU(3) gauge theory as well as in full QCD.
A member of the QCD Taro group proposed to work in the same two-dimensional coupling space but to start blocking from the Wilson action [37]. After two block-spin transformations the coefficients are

$$c_0^{(0)} = 1 - 8c_1^{(0)} \quad c_1^{(0)} = -1.4088 \quad . \tag{2.6}$$

This action is referred to as DBW2 action (Double blocked from Wilson action in two coupling space).

2.2 Numerical results in pure gauge theory using improved actions

2.2.1 The critical temperature $T_c/\sqrt{\sigma}$ and the pressure p/T^4

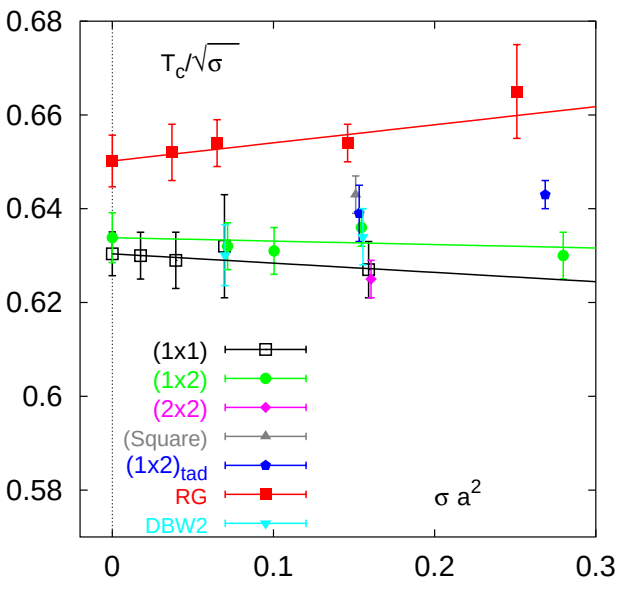

Figure 2.1: The critical temperature $T_c/\sqrt{\sigma}$ as function of the lattice spacing σa^2. For the Wilson action the critical couplings are taken from Boyd et al. *[38], the string tension from Edwards* et al. *[39], for the tree-level and tadpole improved 1×2 and 2×2 action critical couplings and string tension values are from Cella* et al. *[40] and Beinlich* et al. *[41]. The results for the square action can be found in [42], for the DBW2 action in [43] and for the RG action in Okamoto* et al. *[44].*

In this section the cut-off effects in SU(3) thermodynamics will be discussed. One has to distinguish between infrared and ultraviolet dominated quantities. The critical temperature $T_c/\sqrt{\sigma}$ e.g. belongs to the first category since the string tension σ is extracted from the long-range behaviour of the potential and is therefore not sensitive to high momenta but only to the finite size of the volume. This is different for the equation of state. The energy density ϵ for an ideal gluon gas is $(N_c^2-1)\pi^2/45\, T^4$ where the temperature is related to the average momentum by $\bar{p} \propto 3T \propto 3/N_\tau a$. Therefore the equation of state is sensitive to a momentum cut-off induced by a finite lattice spacing. Simulations performed over the past years reflect these considerations. For the transition temperature the cut-off dependence is about 3%. In figure 2.1 all available measurements from pure gauge theory are collected. It is obvious that for all actions the results only slightly change when varying the lattice spacing. The difference between the RG action and all other results is probably due to a systematic difference in the analysis of the heavy quark potential. The value for the critical temperature in the continuum limit has been determined by extrapolating various results at finite lattice spacing to $a = 0$ using a quadratic ansatz in a. For the standard, the tree-level 1×2 and the

RG action the results are $T_c/\sqrt{\sigma}$=0.630(5), 0.634(4) and 0.650(5), respectively.
The situation is completely different for the equation of state (figure 2.2). Here the unimproved Wilson action at $N_\tau = 4$ has cut-off corrections of about 25% to the continuum extrapolated pressure. For the tree-level and tadpole improved 1×2 action and the fixed point action FPIII the situation is much improved. The difference to the continuum curve is already quite small for $N_\tau = 3$ and a reliable extrapolation to the continuum limit can be performed using simulations with $N_\tau = 3$ and 4. This is shown in figure 2.3. The continuum results for the Wilson and 1×2 improved tree-level and tadpole actions agree within errors. Thus in pure gauge theory different discretisation schemes lead to the same continuum limit. In figures 2.2 and 2.3 also the results for the RG action are presented. Although it is designed to give an improvement at intermediate couplings, the pressure at $N_\tau = 4$ shows quite drastic cut-off distortions. For this reason the continuum extrapolation based on $N_\tau = 4$ and 8 lattices gives a slightly different result than the other actions. This effect should vanish when using $N_\tau = 6$ as smallest temporal extension in the extrapolation. The same effect can be observed for the continuum extrapolation of the pressure with the Wilson action.

2.2.2 The high temperature limit

To get an idea why the standard and RG improved action show these strong cut-off effects and the Symanzik improved actions do not, a calculation of the high temperature ideal gas limit of the free energy/pressure for the different actions is quite helpful. This can be done by using the equation $p = -f = 1/V \ln Z$, which can be calculated order by order, $p = -f = -f^{(0)} - g^2 f^{(2)} + \mathcal{O}(g^4)$. The numerical evaluation of the lowest order contribution gives the results plotted in figure 2.4 after normalization with the continuum ideal gas value p_{SB}/T^4.

$$\begin{aligned}
\frac{p_G^{(0)}(N_\tau)}{T^4} &= \frac{-f_G^{(0)}(N_\tau)}{T^4} \\
&= N_\tau^4 \, \frac{1}{(2\pi)^3} \int_0^{2\pi} \mathrm{d}^3\vec{p} \Big[N_\tau^{-1} \sum_{n_0=0}^{N_\tau - 1} \ln \left(\Delta_{FP}^{-1} \left((\vec{p}, (2\pi/N_\tau)\, n_0) \, \mathrm{Det}[\Delta_G^{-1}(\vec{p}, (2\pi/N_\tau)\, n_0)] \right) \right] \\
&\quad - N_\tau^4 \, \frac{1}{(2\pi)^4} \int_0^{2\pi} \mathrm{d}^4 p \Big[\ln \left(\Delta_{FP}^{-1}(p) \mathrm{Det}[\Delta_G^{-1}(p)] \right) \Big] \quad , \qquad (2.7)
\end{aligned}$$

where an infinite spatial volume is chosen, $N_\sigma^3 = \infty$, and the zero temperature contributions are subtracted corresponding to $N_\tau = \infty$. The $n_0 = 0, 1, .. (N_\tau - 1)$ label the discrete Matsubara modes $2\pi \; n_o/N_\tau$ in the temporal direction. $\Delta_{FP}(p)$ is the Fadeev Popov determinant and $\Delta_G^{-1}(p)$ is the inverse free gluon propagator which has been calculated for the different gluon actions in [45].
The Stefan Boltzmann value for the pressure is given by

$$\frac{p_{SB}}{T^4} = (N_c^2 - 1) \, \frac{\pi^2}{15} \quad . \qquad (2.8)$$

Obviously the high-temperature ideal gas behaviour is quite different for the different actions. The corrections are quite small for the 1×2 tree-level improved action already at $N_\tau = 4$ whereas they are large for the Wilson and RG actions. A similar pattern can be found for the pressure in a simulation for a temperature regime of $T \gtrsim 2T_c$. The corresponding actions are plotted in figure 2.5. Thus in pure gauge theory the ideal gas free energy of different actions gives a good indication how well suited an action will be for thermodynamic calculations. One should note that the strong cut-off effects for the free energy in the ideal gas limit are not that pronounced in the simulation. For the Wilson action the 50% effect in the ideal gas limit is reduced to about 25% in a simulation at $N_\tau = 4$, for the RG action a 75% effect is reduced by a factor of 3.

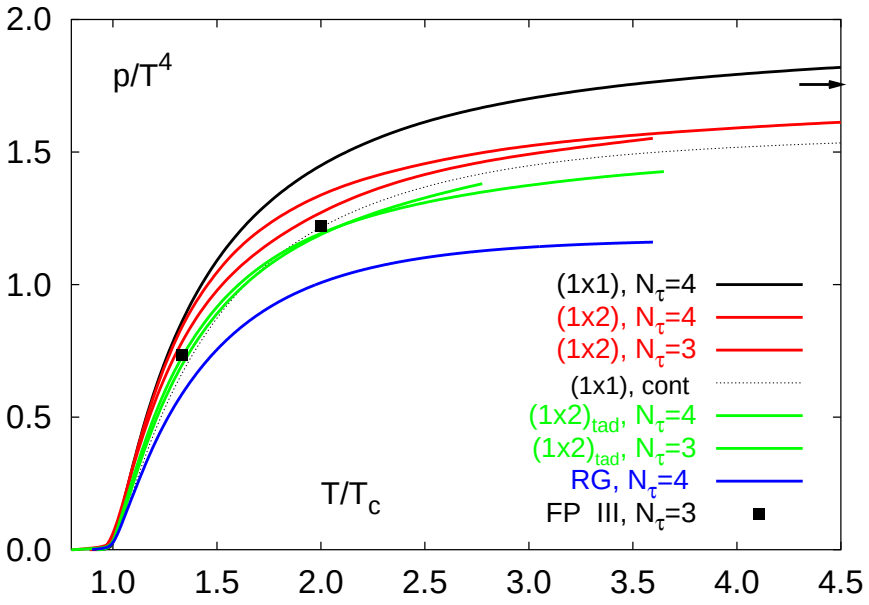

Figure 2.2: The pressure p/T^4 as a function of temperature for different N_τ. Boyd et al. *[38] computed the Wilson action and the continuum extrapolation from their $N_\tau = 6$ and 8 results. The curves for the tree-level and tadpole improved 1×2 action are from Beinlich* et al. *[41]. Okamoto* et al. *[44] calculated the pressure with the RG action, Papa [46] used the fixed point action (FP III).*

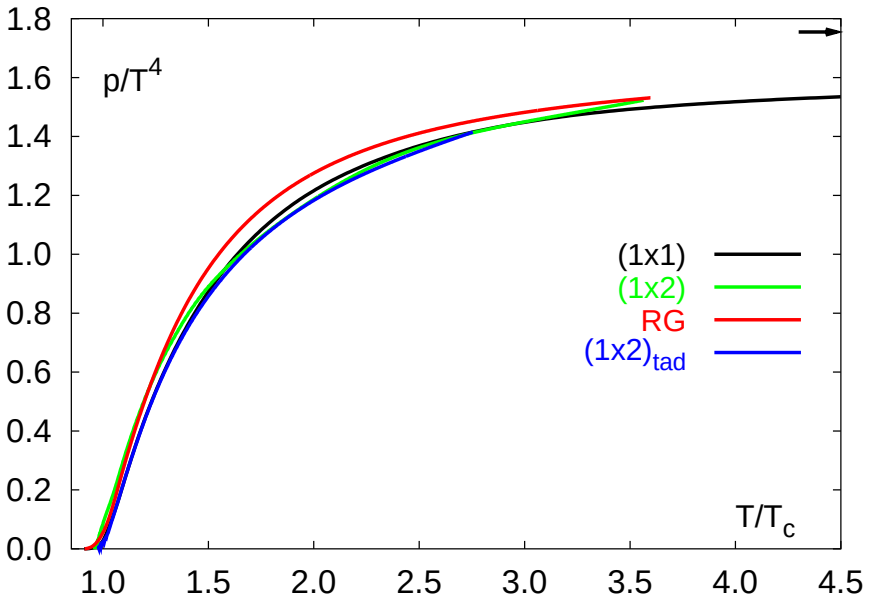

Figure 2.3: Continuum extrapolation of the pressure for the Wilson action ($N_\tau = 6$ and 8), the 1×2 tree-level and tadpole improved action ($N_\tau = 3$ and 4) and the RG action ($N_\tau = 4$ and 8). References are the same as in figure 2.2.

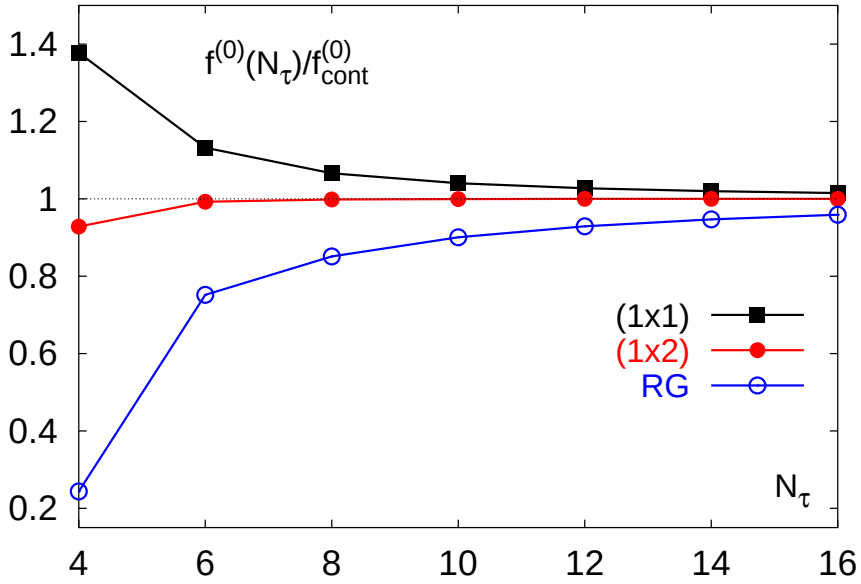

Figure 2.4: The high-temperature ideal gas limit of the free energy normalized to the continuum value for different N_τ and actions.

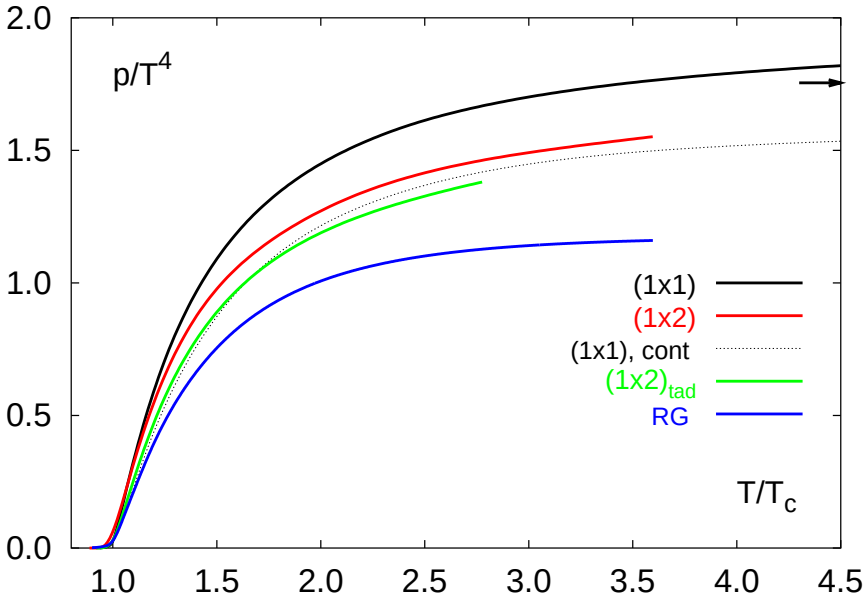

Figure 2.5: The pressure p/T^4 as a function of temperature for $N_\tau = 4$. Results are given for the Wilson action, the tree-level and tadpole improved 1×2 action and the RG action. For references see 2.2.

Even close to the critical temperature the high-temperature limit of the free energy seems to be a good criterion to estimate the cut-off effects at a certain N_τ. Calculations of the surface tension and latent heat using the 1×2 tree level and tadpole improved actions [47] lead to results which have a much reduced cut-off dependence compared to the same quantities calculated with the standard Wilson action [48, 49].

2.2.3 Rotational symmetry in the heavy quark potential

At finite lattice spacing one observes the breaking of rotational symmetry in the heavy quark potential. The potential at distance R measured along the coordinate axis and along off-axis directions does not agree due to distortions of rotational symmetry. This behaviour can be utilized to define a measure for the strength of rotational symmetry breaking. The potential $V(R)$ is fitted to the ansatz $V(R) = V_0 + \sigma\ R + \alpha/R$ where only on-axis points are taken into account in the fit. The following definition of δ_V^2 then measures the relative mean square deviation of the potential values for off-axis directions from the fit [43].

$$\delta_V^2 = \sum_{\text{off}} \frac{\left(V_{\text{fit}}(R) - V_{\text{off}}(R)\right)^2}{V_{\text{fit}}^2(R)\delta^2 V_{\text{off}}(R)} \left(\sum_{\text{off}} \frac{1}{\delta^2 V_{\text{off}}(R)} \right)^{-1} \quad , \tag{2.9}$$

where $V_{\text{fit}}(R)$ denotes the heavy quark potential fitted to only on-axis data and $V_{\text{off}}(R)$ are the off-axis data.
The potential has been determined from the ratio of smeared Wilson loops. Different from what one usually does when calculating the string tension from the long-distance behaviour of the potential also the short distance part of the potential is taken into account in the fit. In figure 2.6 the results for δ_V^2 using the 1×1, the 1×2 tree level and tadpole actions are plotted. As expected the breaking of rotational symmetry gets stronger with increasing lattice spacing. Additionally the improved actions show much smaller distortions than the standard 1×1 action. As for the pressure and other thermodynamic quantities like the latent heat and the surface tension the tadpole action is slightly superior to the tree-level action. In [43] the rotational symmetry violations at lattice spacings larger than $\approx$ 0.2fm ($a\sqrt{\sigma} \gtrsim 0.4$) have been investigated also for the renormalisation group improved actions, RG and DBW2. One finds an even larger improvement of rotational invariance than for the Symanzik 1×2 improved actions.

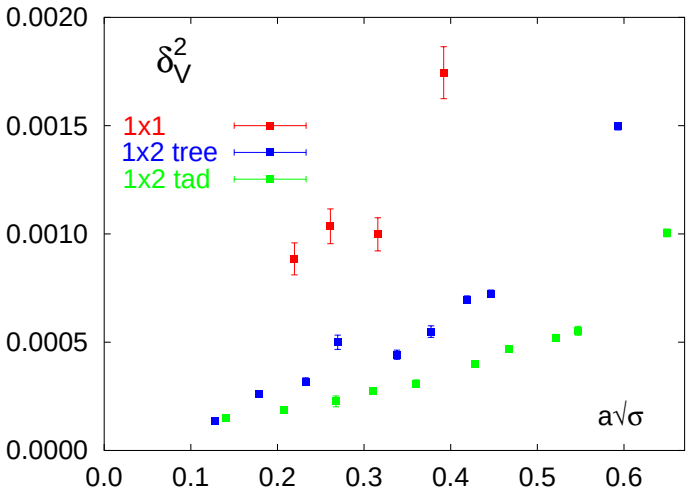

Figure 2.6: Rotational symmetry violations for the 1×1, the 1×2 tree level and tadpole improved actions.

2.3 Improvement of the fermionic sector of QCD

In full QCD thermodynamic calculations very strong cut-off effects for the equation of state with the standard staggered fermion action have been observed when comparing results from temporal lattices of size $N_\tau = 4$ [50] and $N_\tau = 6$ [28]. The effect is even larger than in the pure gauge sector. Therefore the use of improved actions is mandatory in the fermionic sector.
In general infinitely many operators can be added to the one-link derivative of the standard staggered fermion action to take into account higher orders in the discretisation of the derivative. An ansatz for the free staggered fermionic action with bilinear operators has the following form

$$
\begin{aligned}
S_F \;=\; & m \sum_x \bar{\chi}(x)\chi(x) \;+\; \sum_x \bar{\chi}(x) \\
& + \sum_\mu \eta_\mu(x) \sum_{i=1,3,5,\ldots} \Bigg[c_{i,0,0,0} \;[\, \chi(x+i\hat{\mu}) - \chi(x-i\hat{\mu}) \,] \\
& + \sum_{\nu\neq\mu} \sum_{j=0,2,4,\ldots} \Bigg[c_{i,j,0,0} \Big\{ [\, \chi(x+i\hat{\mu}+j\hat{\nu}) - \chi(x-i\hat{\mu}-j\hat{\nu}) \,] \\
& \qquad + [\, \chi(x+i\hat{\mu}-j\hat{\nu}) - \chi(x-i\hat{\mu}+j\hat{\nu}) \,] \Big\} \\
& + \sum_{\rho\neq\mu,\nu} \sum_{k=0,2,4,\ldots} \Bigg[c_{i,j,k,0} \Big\{ [\, \chi(x+i\hat{\mu}+j\hat{\nu}+k\hat{\rho}) - \chi(x-i\hat{\mu}-j\hat{\nu}-k\hat{\rho}) \,] \\
& \qquad + [\, \chi(x+i\hat{\mu}-j\hat{\nu}+k\hat{\rho}) - \chi(x-i\hat{\mu}+j\hat{\nu}-k\hat{\rho}) \,] \\
& \qquad + [\, \chi(x+i\hat{\mu}+j\hat{\nu}-k\hat{\rho}) - \chi(x-i\hat{\mu}-j\hat{\nu}+k\hat{\rho}) \,] \\
& \qquad + [\, \chi(x+i\hat{\mu}-j\hat{\nu}-k\hat{\rho}) - \chi(x-i\hat{\mu}+j\hat{\nu}+k\hat{\rho}) \,] \Big\} \\
& + \sum_{\sigma\neq\mu,\nu,\rho} \sum_{l=0,2,4,\ldots} c_{i,j,k,l} \Big\{ [\, \chi(x+i\hat{\mu}+j\hat{\nu}+k\hat{\rho}+l\hat{\sigma}) - \chi(x-i\hat{\mu}-j\hat{\nu}-k\hat{\rho}-l\hat{\sigma}) \,] \\
& \qquad + [\, \chi(x+i\hat{\mu}+j\hat{\nu}+k\hat{\rho}-l\hat{\sigma}) - \chi(x-i\hat{\mu}-j\hat{\nu}-k\hat{\rho}+l\hat{\sigma}) \,] \\
& \qquad + [\, \chi(x+i\hat{\mu}+j\hat{\nu}-k\hat{\rho}+l\hat{\sigma}) - \chi(x-i\hat{\mu}-j\hat{\nu}+k\hat{\rho}-l\hat{\sigma}) \,] \\
& \qquad + [\, \chi(x+i\hat{\mu}+j\hat{\nu}-k\hat{\rho}-l\hat{\sigma}) - \chi(x-i\hat{\mu}-j\hat{\nu}+k\hat{\rho}+l\hat{\sigma}) \,] \\
& \qquad + [\, \chi(x+i\hat{\mu}-j\hat{\nu}+k\hat{\rho}+l\hat{\sigma}) - \chi(x-i\hat{\mu}+j\hat{\nu}-k\hat{\rho}-l\hat{\sigma}) \,] \\
& \qquad + [\, \chi(x+i\hat{\mu}-j\hat{\nu}+k\hat{\rho}-l\hat{\sigma}) - \chi(x-i\hat{\mu}+j\hat{\nu}-k\hat{\rho}+l\hat{\sigma}) \,] \\
& \qquad + [\, \chi(x+i\hat{\mu}-j\hat{\nu}-k\hat{\rho}+l\hat{\sigma}) - \chi(x-i\hat{\mu}+j\hat{\nu}+k\hat{\rho}-l\hat{\sigma}) \,] \\
& \qquad + [\, \chi(x+i\hat{\mu}-j\hat{\nu}-k\hat{\rho}-l\hat{\sigma}) - \chi(x-i\hat{\mu}+j\hat{\nu}+k\hat{\rho}+l\hat{\sigma}) \,] \Big\} \Bigg] \Bigg] \Bigg] \Bigg] \,,
\end{aligned}
\tag{2.10}
$$

where the coefficients $c_{i,j,k,l}$ have to fulfill the following normalisation condition

$$
\begin{aligned}
1/2 \;=\; & \sum_{i=1,3,5,\ldots} \Bigg[i\, c_{i,0,0,0} \sum_{j=0,2,4,\ldots} \Bigg[2(i+j)\, c_{i,j,0,0} \\
& \sum_{k=0,2,4,\ldots} \Bigg[4(i+j+k)\, c_{i,j,k,0} \sum_{l=0,2,4,\ldots} 8(i+j+k+l)\, c_{i,j,k,l} \Bigg] \Bigg] \Bigg] \quad .
\end{aligned}
\tag{2.11}
$$

This ansatz respects the hyper-cubic structure of staggered fermions necessary to reproduce the correct continuum action.

Different strategies have been followed over the last years how to choose the operators of the improved action and how to fix the coefficients. One approach is based on renormalisation group concepts. The latest version of so-called perfect staggered fermions have been proposed by Bietenholz *et al.* [51]. They constructed a truncated perfect action (TP) which is relatively local compared to earlier attempts with a classical fixed point action [52]. In total the action consists of eight operators with a path length up to three in μ direction and up to two in all other directions, i.e. the coefficients $c_{1,0,0,0}$ ... $c_{3,2,2,2}$ are non-zero. The ideal gas free energy density and the free dispersion relation clearly show a drastic improvement over the standard staggered action [53]. Unfortunately there are still too many non-local operators involved such that this action is not suitable for a full QCD simulation at the present stage of computer resources.
The same is even more true for an on-shell $\mathcal{O}(a^2)$ improved staggered fermion action which has been studied by Luo in 1998 [54]. After elimination of all irrelevant operators one is still left with three bilinear and ten 4-Fermi operators for which it is not even clear how to incorporate them in a simulation. Thus on-shell improvement in the fermionic sector is possible only in tree-level where the linear one-link and three-link operator is sufficient. The coefficients are $c_{1,0,0,0} = 9/16$ and $c_{3,0,0,0} = -1/48$. This action has been proposed by Naik [55] already in 1989 to remove the $\mathcal{O}(a^2)$ corrections and is called Naik action after him. Thermodynamic simulations in 4 flavour QCD [56] showed that the cut-off effects indeed are substantially reduced with the Naik action as will be discussed in the next chapter.

2.3.1 Improvement of rotational symmetry

Another strategy to improve the staggered fermion action has been proposed by Heller *et al.* [32]. They constructed staggered fermion actions with improved rotational symmetry. In general one can take into account any link which fulfills the staggered criteria to reproduce the continuum action. To keep the action as local as possible Heller *et al.* restricted themselves to 1-link and all possible 3-link paths. The ansatz for the fermion matrix M then reads

$$M[U]_{ij} = m\,\delta_{ij} + \eta_i \cdot \Big(c_{1,0,0,0}\; A[U]_{ij} + c_{3,0,0,0}\; B_1[U]_{ij} + c_{1,2,0,0}\; B_2[U]_{ij} \Big)$$

$A[U]_{ij} =$ 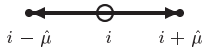

$B_1[U]_{ij} =$ 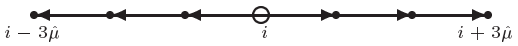

$B_2[U]_{ij} =$ 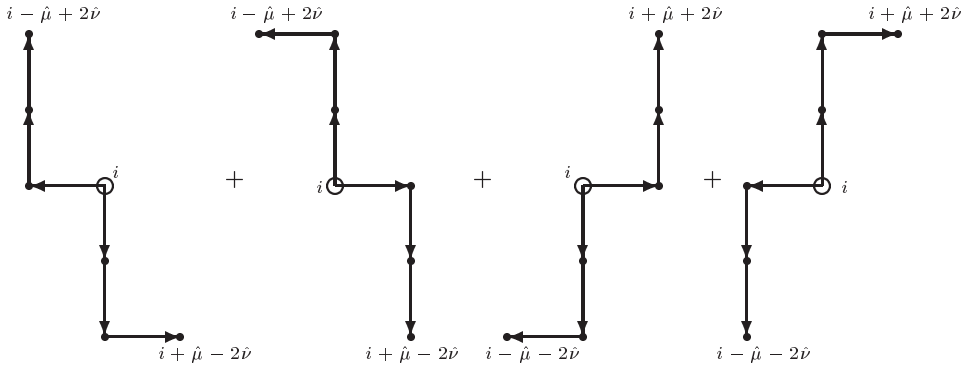

where the tree-level coefficients are fixed by demanding that the correct naive continuum limit is reproduced and that the free fermion propagator* is rotationally invariant up to $\mathcal{O}(p^4)$. The

*The improvement of rotational symmetry has also been calculated to one-loop order by demanding the rotational invariance of the fermion propagator up to $\mathcal{O}(g^2)$ [32].

resulting relations are

$$\begin{aligned} c_{1,0,0,0} + 3\, c_{3,0,0,0} + 6\, c_{1,2,0,0} &= 1/2 \\ c_{1,0,0,0} + 27\, c_{3,0,0,0} + 6\, c_{1,2,0,0} &= 24\, c_{1,2} \end{aligned}$$

A further simplification can be obtained by setting either of the coefficients $c_{1,2,0,0}$ and $c_{3,0,0,0}$ to zero. Choosing $c_{1,2,0,0} = 0$ leads to the Naik action,

$$c_{1,0,0,0} = 9/16 \qquad c_{3,0,0,0} = -1/48 \quad .$$

By setting $c_{3,0,0,0} = 0$ one obtains the so-called p4 action,

$$c_{1,0,0,0} = 3/8 \qquad c_{1,2,0,0} = 1/48 \quad .$$

A more complicated ansatz which compares in complexity to the truncated perfect action (TP) of Bietenholz *et al.* [51] can be used to obtain rotational symmetry of the free fermion propagator up to $\mathcal{O}(p^6)$. It takes into account up to 7-link paths of Euclidean length up to $\sqrt{13}$. A minimal number of operators is realized in the p6m action, in the p6 action two free coefficients can be used for tuning the action. The coefficients together with the ones of the truncated perfect action are collected in table 2.1. Obviously the coefficients of the rotational invariant actions are similar to those of the truncated perfect action.

(i,j,k,l)	$c_{i,j,k,l}$		
	p6m	p6	TP [51]
(1,0,0,0)	0.3375	0.32	0.348194
(1,2,0,0)	0.01875	0.02	0.020490
(1,2,2,0)	0.0023438	0.0010938	0.002240
(3,0,0,0)	0.0072917	0.0047917	0.007609
(1,2,2,2)		0.00125	0.000247
(3,2,0,0)		0.00125	-0.000216
(3,2,0,0)			-0.000384
(3,2,2,2)			-0.000214

Table 2.1: Coefficients for $\mathcal{O}(p^6)$ rotational invariant actions and the truncated perfect point action.

The properties of these actions can be analyzed by calculating the high temperature ideal gas value for the free energy and the dispersion relation for free fermions in lattice perturbation theory or by determining the distortions of rotational symmetry from the heavy quark potential in lattice simulations.

2.3.2 The high-temperature limit

In the pure gauge sector the ideal gas limit of the free energy density is a good indicator of the cut-off effects of thermodynamic quantities in simulations at a certain N_τ. This experience will be used as a guideline to judge the quality of different full QCD actions. The free energy density $f = -T/V \ \ln Z = f_G + f_F$ can be decomposed into an fermionic and gluonic part up to next-to-leading order. Thus the results for the high-temperature limit of the free energy density of the pure gauge sector discussed in the previous section are still valid.
The continuum ideal gas value for the free energy density for n_f massless quark flavour and the colour group $SU(N_c)$ up to $\mathcal{O}(g^2)$ is given by

$$\begin{aligned} \frac{f_{\mathrm{cont},F}}{T^4} = \frac{-p_{\mathrm{cont},F}}{T^4} = \frac{-\epsilon_{\mathrm{cont},F}}{3T^4} &= f^{(0)}_{\mathrm{cont},F}/T^4 + g^2 f^{(2)}_{\mathrm{cont},F}/T^4 + \mathcal{O}(g^3) \\ &= -n_f \frac{7}{180}\pi^2 N_c + g^2 n_f \frac{5}{576}\left(N_c^2 - 1\right) + \mathcal{O}(g^3) \quad (2.12) \end{aligned}$$

In lattice perturbation theory the corresponding contributions can also be calculated order by order using the standard thermodynamic relations, i.e. $p/T = V^{-1} \ln Z$ and $\epsilon = -V^{-1} \partial \ln Z / \partial(1/T)$,

$$p_F = p_F^{(0)} + g^2 p_F^{(2)} + \mathcal{O}(g^3) \tag{2.13}$$

$$\epsilon_F = \epsilon_F^{(0)} + g^2 \epsilon_F^{(2)} + \mathcal{O}(g^3) \tag{2.14}$$

The resulting integrals which have to be evaluated numerically are given in lowest order for a free massless fermion gas,

$$\frac{p_F^{(0)}(N_\tau)}{T^4} = \frac{3}{8} n_f N_\tau^4 \frac{1}{(2\pi)^3} \int_0^{2\pi} \mathrm{d}^3\vec{p} \left[N_\tau^{-1} \sum_{n_0=0}^{N_\tau - 1} \ln\left(\omega^2(\vec{p}) + 4f^2((2n_0+1)\pi/N_\tau)\right) - \frac{1}{(2\pi)} \int_0^{2\pi} \mathrm{d}p_0 \ \ln\left(\omega^2(\vec{p}) + 4f^2(p_0)\right) \right] , \tag{2.15}$$

$$\frac{\epsilon_F^{(0)}(N_\tau)}{T^4} = 3 n_f N_\tau^4 \frac{1}{(2\pi)^3} \int_0^{2\pi} \mathrm{d}^3\vec{p} \left[N_\tau^{-1} \sum_{n_0=0}^{N_\tau - 1} \frac{f^2((2n_0+1)\pi/N_\tau)}{\omega^2(\vec{p}) + 4f^2((2n_0+1)\pi/N_\tau)} - \frac{1}{(2\pi)} \int_0^{2\pi} \mathrm{d}p_0 \ \frac{f^2(p_0)}{\omega^2(\vec{p}) + 4f^2(p_0)} \right] , \tag{2.16}$$

where the zero temperature contributions to p_F/T^4 and ϵ_F/T^4 have been subtracted. The function $\omega^2(\vec{p}) \equiv 4 \sum_{\mu=1}^{3} f^2(p_\mu)$ is introduced and the discrete Matsubara modes $(2n_0+1)\pi/N_\tau$ in the temporal direction are labelled by $n_0 = 0,\ 1, \ldots,\ (N_\tau - 1)$. In the case of the standard, Naik and p4 action, respectively, the momentum dependent terms of the free propagator are given by,

$$f(p_\mu) = \frac{1}{2} \sin(p_\mu) \quad \text{(standard staggered action)} \tag{2.17}$$

$$f(p_\mu) = \frac{9}{16} \sin(p_\mu) - \frac{1}{48} \sin(3p_\mu) \quad \text{(Naik action)} \tag{2.18}$$

$$f(p_\mu) = \frac{3}{8} \sin(p_\mu) + \frac{1}{48} \ 2 \ \sin(p_\mu) \sum_{\nu \neq \mu} \cos(2p_\nu) \quad \text{(p4 action)}. \tag{2.19}$$

In [32] Heller *et al.* calculated the fermionic tree-level and one-loop contributions to the free energy density for the improved actions. Their tree-level results for the standard staggered, Naik and p4 action are plotted in figure 2.7.
The standard staggered action shows strong deviations from the ideal gas limit of $\mathcal{O}(1/N_\tau^2)$ up to quite large N_τ. The contributions at $N_\tau = 4$ deviate from the continuum by more than 100%, at $N_\tau = 8$ they are still larger than 40%. The situation is much improved for the p4 and Naik action, where $\mathcal{O}(1/N_\tau^2)$ deviations are substantially suppressed or eliminated, respectively. They show cut-off corrections of 20% for the Naik and 40% for the p4 action at $N_\tau = 4$. At larger N_τ the situation is even more improved. Both actions approach the continuum value much faster than the standard staggered action, for the p4 action the cut-off effects are only 5% already for $N_\tau = 6$. The more complex actions, p6 and TP, show cut-off distortions for $N_\tau = 4$ of only 13% and 18%, respectively. At larger N_τ the deviation is smaller than 1%. But, as already pointed out, for a full QCD simulation with computer resources available now both actions are too expensive.
The quantity $(\epsilon^{(0)} - 3p^{(0)})/T^4$, which is zero for an ideal gas, is plotted in figure 2.8. Thus deviations from zero indicate the violation of this basic thermodynamic identities due to finite cut-off effects.

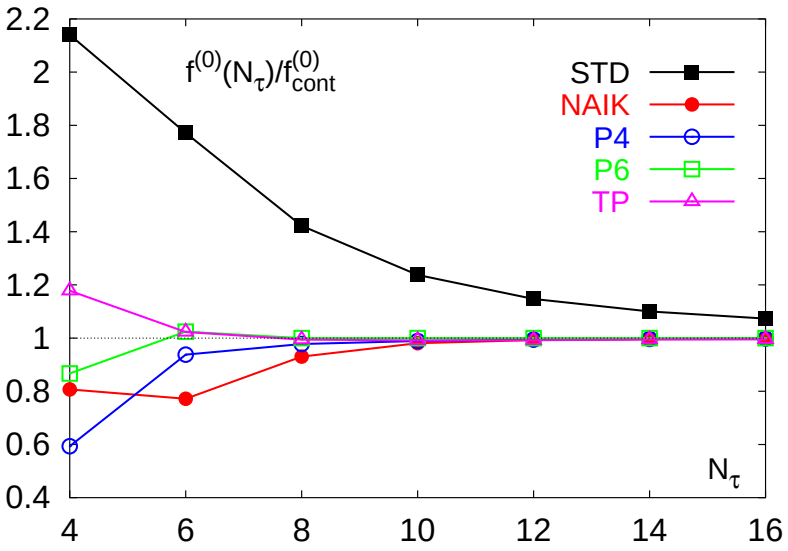

Figure 2.7: Tree-level contribution to the free energy density normalized by the corresponding Stefan-Boltzmann value as a function of N_τ for different fermion actions. The p6 and TP action values are taken from [51].

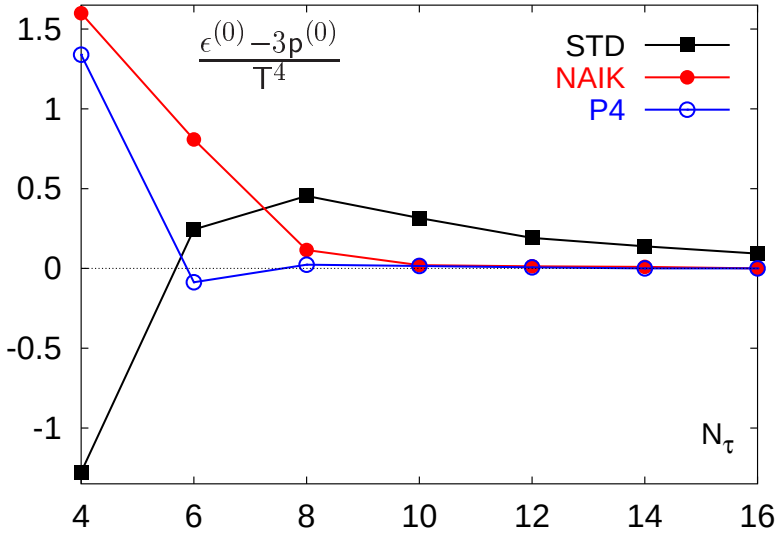

Figure 2.8: Tree-level contribution to $(\epsilon - 3p)/T^4$ as a function of N_τ for different fermion actions.

The approach to zero is very slow for the standard action. As in the case of the free energy the p4 action converges to the continuum already at smaller N_τ than the Naik action.

2.3.3 The dispersion relation

A further indication for the quality of the improvement is the dispersion relation for free massless quarks. The results for the standard, Naik, p4 and p6 action are shown in figure 2.9. In the continuum limit, $a \to 0$, corresponding to small E and p all curves approach the continuum line. Especially the p6 and p4 actions stay quite close to the continuum line for larger momenta.

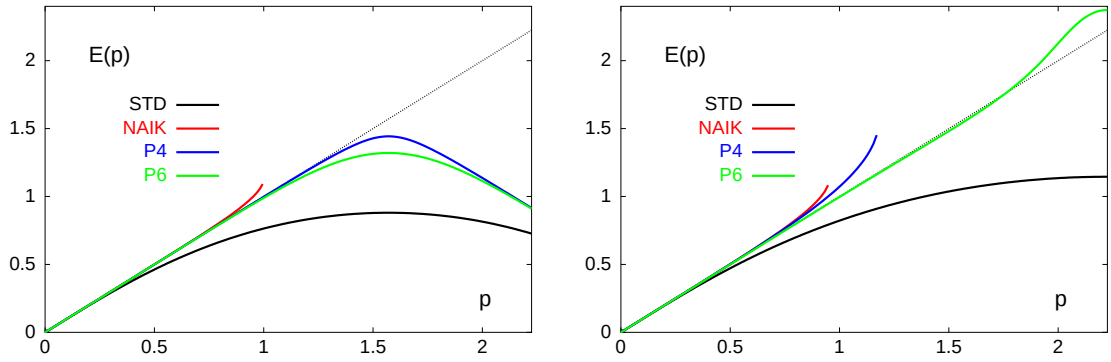

(a) momenta $\vec{p} = (0, 0, p)$

(b) momenta $\vec{p} = (0, p/\sqrt{2}, p/\sqrt{2})$

Figure 2.9: The dispersion relation $E = E(\vec{p})$ for the standard staggered, the Naik, the p4 and the p6 action. The dashed line is the continuum dispersion relation $E = p$.

2.3.4 Rotational symmetry of the heavy quark potential

A final test of the quality of the action is the direct measurement of the breaking of rotational symmetry as it is observed in the heavy quark potential. Also for full QCD the distortions of rotational symmetry are measured in the quantity δ_V^2 as defined by equation 2.9. Three flavour simulations have been performed with the p4 fat[†] action for different bare quark masses $m_q a = 0.10$, 0.20, 0.40 and 0.60 on a lattice of size 16^4. The potential has been determined from the ratio of smeared Wilson loops. To compare the result with a two flavour standard staggered simulation [57] the lattice spacing a has been determined from the string tension and the pseudo-scalar to vector meson mass ratio has been extracted from the corresponding meson correlation functions. In figure 2.10 the results for δ_V^2 are plotted against $(m_{\rm PS}/m_{\rm V})^2$. There are two measurements at the same physical quark mass determined by $(m_{\rm PS}/m_{\rm V})^2$ and the same lattice spacing a. They show that the p4 action reduces the breaking of rotational symmetry in the heavy quark potential substantially, the value of δ_V^2 is smaller by more than a factor of two compared to the standard staggered action.

[†]Fat link improvement will be discussed in the next section. The effect on the rotational symmetry should be small as it is small on the free energy density.

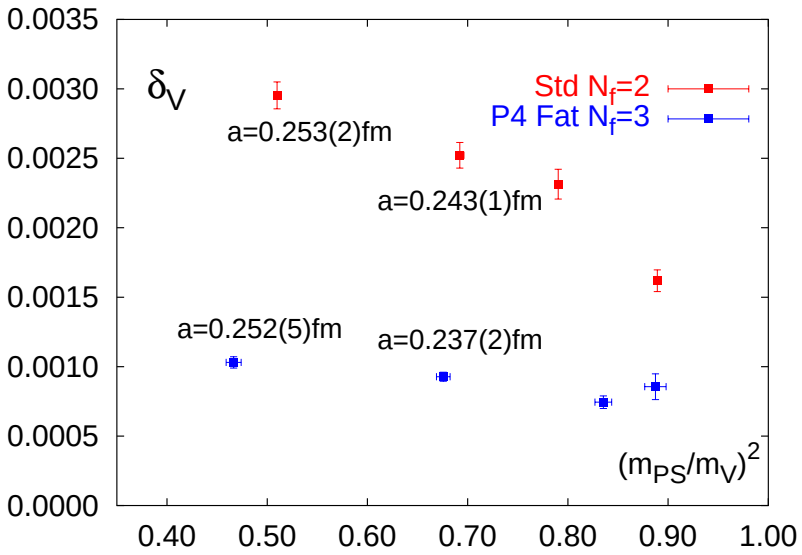

Figure 2.10: The breaking of rotational symmetry in the heavy quark potential measured in the quantity δ_V^2. Comparison of $N_f = 2$ results with the standard staggered action and $N_f = 3$ results for the rotationally improved p4 action.

Finally the success of rotationally improved actions for finite temperature calculations will be discussed in chapter 4. There the reduction of cut-off effects in the pressure will be shown as expected from the discussion of this section.

2.3.5 Improvement of flavour symmetry

From the expansion of the staggered fermion action in chapter 1 it is obvious that the flavour symmetry of the continuum theory is not realized in the staggered formulation. The full chiral symmetry $U(n_f) \otimes U(n_f)$ for n_f quark flavours is reduced to a $U(1)_o \otimes U(1)_e$ symmetry for staggered fermions due to a flavour mixing contribution to the action in $\mathcal{O}(a)$ or $\mathcal{O}(a^3)$, depending on whether unimproved or improved quark fields are used to connect staggered to continuum flavours. Therefore only in the continuum limit the full axial $SU_A(n_f)$ is spontaneously broken which results in 15 massless pseudo-scalar mesons for 4 staggered flavours. At finite lattice spacing a the reduced axial symmetry $U_A(1)$ is realised and only one of the 15 pseudo-scalar mesons becomes massless. This lattice artifact is especially problematic for finite temperature calculations close to the critical temperature. In this temperature regime light pseudo-scalar mesons are expected to contribute to the pressure non-negligible. Thus for finite temperature staggered fermion simulations with small quark masses an improvement of this finite lattice spacing effect is especially desirable. The breaking of flavour symmetry is considered as an effect which is connected to the hypercubic structure of staggered fermions [58]. The different Dirac and flavour components are linear combinations of the staggered fields χ which are connected via gauge fields in the interacting theory. These gauge fields can induce flavour mixing. In momentum space the corresponding picture becomes a gluon which transports sufficient energy to change the flavour content of the fermion it couples to. In the approach of Lagaë and Sinclair [58] the gauge fields are redefined such that for small gauge couplings g the unwanted coupling between gluons and fermions is suppressed. This leads to an improved gauge link that consists of generalized staples which are

quite complicated objects. The simplest choice is the so-called fat-link, which was introduced by MILC [33] already in 1997. It replaces a link U_μ by the sum of this link and the corresponding staple.

$$\begin{aligned} U_{\text{fat}}(x) &= \frac{1}{1+6\omega}\Bigg(U_\mu(x) + \omega \sum_{\nu\neq\mu} U_\nu(x)U_\mu(x+\hat{\nu})U_\nu^\dagger(x+\hat{\mu}) \\ &\qquad + U_\nu^\dagger(x-\hat{\nu})U_\mu(x-\hat{\nu})U_\nu^\dagger(x+\hat{\mu}-\hat{\nu})\Bigg) \end{aligned}$$

$$= \frac{1}{1+6\omega}\Bigg(\longrightarrow + \omega \Bigg) \tag{2.20}$$

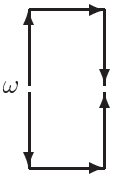

where ω is a weight factor which can be used to tune the action.
The expansion of this fat-link in orders of the lattice spacing is given by

$$\begin{aligned} U_{\text{fat}}(x) &= \mathbb{1} + iga\left[A_\mu(x) + \frac{1}{2}a\partial_\mu A_\mu(x) + \frac{1}{6}a^2\partial_\mu^2 A_\mu(x) + \omega\sum_{\nu\neq\mu} a^2\frac{1}{2}\partial_\nu^2 A_\mu(x) + \mathcal{O}(a^3)\right] \\ &\qquad + \mathcal{O}(a^2g^2) \\ &= U_\mu(x) + \omega\sum_{\nu\neq\mu} iga^3\frac{1}{2}\partial_\nu^2 A_\mu(x) + \mathcal{O}(a^4) + \mathcal{O}(a^2g^2) \end{aligned} \tag{2.21}$$

From this expansion it is clear that in tree level fat-links contribute to the fermion action only at $\mathcal{O}(a^3)$ since they agree with the usual link up to $\mathcal{O}(a^2)$. Since the flavour symmetry breaking is also at most an $\mathcal{O}(a^3)$ effect when the action is expressed in terms of improved fermion fields, it is reasonable to assume that fat-links have an effect on the flavour symmetry. In addition it has been shown by Luo [10] that the fat-link belongs to the set of non-redundant operators which are necessary to construct an $\mathcal{O}(a^2)$ on-shell improved action. This might also be interpreted as an indication that the flavour non-diagonal operators in the expansion of the action are compensated by fat-links.
The effect of fat-links can in the end only be demonstrated in lattice simulations. The mass splitting in the pseudo-scalar channel Δ_{PS}[‡] is generally used as an indicator of flavour symmetry breaking. It measures the difference of the Goldstone and non-Goldstone pseudo-scalar masses. A definition of Δ_{PS} in units of the vector meson mass is used in this work

$$\Delta_{\text{PS}} \equiv \frac{m_{\text{PS}_2}^2 - m_{\text{PS}}^2}{m_{\text{V}}^2} \sim \mathcal{O}(a^2) \tag{2.22}$$

where m_{PS} is the mass of the Goldstone pseudo-scalar and m_{PS_2} the mass of the non-Goldstone pseudo-scalar meson.
In first quenched studies with standard and improved gluon actions and the standard staggered action it has been shown that the pion splitting can be substantially reduced by using fat-links. The simulation by the MILC group [33] has been performed with the standard gluon action on lattices of size $20^3 \times 48$ at β=5.85. In Bielefeld a similar calculation using the tree-level improved 1×2 action on $16^3 \times 30$ lattices at β=4.1 has been carried out [59]. Bare quark masses of $m_q a = 0.05$, 0.02 and 0.01 have been used in the meson spectrum calculation. The result for Δ_{PS} extracted from 30 and 57 independent configurations, respectively, are shown in figure 2.11. For both gluon actions fat-links lead to a reduction of the pion-splitting of more than 50%. The effect of varying

[‡]In the following Δ_{PS} will be referred to as *pion splitting* as it is common in the literature.

the quark mass is relatively small.
Since the lattice spacing of the simulation with the improved action is larger than the one with the standard action the influence of different gluon actions on the pion splitting cannot be extracted from figure 2.11. This analysis has also been performed by the MILC group [60] with the result that a one-loop tadpole improved gluon action substantially reduces the pion-splitting already without fat-links. When interpolating the Bielefeld results to $m_{\mathrm{PS}}/m_{\mathrm{V}} = 0.5$ and comparing at the same lattice spacing it becomes clear that this is to some smaller extent also true for the tree-level improved 1×2 action [61].
To study the influence of improvement of rotational invariance on the flavour symmetry the 57 quenched configurations have also been analysed with the Naik[§], p4 and p6 action. In figure 2.12 no difference in the pion splitting for standard, Naik and p4 action are visible. At the largest quark mass $m_q a = 0.05$ the meson spectrum has been calculated also for the p6 action. Again no improvement over the standard action is visible.
Additionally this analysis could show that fat links work as well for rotationally improved actions as they work for the standard staggered action. This is also true when only the one-link path in the p4 action is fattened (green points in figure 2.12). A final test of the reduction of the pion splitting has been performed in full QCD where the fat-links influence the dynamics of the system. The fat-links in this case are only incorporated in the one-link part of the fermion matrix. On the same configurations on which the deviations from rotational symmetry have been analyzed in section 2.3.4 a measurement of the pion splitting has been performed. Figure 2.13 clearly shows that at the same lattice spacing the fattened action reduces the pion splitting by nearly 50 %.
Finally the effect of fat-links on QCD thermodynamics will be discussed. In lattice perturbation theory the one-loop contribution to the fermion free energy has been calculated taking into account different values of the fat-link parameter ω in the fermion action [32]. At leading order fat-links do not contribute to the ideal gas value. Figure 2.14 indicates that fat-links slightly reduce the deviations from the continuum free energy but this effect is small compared to the improvement of rotational symmetry in the fermion action.

action	ω	β_c	$T_c/\sqrt{\sigma}$	$m_{\mathrm{PS}}/m_{\mathrm{V}}$
std	0.0	5.443 (5)	0.470 (3)	0.510 (5)
	0.2	5.249 (3)	0.473 (13)	0.656 (9)
p4	0.0	3.906 (4)	0.562 (17)	0.563 (8)
	0.2	3.778 (12)	0.552 (16)	0.716 (11)

Table 2.2: The critical temperature and the meson masses for the standard and p4 action at a bare quark mass of $m_q a = 0.20$ for $N_f = 2$. Only the statistical error for the string tension and the meson mass ratio are taken into account. An additional uncertainty due to the error in the critical coupling is ignored.

On the other hand the inclusion of fat-links in the action has an influence on $(m_{\mathrm{PS}}/m_{\mathrm{V}})^2$ which is proportional to the quark mass. At the same bare quark mass the m_{PS} to m_{V} ratio is larger for the fat action at the $N_\tau = 4$ critical point than for the non-fat action. In table 2.2 results from a simulation at a bare quark mass of $m_q a = 0.20$ with the standard and p4 action with a fat-weight of $\omega = 0.0$ and 0.20 are gathered. Obviously the difference in $m_{\mathrm{PS}}/m_{\mathrm{V}}$ for the standard and p4 action is much smaller than for the fat and non-fat actions. Additionally fat links lead to a shift in the pseudo-critical coupling β_c for the same fermion action, standard or p4, respectively. The critical temperature on the other hand does depend on the choice of the fermion action and remains more or less unchanged for different fat-weights. Thus one has to perform a simulation at a smaller bare quark mass for the fat action than for a non-fat action in order to work at the same physical quark mass.

[§]The Naik results are taken from the diploma thesis of Axel Bicker [61].

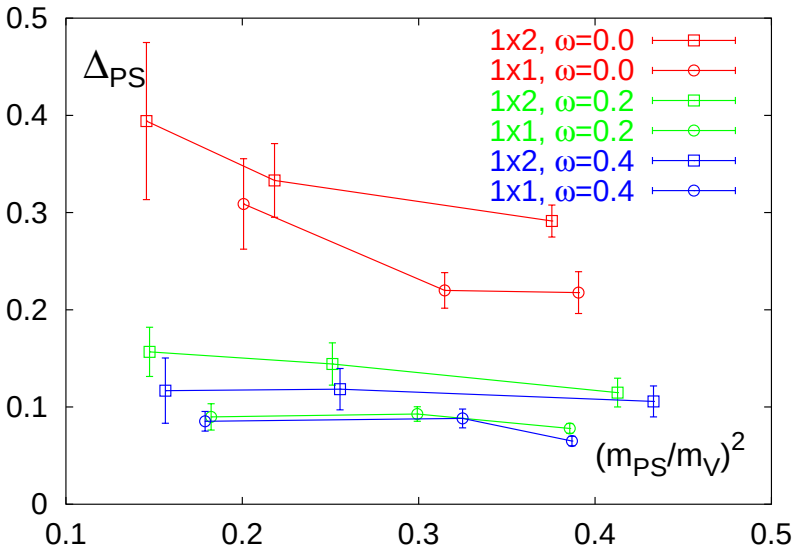

Figure 2.11: The pion splitting Δ_{PS} as a function of the pseudo-scalar to vector meson mass ratio with standard and tree-level improved gluon action for different fat-link parameters ω.

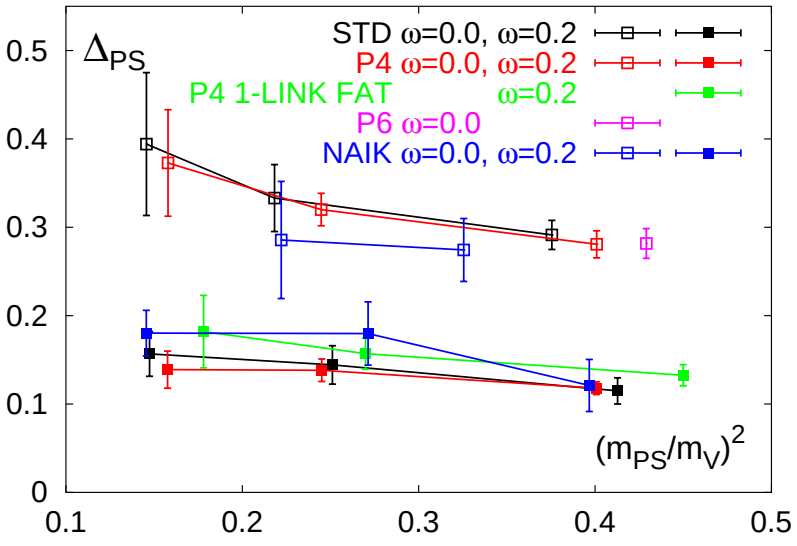

Figure 2.12: The pion splitting Δ_{PS} as a function of the pseudo-scalar to vector meson mass ratio with standard staggered, Naik and p4 action on 57 quenched configurations produced with the tree-level 1×2 gluon action.

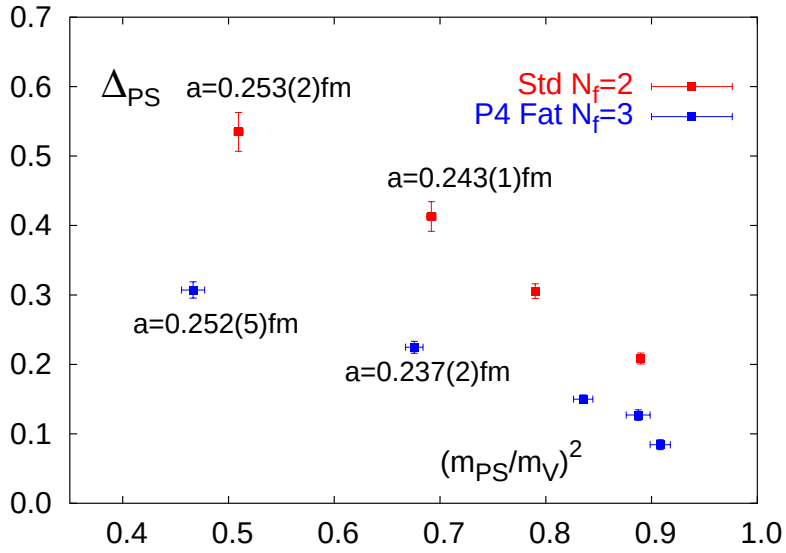

Figure 2.13: The pion splitting $\Delta_{\rm PS}$ as a function of the pseudo-scalar to vector meson mass ratio for $N_f = 2$ and $N_f = 3$ for the non-fat standard staggered and one-link fat p4 action, respectively.

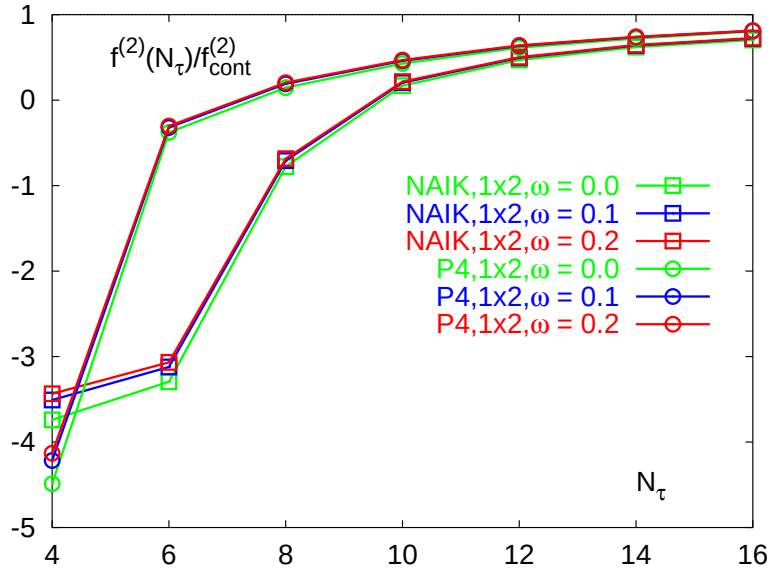

Figure 2.14: The one-loop contribution to the free-energy for different fat-link parameters.

2.4 Computational costs of QCD simulations with improved actions

In this section the computer time required for full QCD simulations will be discussed. Since the gluonic part of the action contributes negligible to the computational effort in the hybrid algorithm, only the fermionic part will be analyzed. There are two basic parts in the calculation which can be quite time consuming. The first one is the matrix multiplication which is part of the conjugate gradient method, the other one is the force calculation. In table 2.3 the number of operations for the different improvement schemes relative to the standard staggered action are given. An additional factor, coming from the enhanced computation of products of link variables for improved actions, is not taken into account. The relative time has been measured on a Quadrics QH2 with 256 nodes. The force computation and the CG matrix inversion have to be performed in each time step of

action	force computation	matrix multiplication	# CG steps	time/CG
std	1	1	1	1
Naik	1+3	1+1	$\approx$1.1	2.5-2.6
p4	1+36	1+6	$\approx$0.7	12-14
fat link	1+18	1	0.6-0.7[¶]	$\gtrsim$1

Table 2.3: Number of operations in the Hybrid algorithm for different improved action relative to the standard action.

the molecular dynamic trajectory. The number of matrix multiplications in the CG algorithm is roughly inverse proportional to the bare quark mass. Thus for small quark masses the matrix inversion dominates the computational effort. Only if highly non-local fat-links as discussed by Orginos *et al.* [62] are used, the force computation can be of equal importance than the matrix product.
From table 2.3 one can read off that the p4 action requires a factor seven times operations than the standard staggered action. On the other hand it turns out that in a simulation the number of steps in a CG inversion is reduced when the p4 action or fat-links are used. This is probably due to their non-local and two-dimensional structure. The corresponding values are given in the fourth column of table 2.3. The number of steps for a combined p4 and fat-link improved action compared to the standard action is roughly the product of the number of steps which are required for both actions alone.
Finally the relative amount of computer time for a conjugate gradient iteration per step is shown in column 5. In real computer time the theoretical factor 2 for the Naik action becomes a factor of 2.5-2.6, the factor 7 for the p4 action becomes a factor of 12-14. The additional communication on the Quadrics parallel machine is responsible for this increase. This is especially true for the additional L-shaped operator in the p4-action which makes remote memory accesses necessary in two directions.
Adding up everything together the p4 fat action is about a factor of 9 more time consuming than the corresponding standard fat action. For the Naik fat action the ratio is about 3.

2.5 Discussion

In this chapter different aspects of improvement of staggered fermion actions have been discussed. It has been shown that there are methods to improve the flavour and the rotational symmetry. The

[¶]The ratio depends on the value of the fat-weight. Increasing the fat-weight reduces the number of steps.

first will become important for small quark masses since then the correct meson spectrum should be reproduced. In finite temperature calculation this is important close to the critical point.
In calculations of the equation of state with the standard staggered action very strong cut-off effects show up at $N_\tau = 4$. When additionally taking into account the slow convergence of the high-temperature free energy to its ideal gas value it is probably necessary to perform simulations on lattices of temporal size 8 and 10 to be able to extrapolate to the continuum reliably. For the improved actions a temporal extension of 4 and 6 might already be sufficient.
In table 2.4 a rough estimate of the relative computer time for different actions is given under the assumption that the same quark mass m/T is used in the simulation and that the ratio N_σ/N_τ is set to 4 to keep the volume approximately constant. Additionally it is assumed that the number of conjugate gradient steps is proportional to the bare quark mass. To keep the error induced by the finite step size of the Hybrid R algorithm sufficiently small the step size has also to be reduced proportional to the bare quark mass. The autocorrelation of the Hybrid R algorithm is proportional to (ξ/a) where (ξ/a) is the correlation length of the system. This would then accumulate to a computer time proportional to $1/a^7$ or N_τ^7 when the critical temperature is relatively constant for different lattice spacings.
In addition one has to have in mind that in thermodynamic calculations in quantities like the equation of state p/T^4 the signal is suppressed with $1/N_\tau^4$. In order to have the same signal to noise ratio this factor should also be taken into account. Then the computer time would add up to a factor of N_τ^{11}.
In table 2.4 the numbers for the simulation for different N_τ and actions are gathered. In the last column the total computer time for the calculation of the equation of state normalized by the time required for the standard action is given. The dramatic increase with N_τ is obvious. A simulation with $N_\tau = 6$ and 8 using the standard action is a factor of 8.1 or 2.7 more time consuming than a $N_\tau = 4$ and 6 simulation with the Naik or p4 action, respectively.

action	N_τ	N_σ^3	mass	rel. time	tot. time
std	4	16^3	m_0	1	1
	6	24^3	$2/3m_0$	1	87
	8	32^3	$1/2m_0$	1	2048
	10	40^3	$2/5m_0$	1	23842
	12	48^3	$1/3m_0$	1	177147
Naik	4	16^3	m_0	3	3
	6	24^3	$2/3m_0$	3	261
	8	32^3	$1/2m_0$	3	6144
p4	4	16^3	m_0	9	9
	6	24^3	$2/3m_0$	9	783
	8	32^3	$1/2m_0$	9	18432

Table 2.4: Number of operations in the Hybrid algorithm for different improved action relative to the standard action.

Chapter 3

The finite temperature phase transition in QCD with 2+1 quark flavours

QCD predicts a phase transition from a hadronic phase with confined quarks and gluons at low temperatures to a plasma phase with liberated quarks and gluons at high temperatures. The nature of the phase transition depends on the number of flavours and the quark masses. For the quenched theory with zero quark flavours the first order nature of the deconfinement transition has been established by Fukugita *et al.* [63] in lattice simulations with the standard gluon action. With dynamical quarks the $Z(3)$ symmetry present in the quenched theory is no longer a symmetry of the action and therefore the Polyakov loop is not a proper order parameter although it still serves as a good indicator of the deconfining phase transition. On the other hand for small quark masses there is a chiral phase transition from a phase with spontaneously broken chiral symmetry at low temperatures to a phase with restored chiral symmetry at high temperatures. This is true as long as the explicit breaking of chiral symmetry in the Lagrangian through the mass term is not too strong. Strictly speaking there is no chiral order parameter except at zero quark mass.

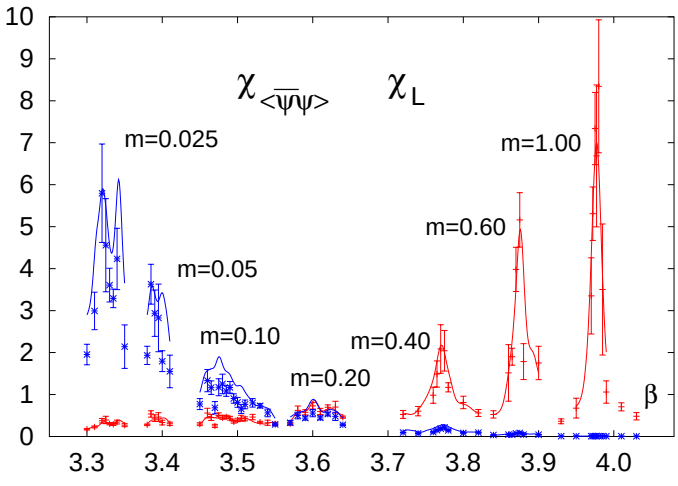

Figure 3.1: The susceptibility of the Polyakov loop and chiral condensate in 3 flavour QCD.

In a lattice simulation with the improved p4 action the quark mass has been varied from heavy to light quarks. The effect on the susceptibility of the chiral condensate and the Polyakov loop is illustrated in figure 3.1 for three quark flavours. One clearly observes that the deconfining transi-

tion smoothly turns into a chiral transition. A similar behaviour has been observed in two flavour QCD with an unimproved action [57].
In addition to lattice calculations the nature of the phase transition has also been studied in effective models which respect the symmetries of QCD. The three-states Potts model in three dimensions has the same Z(3) symmetry as quenched QCD and is therefore expected to lie in the same universality class as zero flavour QCD. Results from this model will be discussed in the next section.

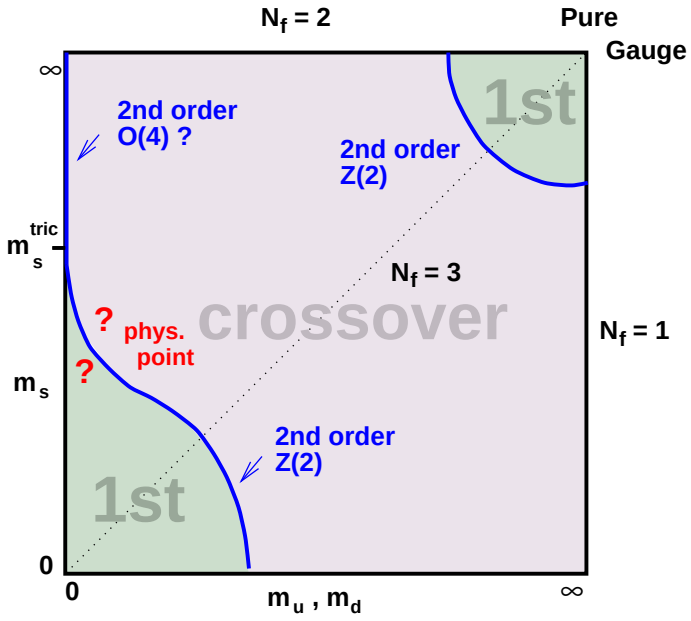

Figure 3.2: The phase diagram of QCD for 2+1 quark flavours.

In the case of small quark masses Ginsburg-Landau effective theories respecting the chiral symmetry of QCD, so-called linear σ models, have been studied in the past. The $SU(2) \times SU(2)$ and $SU(3) \times SU(3)$ σ models [64] suggests a second order transition with O(4) critical exponents for two degenerate quark flavours and a first order transition for three degenerate quarks in the limit of zero quark mass. The second order line in the phase diagram runs into a tricritical point and then continues according to $m_u, m_d \propto \left(m_s^{tric} - m_s\right)^{\frac{2}{5}}$ [65] separating the first order from the crossover region. On the line of three degenerate quarks the second order phase transition should scale with Z(2) critical exponents for the chiral as well as the deconfinement transition [66]. These predictions are schematically presented in the $(m_{\mathrm{up/down}}, m_{\mathrm{strange}})$-plane of figure 3.2 and will be reviewed in the following sections.
Lattice results from simulations with staggered and Wilson fermions have been obtained for different number of flavours and quark masses during the past years. They will be compared to σ model predictions and results from a simulation of three quark flavours with the p4 improved staggered fermion action.

3.1 The deconfinement transition

The finite temperature deconfinement transition for heavy quarks will be investigated for three quark flavours in the staggered fermion formulation with an improved p4 action. The case of infinite quark mass has been intensively investigated in the past. Using the standard gluon action Fukugita *et al.* [63] established the first order nature of the phase transition by inspecting the finite size scaling of the Polyakov loop susceptibility χ_L. The maximum of χ_L should scale with the volume for first order transitions and like $V^{\gamma/d\nu}$ with some critical exponents for a second order transition. For a crossover $\chi_L^{\max}$ should approach some constant value when the volume is sufficiently large. In figure 3.3 results for the maximum of the susceptibility are plotted for the standard [63] and improved gluon actions [41, 40]. Scaling fits to the data lead to results for the exponent $\gamma/d\nu$ of 1.01(6), 0.96(11), 0.98(2) and 0.95(2) for the standard ($N_\tau = 4$), the tree-level 1×2 ($N_\tau = 3, 4$) and tadpole 1×2 ($N_\tau = 4$) actions, respectively. These values should be compared to the second order Ising, O(2) or O(4) exponents of 0.653. There is thus great evidence from different discretisation schemes of SU(3) pure gauge theory that the corresponding transition is first order. The fact that $N_\tau = 3$ and $N_\tau = 4$ results of the tree level 1×2 action are consistent with unity strongly suggests a first order transition also in the continuum limit. The same conclusion can be drawn by investigating the surface tension. After infinite-volume and continuum extrapolation it is fixed to a small but non-vanishing value of $\sigma/T^3 = 0.0155(16)$ [47] indicating a first order transition.

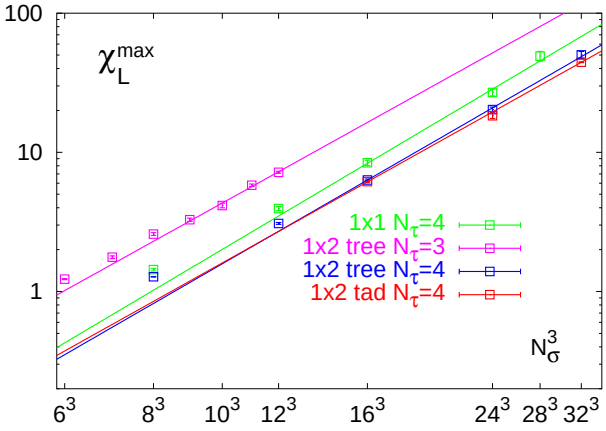

Figure 3.3: The peak height of the Polyakov loop susceptibility as a function of the volume in pure gauge theory. Straight lines are fits to the data for the three largest volumes available for each action.

The case where dynamical quarks are included has not been studied that extensively in the past. In addition to the three flavour study of this work there exist one flavour results [67] and a two flavour simulation [68] on $6^3 \times 2$ lattices with a pre-Hybrid Monte-Carlo algorithm. An up-to-date calculation has been started by Lütgemeier [57] and is now being completed by Schmidt [69] with standard staggered fermions.

A first step in the investigation of the deconfining phase transition can be the study of an effective theory of QCD with heavy quarks. Svetitsky and Yaffe [70] argued that this is the three-states Potts model in three dimensions for the pure gauge case. In the full theory integrating out the quark fields leads to an external field in the Z(3) spin theory [71]. A first numerical calculation of the spin system with external field was carried out by DeGrand and DeTar in 1983 and has now been pushed to very high precision by Stickan in his diploma thesis [72].

A slightly different approach has been realized by Hasenfratz *et al.* [74] who simulated an effective model where the hopping parameter expansion for Wilson fermions is truncated at leading or next-to-leading order. By extrapolating the gap in the order parameter to zero the critical field at the endpoint of the first order transition has been determined to be $h'_{crit} = 0.055$. Translating this into the bare quark mass gives $m/T \approx 4.2$ for three flavours. This value is in agreement with a mean-field analysis of this model by Green and Karsch[75].

3.1.1 The three states Potts model in three dimensions with external field - An effective model for QCD with heavy quarks

In this section the high-temperature and strong-coupling limit of QCD with heavy quarks will be discussed. After integrating out the Grassman variables of the QCD action one obtains the effective action

$$\begin{aligned} S_{QCD} &= \beta S_G + S_F \\ &= \beta S_G + \sum \bar{\psi} M(U) \psi \\ &\longrightarrow \quad S_{eff} = \beta S_G + \mathrm{tr}\ \ln M(U). \end{aligned} \tag{3.1}$$

The gauge part can be treated in the high temperature and strong coupling limit corresponding to small N_τ and small a_τ/a. In the anisotropic gauge action given in equation 1.47 the spatial part is then suppressed with a_τ/a. Finally choosing the special case $N_\tau = 1$ and replacing elements of $SU(3)$ with elements of $Z(3)$ the temporal part of the action reduces to that of a three dimensional $Z(3)$ spin or the three state Potts model

$$\begin{aligned} U_{4\mu}(x) &= U_4(x) U_\mu(x) U_4^\dagger(x+\hat{\mu}) U_\mu^\dagger(x) \quad \text{for } N_\tau = 1 \\ &\to \quad z_x\ z^\star_{x+\mu} \quad \text{for } SU(3) \to Z(3) \\ \Rightarrow \beta S_G &\longrightarrow \beta \frac{a}{a_\tau} \sum_{x,\mu} \mathrm{Re}\ z_x^\star z_{x+\mu} \ , \end{aligned} \tag{3.2}$$

where z_x are elements of $Z(3)$.
For the contributions from the fermion degrees of freedom the hopping parameter expansion for Wilson fermions can be applied which is valid for small κ. The hopping parameter can be related to the quark mass when κ and a_τ/a are small

$$\kappa \approx \frac{1}{2} e^{-m\ a_\tau} \quad . \tag{3.3}$$

Once again if N_τ is chosen to be one and the SU(3) group elements are replaced by elements of $Z(3)$ the fermionic action reduces to a function of Z(3) elements.

$$\begin{aligned} M &= 1\!\!1 - \kappa a_\tau/a M_{\text{spatial}} - \kappa M_{\text{temporal}} \\ \Rightarrow \mathrm{Tr}\ \ln M &\approx \mathrm{Tr}\ \ln(1\!\!1 - \kappa M_{\text{temporal}}) \\ &= h_0 + h(\kappa) \sum_x \mathrm{Re} z_x \end{aligned} \tag{3.4}$$

Gauge and fermionic part then have the form of a three states Potts model with real external field $h(\kappa)$

$$\beta S_G + S_F \longrightarrow \beta \frac{a}{a_\tau} \sum_{x,\mu} \mathrm{Re}\ z_x^\star z_{x+\mu} + h(\kappa) \sum_x \mathrm{Re} z_x \quad , \tag{3.5}$$

where for small κ the relation $h(\kappa) \approx 24\kappa$ holds. Thus the bare quark mass is related to the external field of the Potts model via the equation $h = 12\exp(-m/T)$; the external field grows with decreasing quark mass. At some critical value of the external field the explicit breaking of $Z(3)$ symmetry is expected to be that strong that the first order transition of the Potts model for zero field disappears. The endpoint of the first order transitions should be a second order critical point. A numerical study can determine this critical endpoint and the critical exponents of the second order transition. Due to the relation between the quark mass in QCD and the external field in the Potts model one might hope that results on the universality class of the transition carry over from the Potts model to QCD as they did for zero external field or infinite quark mass. In that case both transitions have turned out to be first order [63, 73]

Numerical results

In a first numerical study DeGrand and DeTar [71] performed simulations on lattices of maximal size 30^3 and looked for tunneling events between two states. This lead to an estimate of the critical external field of $10^{-3} < h_{crit} < 10^{-2}$ or to a bare quark mass of $4.8 < m/T < 7.1$
A very recent numerical calculation of the Potts model has been carried out by Stickan [72] on volumes ranging from $L^3 = 30^3$ to 70^3. The energy $E = \sum_{x,\mu} \mathrm{Re}\ z_x^\star z_{x+\mu}$ and magnetisation $M = \sum_x \mathrm{Re}\ z_x$ have been calculated at several (β, h) values with a statistics of up to 140000 iterations close to the critical point using the Wolf cluster update [95]. Stickan utilized methods previously applied to the determination of the universality of the second order endpoint of the liquid gas transition [76] and the electroweak phase transition [77]. A first step in this procedure is the exact determination of the critical endpoint. One can think of different criteria for the distinction between a first order and a continuous phase transition.

- The existence or non-existence of a two state signal in the Polyakov loop or the action indicating a non-zero or vanishing latent heat.

- The surface tension calculated from the maximum and minimum of the order-parameter distribution P according to

$$\frac{\sigma_V}{T^3} = \frac{1}{L^{d-1}} \ln\left(\frac{P_{min}}{P_{max}}\right) \quad . \tag{3.6}$$

- The finite volume scaling of the peak height of the order parameter susceptibility characterizes the nature of the transition: scaling like V for first order and like $V^{\gamma/d\nu}$ for second order transitions. For a crossover the peak height should approach some maximum value.

- The intersection of the fourth Binder cumulant for different lattice sizes defines the critical point.

$$C_4(M) \quad = \quad \frac{\langle (\Delta M)^4 \rangle}{\langle (\Delta M)^2 \rangle^2} \tag{3.7}$$

  with $\Delta\mathcal{O} \equiv \mathcal{O} - \langle \mathcal{O} \rangle$.

To obtain reliable results an infinite volume extrapolations of the latent heat and surface tension seems to be necessary. Only then one makes sure that non-zero values of σ_V and $\Delta\epsilon$ on finite volumes survive in the limit of infinite volume.
The determination of the pseudo-critical coupling in β at fixed h is quite unproblematic. Compatible results for β_c have been extracted from the peak position of the magnetic and energy susceptibilities and the criterion that the probability distribution of the order parameter is symmetric. This is characterized by the vanishing of the third cumulant $C_3(M) = 0$.

$$C_3(M) \quad = \quad \frac{\langle (\Delta M)^3 \rangle}{\langle (\Delta M)^2 \rangle^{3/2}} \tag{3.8}$$

To find the critical point in h-direction the peak heights of the magnetic susceptibility at different external fields h for several volumes are analysed and plotted in figure 3.4. The volume dependence

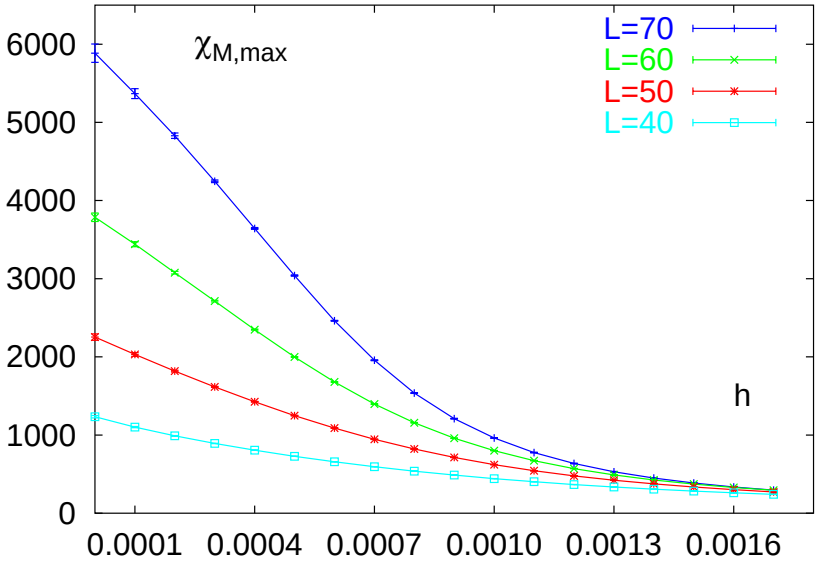

Figure 3.4: The peak height of the magnetic susceptibility as a function of the external field for different volumes.

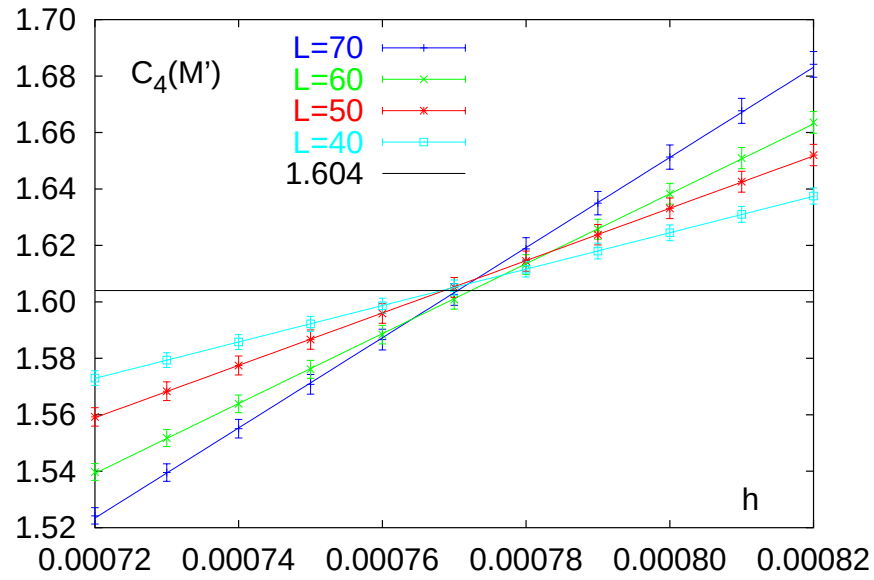

Figure 3.5: The intersection of Binder cumulants as a function of the external field for different volumes.

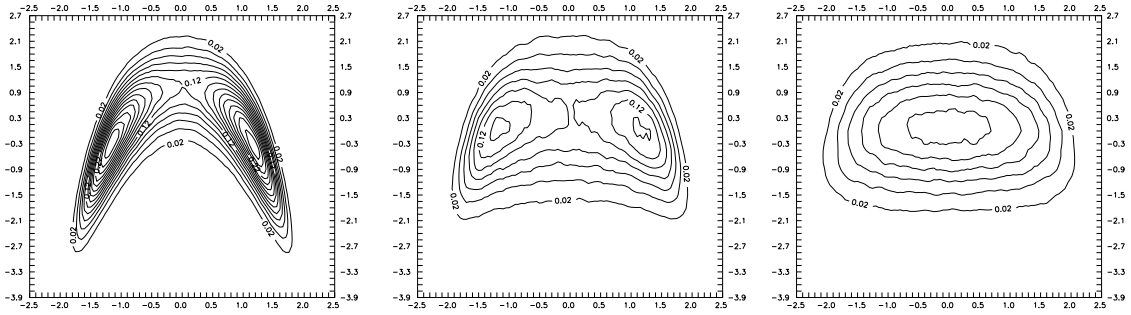

(a) Ising (b) $O(2)$ (c) $O(4)$

Figure 3.6: The distribution of E'- and M'-like observables for different spin models at the critical point. The horizontal axis shows $\Delta M'$, the vertical axis $\Delta E'$.

clearly reduces when the value of the field is increased. At some point no volume effects are visible any more, a clear sign for a crossover. However, it does not seem possible to fix the exact position of the endpoint. To reliably determine the endpoint and the universality class the concept of decorrelating energy and magnetic-like observables has to be introduced. For the liquid gas and electroweak transition it has been shown that a linear mapping of a small area in parameter space around the critical point to the corresponding area in the Ising model can be found and that all three systems behave in exactly the same way in this area.
Since the magnetisation for non-zero external field is no longer an exact order-parameter one cannot expect to read off the same scaling properties at the critical endpoint as for the proper order parameter of a system in the same universality class. A non-zero field effectively leads to a mixing of E- and M-like observables. Therefore one defines new observables E' and M' which are the result of a coordinate transformation and in two dimensions is simply given by

$$\begin{aligned} E' &= A_{11}\ E + A_{12}\ M \\ M' &= A_{21}\ E + A_{22}\ M \quad , \end{aligned} \tag{3.9}$$

where A is the basis transformation matrix which diagonalizes the fluctuation matrix F in $E-M$ space. F is defined as

$$F = \begin{pmatrix} \langle(\Delta E)^2\rangle & \langle(\Delta E)(\Delta M)\rangle \\ \langle(\Delta E)(\Delta M)\rangle & \langle(\Delta M)^2\rangle \end{pmatrix} \tag{3.10}$$

The new E'- and M'-like observables are now orthogonal in coupling space.
The order parameter distribution $P(M')$ for a first order transition determines the surface tension and for a second order critical point it should show a universal form independent of the volume. Thus the ratio of the minimum and maximum has a fixed universal value which in the Potts model at $h = 7.7 \cdot 10^{-4}$ turned out to be 2.23(11) clearly in agreement to the Ising value of 2.173(4). Also the infinite volume extrapolation of the surface tension 3.6 which takes into account different finite volume corrections [79]

$$\frac{\sigma_V}{T^3} = \frac{\sigma}{T^3} + \frac{a}{L^{d-1}} + \frac{b\ln(L)}{L^{d-1}} \tag{3.11}$$

leads to a vanishing of σ/T^3 at about $h = 7.5 \cdot 10^{-4}$. Thus using this criterion a critical field of $h_c = 7.5(5) \cdot 10^{-4}$ has been found.

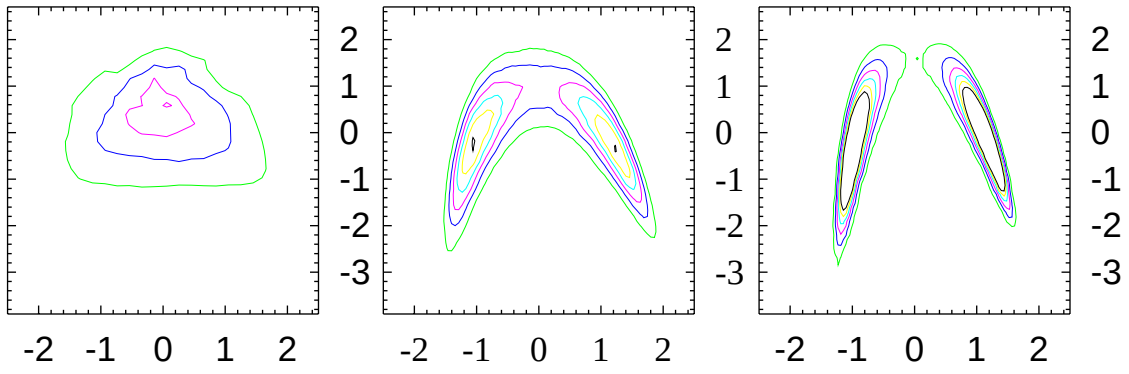

(a) $(\beta_c, h > h_c)$ (b) (β_c, h_c) (c) $(\beta_c, h < h_c)$

Figure 3.7: The joint E'- and M'-like distribution for the Potts model at the pseudo-critical point β_c for different values of the external field on a volume of 70^3. In (a) couplings in the crossover region, in (b) at the critical point and in (c) in the first order region are displayed. The horizontal axis shows $\Delta M'$, the vertical axis $\Delta E'$.

Additionally the intersection of the fourth Binder cumulant for M' at β_c can be used to determine the critical value of the external field h. In figure 3.5 the results for the four largest volumes are plotted. All curves intersect within a range in h of $7.6 \cdot 10^{-4}$ and $7.8 \cdot 10^{-4}$, thus the critical endpoint can be determined to very high precision $(\beta_c, h_c) = (0.54939(1), 7.7(1) \cdot 10^{-4})$. The value of the fourth cumulant at the intersection point is characteristic for the universality class. One finds a $C_4(M')$ of 1.603(4) at h_c for the largest volume which is in very good agreement with the universal Ising value of 1.604(1) [78] and clearly disagrees with the $O(2)$ and $O(4)$ values of 1.092(3) and 1.233(6), respectively. A further universal quantity is the critical exponent γ/ν which characterizes the scaling of the order parameter susceptibility with the volume. At (β_c, h_c) a value of 1.933(6) has been calculated, to be compared to 1.96 for the Ising, $O(2)$ and $O(4)$ universality class. For larger or smaller values of h the exponent approaches zero or three as it should for a crossover or first order transition, respectively.
Finally the universal joint E'- and M'-like distribution at the critical point can be analysed. They are normalized such that $\langle(\Delta M')^2\rangle = 1$ and $\langle(\Delta E')^2\rangle = 1$. For the different universality classes discussed in connection with the Potts model and QCD, the Ising, O(4) and O(2) joint distributions are plotted in figure 3.6. They can now be compared to the results from the three-states Potts model at the pseudo-critical coupling (β_c, h_c) determined by the intersection of the cumulants. The distribution is plotted in figure 3.7 not only for the critical point (β_c, h_c) which agrees to very high precision with the Ising distribution, but also for two values of the pseudo-critical coupling which lie in the crossover and in the first order region. Thus not only the universal Ising intersection point of the cumulant and the critical exponent γ/ν, but also the joint probability distribution is that of the Ising model in three dimensions. If the connection between the Potts model and QCD carries over to non-zero external field and large quark masses, respectively, then the QCD critical endpoint in the deconfinement region should also be that of the Ising model. Numerical evidence for or against this will be presented in the next section.

				pseudo-critical couplings β_c			
$m_q a$	N_σ	# β	# iter.	max(χ_S)	max(χ_L)	max($\chi_{\langle\bar\psi\psi\rangle}$)	$C_3(L)=0$
0.20	8	16	39250	3.5184 (462)	3.6216 (27)	3.6204 (32)	3.6129 (29)
	12	5	18700	3.5986 (25)	3.6020 (32)	3.6004 (18)	3.6001 (32)
	16	8	29650	3.5998 (14)	3.6017 (17)	3.6000 (33)	3.6024 (13)
0.40	8	11	36600	3.7756 (64)	3.7848 (23)	3.7808 (27)	3.7836 (24)
	12	3	11700	3.7810 (24)	3.7781 (17)	3.7797 (16)	3.7762 (20)
	16	5	16250	3.7653 (16)	3.7719 (33)	3.7746 (40)	3.7692 (28)
0.60	8	12	33100	3.7983 (159)	3.8865 (17)	3.8806 (12)	3.8812 (16)
	12	4	16500	3.8718 (47)	3.8770 (16)	3.8798 (38)	3.8760 (11)
	16	6	41750	3.8210 (233)	3.8766 (6)	3.8764 (6)	3.8744 (9)
0.70	16	4	24000	3.7983 (159)	3.8865 (17)	3.8806 (12)	3.8812 (16)
0.80	16	3	25300	3.9358 (18)	3.9377 (10)	3.9368 (14)	3.9382 (17)
1.00	8	8	21750	3.9680 (6)	3.9686 (27)	3.9663 (11)	3.9690 (28)
	12	5	24520	3.9717 (39)	3.9712 (22)	3.9711 (15)	3.9704 (19)
	16	8	101300	3.9771 (15)	3.9778 (10)	3.9808 (16)	3.9770 (11)
∞	8	10	129000	4.0554 (27)	4.0745 (17)	-	4.0685 (14)
	12	14	154900	4.0708 (27)	4.0708 (6)	-	4.0684 (7)
	16	8	157500	4.0719 (7)	4.0715 (5)	-	4.0704 (6)
	24	3	75200	4.0724 (4)	4.0722 (4)	-	4.0719 (3)
	32	1	46800	4.0733 (4)	4.0729 (3)	-	4.0729 (4)
	∞	-	-	4.0732 (4)	4.0730 (3)	-	4.0729 (4)

Table 3.1: Pseudo-critical couplings for different masses and volumes.

3.1.2 Numerical results from lattice QCD with three degenerate quarks

To investigate the second order endpoint of the deconfinement transition in three flavour QCD simulations with the p4 improved staggered fermion action have been performed. The standard Hybrid R algorithm has been used with a step size of 0.08 for the smallest and 0.10 for the other quark masses. This choice probably leads to results which are not free of systematic errors. On the other hand one would not expect that the effect is large enough to change the universality class of the transition.
The quark masses under consideration are $m_q a$ = 0.20 0.40 0.60 0.70, 0.80 and 1.00. To get an impression of the finite size effects simulations on $8^3 \times 4$, $12^3 \times 4$ and $16^3 \times 4$ have been performed. The pseudo-critical couplings have been determined from the peak position of the susceptibilities of the action, the chiral condensate and the Polyakov loop. Additionally the third "magnetic" cumulant $C_3(L)$ has been analyzed. Since it should vanish at the critical point it also defines a pseudo-critical coupling. From all observables except from the action susceptibility one obtains a good signal for all quark masses and lattice sizes. All results for the critical couplings are collected in table 3.1 together with the total number of iterations and β values. A jackknife analysis has been performed to determine the mean value and the error.
In most cases the values for β_c coming from the peak position from χ_L and $\chi_{\langle\bar\psi\psi\rangle}$ and from the

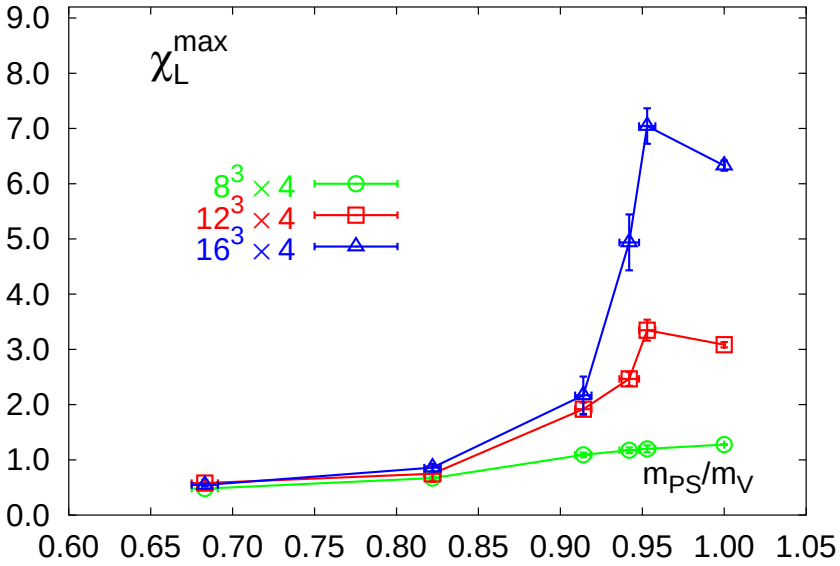

Figure 3.8: The peak height of the Polyakov loop susceptibility as a function of the pseudo scalar to vector meson mass ratio for different volumes.

third cumulant coincide within errors for fixed volumes. The finite size effects lead to discrepancies of β_c which are larger than the assigned errors. Thus the infinite volume critical couplings are probably not reached at the largest volume of $16^3 \times 4$. This is expected since an analysis of the pure gauge data shows that only a volume as large as $32^3 \times 4$ is within errors in agreement with the infinite volume extrapolated value. Details of the extrapolation are given in [41].
To find the endpoint of the first order region the different quantities discussed in the previous section are analyzed. In figure 3.8 the maximum of the Polyakov loop susceptibility is plotted for different masses and lattice sizes. For small masses the volume dependence clearly vanishes whereas for the larger masses an increase of the maximum with volume shows up. One thus finds the expected behaviour for a crossover and first order region. The results qualitatively also agree with the ones from the Potts model. The fact that the maxima for $m_q a = 1.00$ are within errors equal to the corresponding pure gauge values is not quite understood. One might speculate that at such a quark mass the system already behaves like a quenched system.

$\max(\chi_L)=k \cdot V^{\gamma/d\nu}$		
mass	k	$\gamma/d\nu$
0.20	0.233	0.158
0.40	0.660	0.143
0.60	0.00613	0.804
1.00	0.00541	0.862
∞	0.00179	0.982

Table 3.2: The critical exponent $\gamma/d\nu$ and the factor k extracted from the finite volume scaling fit of the peak height of the Polyakov loop susceptibility on lattices of spatial size 12^3 and 16^3.

From pure gauge simulation one knows that the volumes considered here are too small to see the correct finite size scaling in the maximum of the susceptibilities. Nevertheless it has been performed using results from the 12^3 and 16^3 lattices. The order parameter susceptibility scales like $V^{\gamma/d\nu}$ where the exponent is one for first order transitions and zero for a crossover. In principle one should allow for an additional constant in the fit to also cover the regular part of the susceptibilities, $\max(\chi) = c + k \cdot V^{\gamma/d\nu}$. This should be especially important in the crossover region since there no scaling with the volume is expected. The scaling plots are shown in figure 3.9

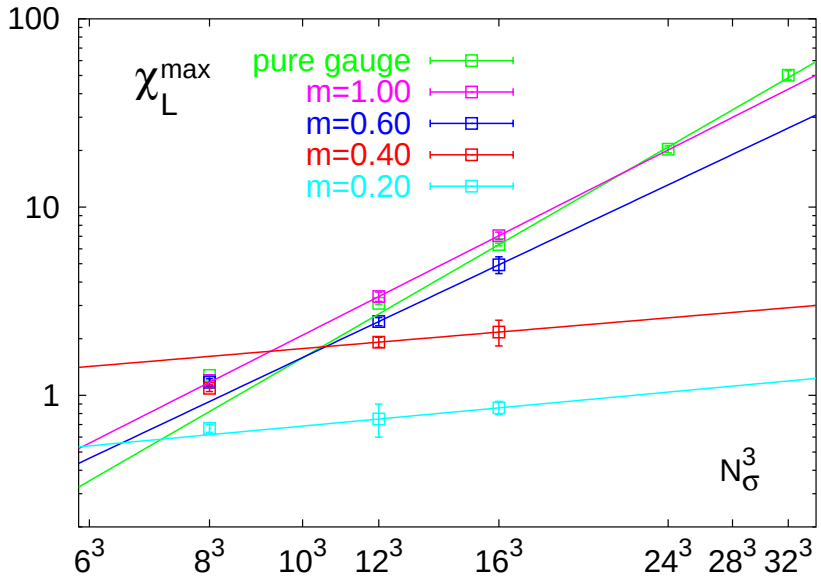

Figure 3.9: Scaling of the peak height of the Polyakov loop susceptibility as a function of the volumes.

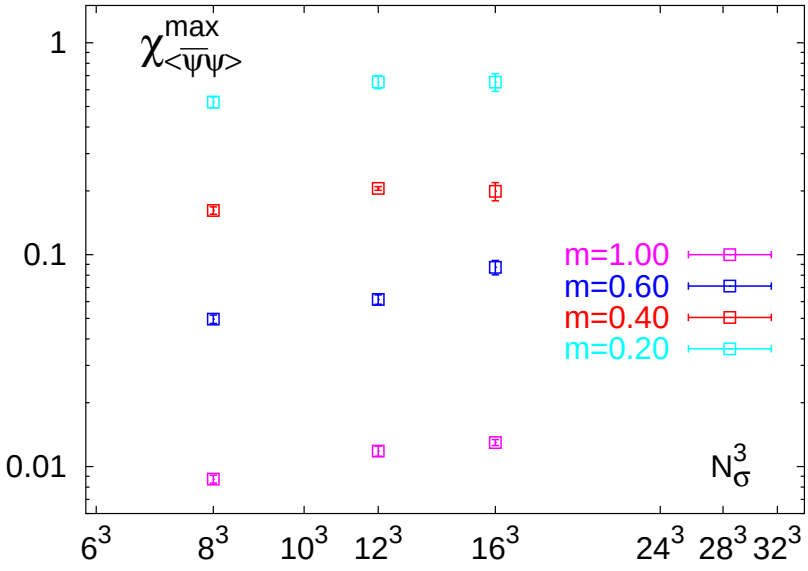

Figure 3.10: Scaling of the peak height of the chiral susceptibility as a function of the volumes.

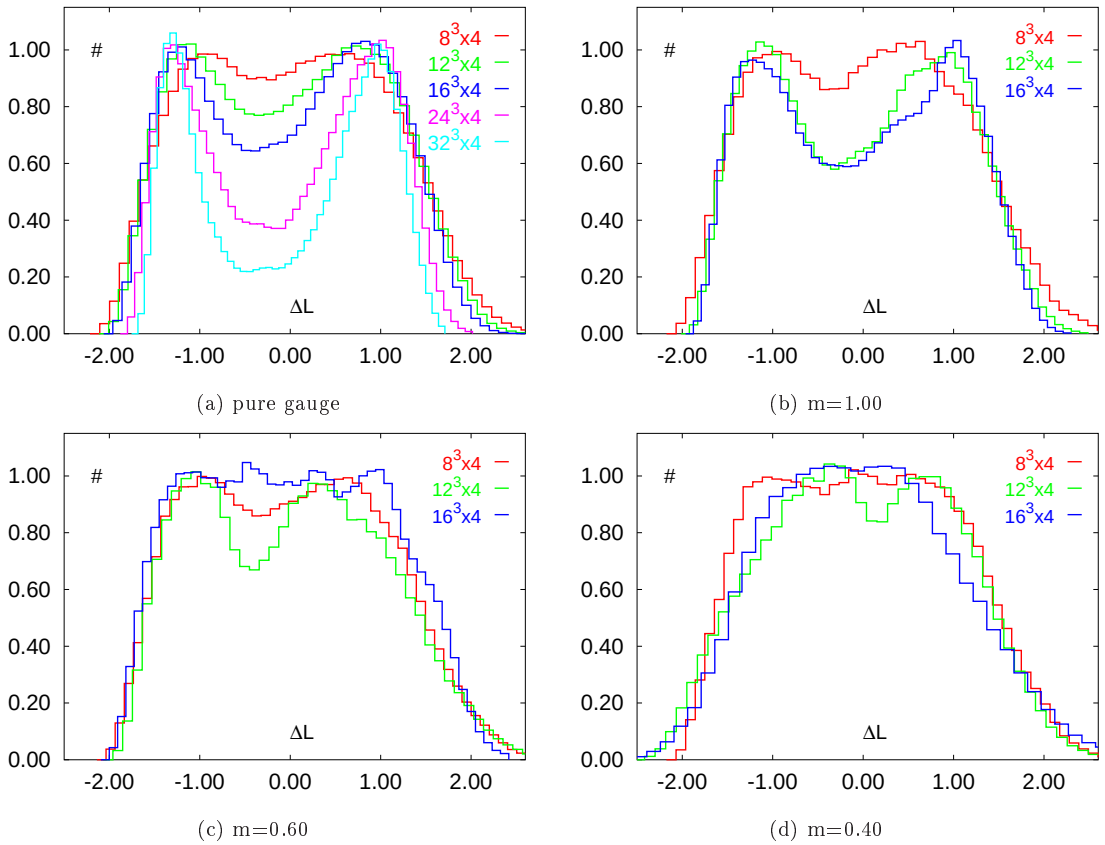

(a) pure gauge (b) m=1.00

(c) m=0.60 (d) m=0.40

Figure 3.11: The Polyakov loop distribution for different quark masses and lattice sizes.

and 3.10 for the peak height of the Polyakov loop and chiral susceptibility, respectively. For $\chi_L^{\max}$ a fit without constant has been included in the figure. The fit parameters are collected in table 3.2. For the three largest quark masses k is small and the exponent $\gamma/d\nu$ is close to one as one would expect for a first order transition. As can already be read off from the figure 3.9 the two smallest quark masses show a quite different behaviour. $\chi_L^{\max}$ does only change weakly with the volume, which is also reflected in the small exponent and large factor k. Of course in principle one should have used a fit with an additional constant, but the quality of the data did not allow for such an ansatz. If assuming the predicted Ising universality class with an exponent of 0.65 for the second order endpoint the critical mass would be in the range between $m_q a = 0.40$ and 0.60.
Since only the disconnected part is taken into account in the chiral susceptibility it is a priori questionable if the correct scaling can be extracted from it. In two flavour simulations the contribution from the connected part turned out to be large at large quark masses and for three flavours it should diverge at the critical point in the chiral limit. The volume dependence of the maximum of $\chi_{\langle\bar{\psi}\psi\rangle}^{\max}$ is quite small for all mass values considered (see figure 3.10). Also for the two largest masses, which show a strong scaling with the volume for the Polyakov susceptibility, no such behaviour has been found.
A further criterion examined is the surface tension. In figure 3.11 the change of the Polyakov loop distribution with the volume is plotted for different values of the quark mass with the maximum

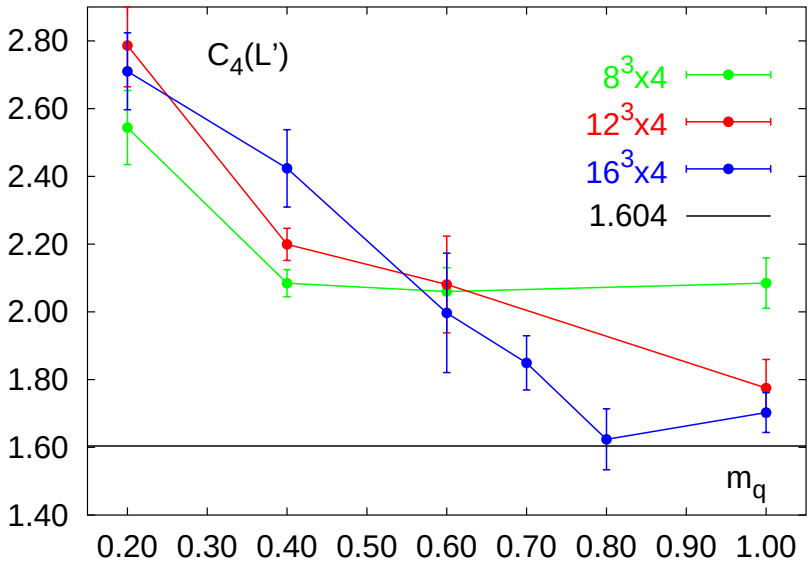

Figure 3.12: The fourth Binder cumulant $C_4(L')$ plotted against the quark mass for different lattice volumes.

normalized to one. The formula to calculate the surface tension from the order parameter distribution $P(L)$ then reads $\sigma_V/T^3 = 1/L^{d-1} \ln(P_{min})$. For the pure gauge case and $m_q a = 1.00$ a minimum in the distribution develops which decreases or at least stays constant with increasing volume. This will result in a finite surface tension in the infinite volume limit. For quark masses $m_q a \lesssim 0.60$ the minimum of the distribution vanishes with increasing volume, thus the surface tension approaches zero in the limit $V \to \infty$.
As for the Potts model the method of decorrelating energy- and magnetic-like observables has been applied. For QCD with heavy quarks the gluonic action takes the role of the energy and the Polyakov loop the one of the magnetisation of a spin system. The basis transformation has been applied to the vector (S_G, L) yielding

$$\begin{aligned} S' &= A_{11}\ S_G + A_{12}\ L \\ L' &= A_{21}\ S_G + A_{22}\ L \quad , \end{aligned} \tag{3.12}$$

with the basis transformation matrix A. It diagonalizes the fluctuation matrix F in $S_G - L$ space. F is defined as

$$F = \begin{pmatrix} \langle(\Delta S_G)^2\rangle & \langle(\Delta S_G)(\Delta L)\rangle \\ \langle(\Delta S_G)(\Delta L)\rangle & \langle(\Delta L)^2\rangle \quad . \end{pmatrix} \tag{3.13}$$

In two dimensions the transformation is simply a rotation about the angle α. For the largest lattice size, $16^3 \times 4$, α at the pseudo critical point turned out to be as small as $1.75°$ for infinite quark masses and increases to $6.12°$ for the smallest mass considered, $m_q a = 0.10$. The angles at intermediate couplings are collected in table 3.3. The results thus show that for large quark masses the Polyakov loop nearly is a proper order parameter which is contaminated by contributions from the action at smaller masses.
The intersection of the fourth cumulant which for the Potts model gave the most precise result for the determination of the second order critical point, is plotted in figure 3.12. Due to the large errors in the quantity it is difficult to find a universal intersection point. At a bare quark mass of $m_q a = 0.60$ the values of $C_4(L')$ are consistent within errors for all volumes, but do not agree with

$m_q a$	∞	1.00	0.80	0.70	0.60	0.40	0.20	0.10
α	1.75°	1.77°	1.81°	2.12°	2.10°	2.80°	5.56°	6.12°

Table 3.3: The angle of the rotation in S_G-L space at the pseudo critical point for $16^3 \times 4$.

the Ising number of 1.604(1) and even less with the $O(2)$ and $O(4)$ results of 1.233(6) and 1.092(3), respectively. Taking this seriously would rule out that the QCD deconfinement transition is in the universality class of any of the spin models discussed so far. On the other hand the volumes considered in this work are still quite small and therefore the results presented here have to be confirmed on larger volumes before being conclusive. This is especially true since for the largest spatial volume of 16^3 $C_4(L')$ reaches the universal Ising value at a quark mass of $m_q a = 0.80$, thus the Ising universality is not out of reach.
Finally the joint probability distributions of the rotated Polyakov loop L' and the rotated action S' are investigated on the largest lattice size $16^3 \times 4$. They are plotted in figure 3.13 for masses ranging from $m_q a = 0.20$ to ∞. The two smallest quark masses show a rotationally symmetric distribution which compares to the Potts distribution being in the crossover region (figure 3.7(a)). The quenched and $m_q a = 1.00$ distributions also look quite similar confirming the first order nature of the transition already deduced from the volume scaling of the Polyakov loop susceptibility. For the intermediate mass values one finds a certain structure in the distribution which shows features of the Ising or $O(2)$ distribution. The histogram at a quark mass of $m_q a = 0.80$, where the fourth Binder cumulant has the Ising value, shows a form which is closest to the $Z(2)$ one. However, for the joint distributions to be conclusive the lattice volume and the statistics seems to be too small. Combining the results from different observables one can conclude that the three flavour deconfining phase transition occurs at bare quark masses between $m_q a = 0.40$ and 1.00 for improved staggered fermions. This corresponds to a quite large physical quark mass of $m_{\mathrm{PS}}/m_{\mathrm{V}} = 0.914(5)$ to $0.953(6)$. Methods previously applied to liquid-gas systems, the electroweak-transition and the Potts model have been used to construct magnetic- and energy-like observables. In principles these methods seem to work also in QCD, but require a high statistics and large enough volumes.

3.1.3 The deconfinement transition with one and two flavours

A one flavour calculation using Wilson fermions has been carried out by Alexandrou *et al.* [67] on lattices of size $8^3 \times 4$, $12^4 \times 4$ and $16^3 \times 4$. From the tunneling rate of the Polyakov loop and the scaling of the susceptibilities the authors concluded that for $\kappa = 0.05$ and 0.12 the transition is first order and a crossover, respectively. For an intermediate κ of 0.10 the signals are no longer that clear and no conclusion can be drawn. As for the three flavour staggered results a larger lattice size would be needed to determine the critical endpoint more precisely. In an effective model the same authors found a value for the bare quark mass at the endpoint of the transition of $m_q a = 1.4$, a similar large value as for the three flavour study.
For two staggered flavours using the unimproved action in the gauge and fermionic part [57, 69] a similar analysis to the one in this work is being performed. The calculations qualitatively agree with the three flavour results. Even on a $16^3 \times 4$ and $24^3 \times 4$ lattice the intersection of the fourth cumulants is not conclusive with a statistics of up to 100000 iterations. The same is true for the joint probability distributions.

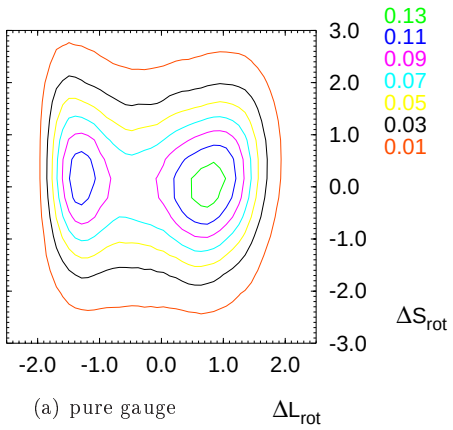

(a) pure gauge

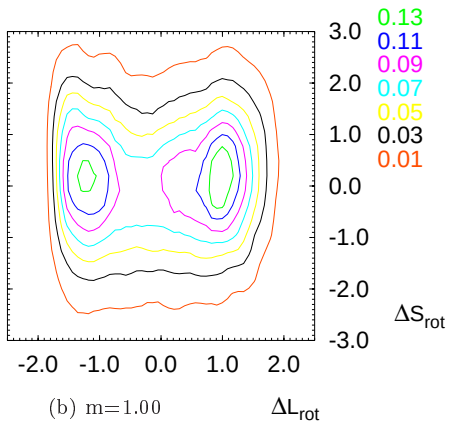

(b) m=1.00

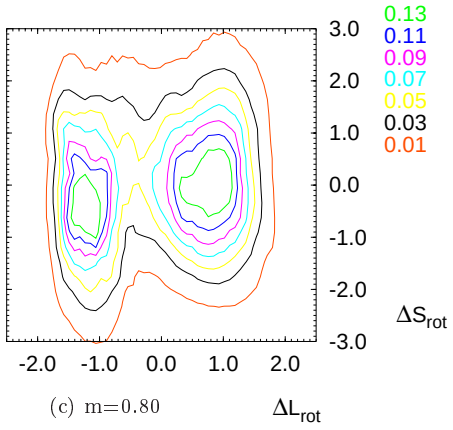

(c) m=0.80

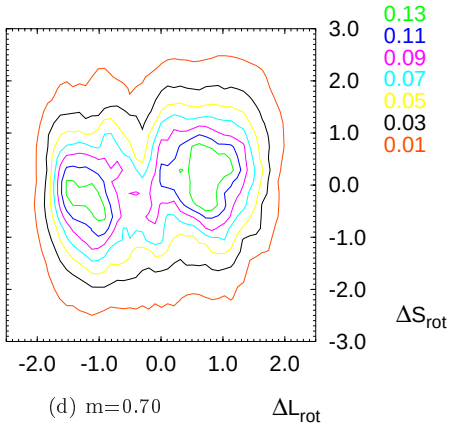

(d) m=0.70

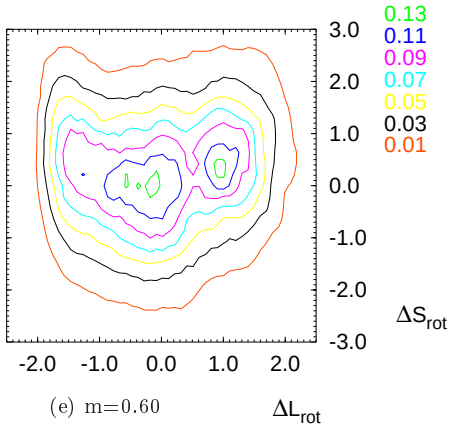

(e) m=0.60

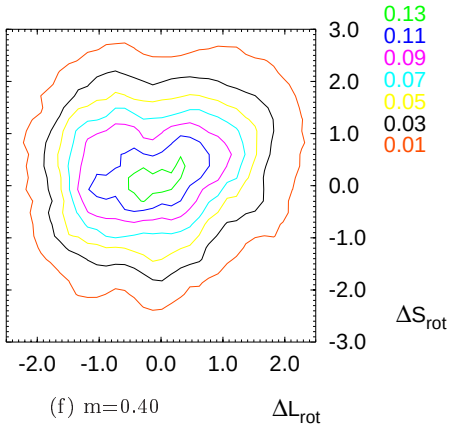

(f) m=0.40

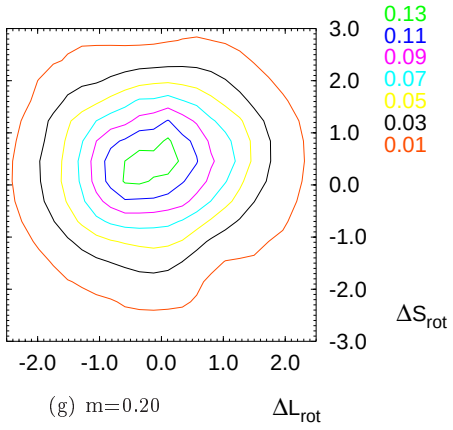

(g) m=0.20

Figure 3.13: The distribution of E- and M-like observables for different quark masses.

3.2 The chiral transition

In this section the finite temperature chiral phase transition of QCD will be discussed. For two quark flavours recent lattice results will be compared to σ-model predictions. In the case of three light flavours the analysis of the chiral $SU(3) \otimes SU(3)$ σ-model will be reviewed in some detail. Finally the lattice results obtained with improved staggered fermions will be discussed and compared to findings with standard staggered and Wilson fermions.

3.2.1 The two flavour chiral transition

Simulations with two flavours using standard staggered quarks performed by different groups [96, 98, 102] with lattice bare quark masses ranging from $m_q a = 0.008$ to 0.075 do neither show evidence for a first order transition nor do they contradict a second order transition in the chiral limit $m_q a = 0$. From renormalization-group arguments it follows that the scaling laws for the different fermionic susceptibilities have the form $\chi_i^{max}(m_q a) \propto (m_q a)^{-z_i}$, where the index i denotes the various derivatives of the free energy with respect to the reduced temperature and/or the quark mass. Hyper-scaling laws relating the critical exponents z_i are approximately satisfied in different studies. On the other hand the critical exponents extracted do not agree with the $O(2)$ or $O(4)$ exponents. The authors of [102] additionally claim that the agreement becomes worse for the smallest quark mass of $m_q a = 0.008$. For this reason the determination of the universality class of the two flavour chiral transition still remains an open problem for unimproved staggered fermions. Unimproved Wilson fermions together with the standard gluon action are plagued by strong lattice artifacts such that no conclusions on the chiral transition can be extracted [99]. The situation is much improved when the RG gluon action is used [100]. Then the subtracted chiral condensate can be successfully described by a scaling function with $O(4)$ critical exponents indicating that the chiral transition is second order and lies in the universality class of the $O(4)$ sigma model. This result is surprising since the chiral properties of Wilson fermions are not expected to be very good.

3.2.2 Ising universality class for the 2+1 flavour chiral transition - Predictions from linear sigma models

In the case of three degenerate massless quark flavours Pisarski and Wilczek [64] investigated a linear sigma model respecting the global $SU(3) \otimes SU(3)$ chiral symmetry of three flavour QCD. The lack of an infrared stable fixed point in this model lead to their conclusion that the chiral transition is of first order driven by fluctuations. In addition to this renormalisation group analysis Frei and Patkós [80] investigated the sigma model by a saddle point approximation of the free energy and confirmed the first order nature of the chiral transition. In [81, 82] Meyer-Ortmanns *et al.* showed that in the case of non-vanishing pseudo-scalar meson masses the chiral transition changes to a smooth crossover. It is therfore expected that the line of first order transitions ends in a second order chiral critical point when increasing the quark mass from zero to some value $(m_{\mathrm{up/down}}, m_{\mathrm{strange}})_{\mathrm{crit}}$.
The universality class of this 2nd order phase transition has been analyzed by Gavin *et al.* [66]. The effective model with the global $SU(3) \otimes SU(3)$ chiral symmetry is the same as in [64, 80, 81, 82]. The Lagrangian density, which is constructed like in Landau theory as a function of the order parameter $\phi \propto \langle \overline{q_L} q_R \rangle$, is given by

$$\begin{aligned} \mathcal{L}_{\mathrm{chiral}} &= \mathrm{tr}\ |\partial_\mu \phi|^2 + \mu^2 \mathrm{tr}\ \left(\phi^\dagger \phi\right) - \sqrt{6}\left(\det(\phi) + \det(\phi^\dagger)\right) \\ &\quad + (g_1 - g_2)\left(\mathrm{tr}\ \phi^\dagger \phi\right)^2 + 3 g_2 \mathrm{tr}\ \left(\phi^\dagger \phi\right)^2, \end{aligned} \tag{3.14}$$

where the field ϕ is defined by $\phi = \sum_{a=0}^{8}(\sigma_a + i\pi_a)\lambda^a$. The $\lambda_i, (i = 1..9)$ are the Gell-Mann matrices and the σ_a and π_a are the scalar and pseudo-scalar components of the nonet.
The different parts in the chirally symmetric Lagrangian are the kinetic term, the mass term with a mass parameter μ^2, terms quartic in ϕ to provide the possibility of a spontaneous symmetry breakdown and a $\det(\phi)$ term to reproduce the $U(1)$ anomaly correctly which is responsible for the mass splitting in η and η'. To incorporate the effect of non- vanishing pseudo-scalar meson masses an explicit symmetry breaking term along two directions of the group generators are introduced into the Lagrangian

$$\mathcal{L} = \mathcal{L}_{\text{chiral}} + h_0\sigma_0 + h_8\sigma_8 \quad . \tag{3.15}$$

The fields h_0 and h_8 correspond to external magnetic fields in spin systems and account for the non-vanishing of the pseudo-scalar masses (explicit breaking of the chiral symmetry) and the mass splitting between different iso-spin multiplets (explicit breaking of the flavour $SU(3)$). In QCD this corresponds to finite non-degenerate quark masses.
Gavin *et al.* [66] could show that in mean field theory this model reproduces the scalar and pseudo-scalar meson spectrum reasonably well when fitting to the masses of π, η, η' and the pion decay constant f_π. Thus the model can be regarded as a appropriate effective model for QCD.
In the case of the flavour SU(3) symmetry, $h_8 = 0$, the Lagrangian reduces to the potential for a constant field Σ_0

$$\mathcal{L} \quad = \quad -h_0\Sigma_0 + \frac{1}{2}\mu^2\Sigma_0^2 - \frac{c}{3}\Sigma_0^3 + \frac{g_1}{4}\Sigma_0^4 \quad . \tag{3.16}$$

For zero external field h_0 the transition is driven first order by the cubic term in the Lagrangian and the strength of this transition is reduced by switching on the external field. The transition turns second order when there is only one extremum in the Lagrangian or Landau free energy. The critical values are given by $h_0^{crit} = c^3/(27g_1^2)$, $\Sigma_0^{crit} = c/(3g_1)$ and $\mu_{crit}^2 = c^2/(3g_1)$. Inserting these results into the mass formula leads to a massless $\sigma_{\eta'}$. All other mesons are massive. Since this model has the same phase diagram as the liquid-gas system and there is only one scalar order parameter it is in the same universality class as the liquid gas system, which is the one of the Ising model in three dimensions.
The authors claim that this is also true for the case of $h_0 \neq 0$ where the flavour $SU(3)$ symmetry is broken. Numerically they still obtain one massless field with the universality class of the Ising model. Thus not only in the case of three degenerate quark flavours but also along the $(m_{\text{up/down}}, m_{\text{strange}})_{\text{crit}}$ line one should see $Z(2)$-scaling.

3.2.3 Numerical results from lattice QCD for 3 quark flavours

As pointed out in the previous section for three flavours one expects a region of first order chiral phase transitions to emerge when the quark mass approaches zero. Since previous lattice results from staggered [97, 98] and Wilson [99] fermions lead to quantitatively very different values for the onset of this first order region a new calculation with the p4-improved staggered fermion action has been performed at bare quark masses of $m_q a = 0.01$, 0.025 and 0.05. The lattice sizes under investigation are $8^3 \times 4$ and $16^3 \times 4$ for the two heavier masses. With decreasing quark mass the chiral order parameter $\langle\bar{\psi}\psi\rangle$, plotted in figure 3.14, shows a steeper drop but no clear sign of a discontinuity. The finite size effects in this quantity are small since the results of the two lattice sizes coincide within errors. This is different for the distribution of the chiral condensate reweighted to the appropriate pseudo-critical couplings (figure 3.14). Here one observes a clear broadening of the distribution for the small lattice which is much reduced for the larger lattice. In [27] the same effect shows up for two flavours where even a double-peak structure in the distribution on $8^3 \times 4$ lattices disappears when going to larger lattices. Taking this into account the broad distribution at the smallest quark mass $m_q a = 0.01$ which might be interpreted as a

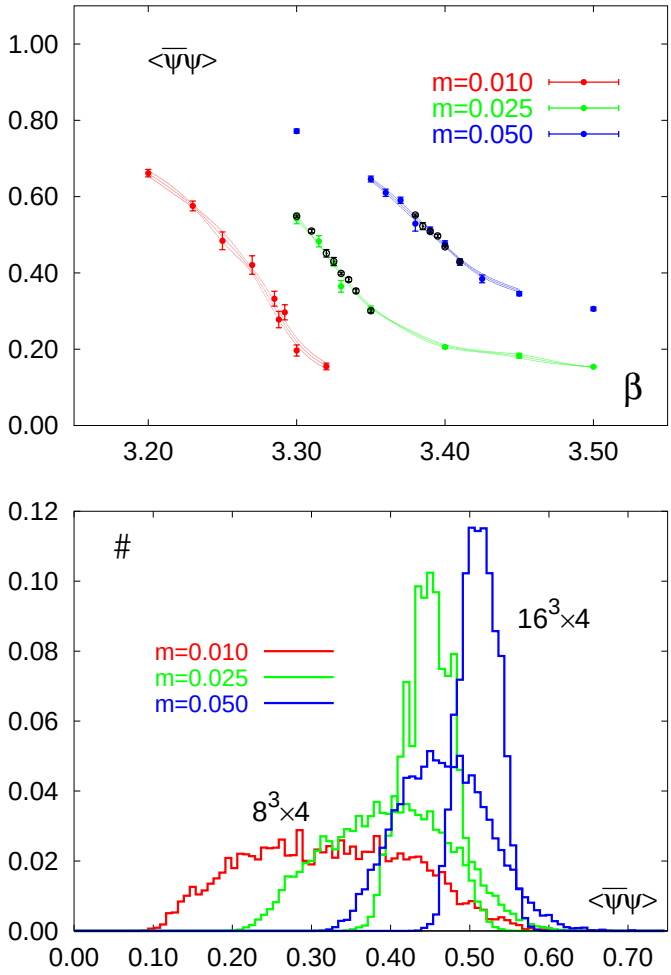

Figure 3.14: The chiral order parameter as a function of the coupling β and the histogram of $\langle\bar{\psi}\psi\rangle$ reweighted to β_c for three flavours of improved staggered quarks on lattices of $8^3 \times 4$ and $16^3 \times 4$ (black data points).

superposition of two single peaks, will probably not survive in the infinite volume. Thus we have an upper bound for the first order region from improved staggered fermions of $m_q a = 0.01$.

In principle all quantities discussed for the deconfinement transition could also be analysed here. In table 3.4 the pseudo-critical couplings are collected which have been extracted from the susceptibility of the action, the Polyakov loop and the chiral condensate and from the vanishing of the third chiral cumulant. For some observables no determination was possible or a large error had to be assigned to β_c. In general the values agree for different observables at a fixed volume.

In figure 3.15 a clear increase of $\max(\chi_{\langle\bar{\psi}\psi\rangle})$ with decreasing quark mass is visible whereas $\max(\chi_L)$ slightly decreases. This indicates that the chiral transition strengthens and the deconfining transition gets weaker. The volume dependence of the maximum of the chiral and Polyakov loop susceptibilities turned out to be small for the mass values investigated. Thus also the volume scaling of the susceptibilities exhibits no sign for the onset of the first order region. The fourth cumulants, which at the critical point should intersect

				pseudo-critical couplings β_c			
$m_q a$	N_σ	# β	# iter.	$\max(\chi_S)$	$\max(\chi_L)$	$\max(\chi_{\langle\bar{\psi}\psi\rangle})$	$C_3(\chi_{\langle\bar{\psi}\psi\rangle}) = 0$
0.01	8	9	10300	3.2865 (98)	3.2887 (65)	3.2841 (57)	3.2831 (42)
0.025	8	8	14000	3.3265 (93)	3.3318 (24)	3.3281 (25)	3.3284 (23)
	16	6	8200	-	3.3428 (159)	3.3194 (21)	-
0.05	8	11	16250	-	3.4018 (35)	3.3930 (201)	3.3851 (74)
	16	4	4500	3.3866 (47)	3.3950 (150)	3.3877 (26)	3.3872 (120)
0.10	8	12	25100	3.4637 (34)	3.4864 (25)	3.4842 (151)	3.4816 (113)
	16	9	15350	3.4752 (10)	3.4856 (138)	3.4756 (14)	3.4763 (11)

Table 3.4: Pseudo-critical couplings for different masses and volumes.

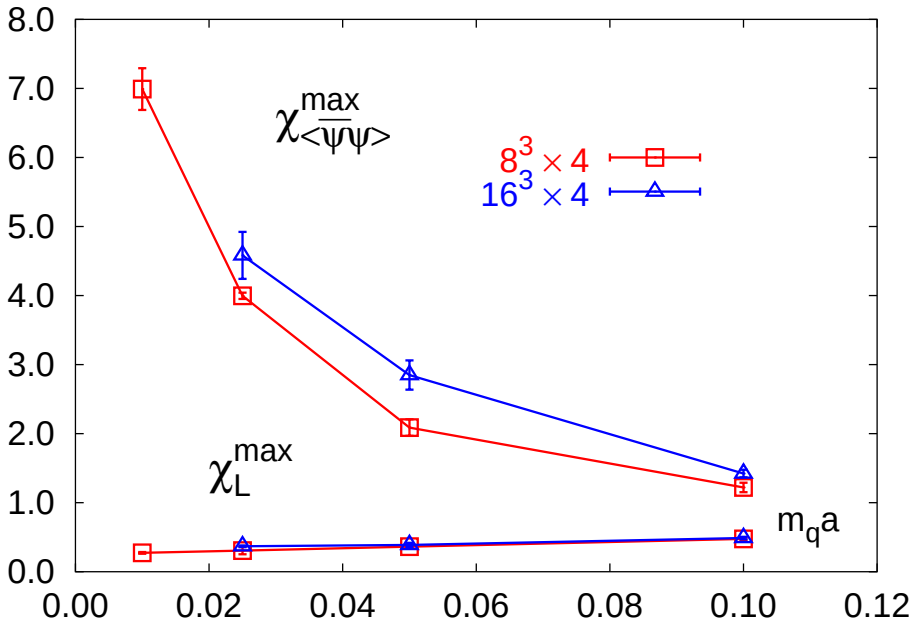

Figure 3.15: The maximum of the chiral and Polyakov loop susceptibility as a function of the bare quark mass for the lattice volumes $8^3 \times 4$ *and* $16^3 \times 4$.

at a universal value for different volumes, stay quite constant in a range between 2.2 and 2.8 for both volumes considered. This should be compared with the Ising, $O(4)$ and $O(2)$ universality classes discussed in connection with QCD, which have intersection points at 1.604, 1.233 and 1.092, respectively.

For standard staggered fermions [97, 98] two-state signals in the chiral condensate have been found for small quark masses. The discontinuity in $\langle \bar{\psi}\psi \rangle$ was extrapolated to zero to find the critical mass where the transition turns second order; they found $m_c a = 0.034$ corresponding to $m_c \approx 23$ MeV [98] in physical units when assuming a critical temperature of 180 MeV at the transition point. A scaling fit in $(m - m_c)^{-z}$ lead to a critical exponent z of 0.67(3) which is relatively close to the $Z(2)$ exponent 0.79. On the other hand, considering the results obtained for the Potts model [72] the determination of the first order endpoint by extrapolating to zero discontinuity in the order parameter seems not to be the appropriate procedure. One should instead look for a vanishing surface tension in the infinite volume limit or the intersection of the fourth Binder cumulant. In summary the staggered fermion action simulations thus suggest that the regime of first order transitions starts at very small quark masses of about 23 MeV. It is pushed to even smaller values of < 14MeV* when an improved action is used.

In contrast to the staggered formulation, results obtained with Wilson fermions suggest a first order transition already for rather large quark masses of 140MeV [99]. But one should note that the Wilson data do not seem reliable since they lead to an unphysically large discontinuity of the action at the transition point (figure 3.16) The latent heat can be calculated from the gap in the plaquette expectation value of the different phases using the formula $\Delta\epsilon/T^4 = -36 N_\tau^4 \, R_\beta \, \Delta\text{Plaq}$,

*Again a critical temperature of 180MeV has been assumed to set the scale. For the p4 fat link improved action at larger quark masses the same pseudo scalar to vector meson mass ratio as for standard staggered fermions shows up at half the bare quark mass. Therfore an additional factor of two has been introduced when the bare quark mass is expressed in physical units.

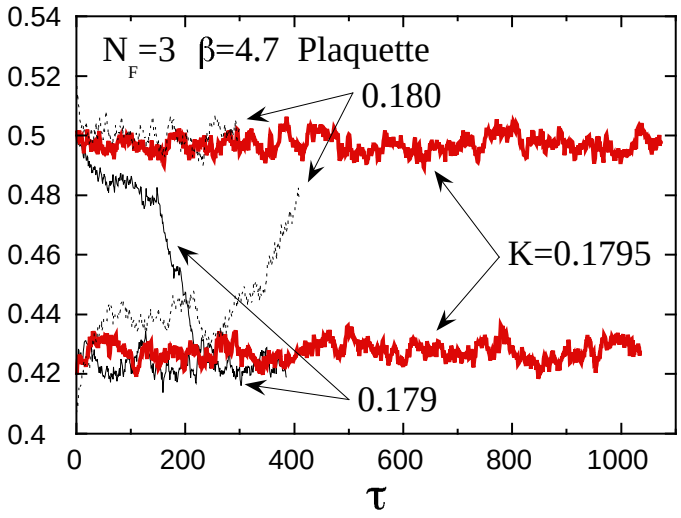

Figure 3.16: The time history of the plaquette for runs close to the critical point with standard Wilson fermions [99]. The red curve shows a run which gives a two state signal depending on the preparation of the system; cold or hot start.

which gives a value of $\Delta\epsilon/T^4 = 73.5$. This is about a factor of five larger than the Stefan-Boltzmann value at infinite temperatures, $\epsilon_{SB}/T^4 = 15.6$. Even when taking into account that there are strong cut-off effects for Wilson fermions which might lead to an overshooting over the Stefan-Boltzmann value by a factor of two, there seem to be other lattice artifacts involved, which are not well under control for unimproved Wilson fermions. As already mentioned it turned out in two flavour simulations that the use of an RG improved gluon action together with standard Wilson fermions reduces the lattice artifacts significantly [100]. Unfortunately for three flavours only exploratory simulations have been performed with this combination of quark and gluon actions [101].

The physical transition

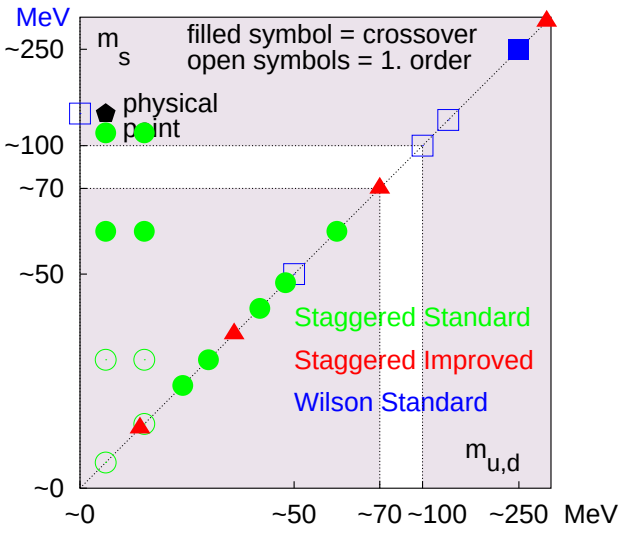

Figure 3.17: The order of the phase transition for 2+1 flavour simulations using standard staggered [97, 98], improved staggered and standard Wilson [99] actions.

Collecting all data available for 2+1 flavour simulations the staggered data give a consistent result whereas the data from Wilson fermions disagree with them (figure 3.17). This discrepancy then also leads to different results for the order of the phase transition at the physical point of two light and one heavier strange quark. For three staggered flavours the first order region already ends at a quark mass of about $14 - 25$ MeV and standard staggered simulations with two light and one heavier quark show no first order signal at quark masses even smaller than the physical one. The physical transition therefore very likely is a crossover. The prediction of a first order physical transition from Wilson fermions seems to be questionable for the problems with an unphysical action discontinuity mentioned above.
The order of the QCD phase transition has consequences for cosmological models and heavy ion collisions which will shortly be mentioned. In connection with the evolution of the early universe the QCD transition has been discussed as a source of matter inhomogeneities

created during the transition [83]. Remnants of these structures would only be visible until today if the transition was strongly first order. For pure gauge theory the latent heat and the surface tension calculated on the lattice [45] lead to results for the density fluctuations which are too small to explain the structure of the universe as it is observed today. For a continuous transition in full QCD, as predicted by staggered fermions, no observable consequences are expected. Rajagopal and Wilczek [65] discussed a continuous second order transition in the context of heavy ion collisions. Due to the divergence of the correlation length large volumes of space would be correlated and might lead to fluctuations in the ratio of charged to neutral pions. On the other hand in the physical world a non-zero quark mass would restrict the correlation length and no correlated volumes of space would emerge. Thus, if the QCD plasma cools through the transition while staying close to thermal equilibrium then no dramatic effect occurs and the QCD transition is a smooth crossover.

3.3 Conclusions

In this chapter the properties of the confinement-deconfinement and chiral phase transitions of QCD have been investigated for three degenerate quark flavours using the p4 improved staggered fermion and the tree-level improved 1×2 gluon action. In the regime of heavy quarks the first order phase transition gets weaker and finally disappears when the quark mass is reduced from infinity to some still large value. Using methods previously applied for the Potts model and the electroweak theory in lattice simulations, the critical endpoint for the first order region has been limited to the mass interval of $m_{\mathrm{PS}}/m_{\mathrm{V}} = 0.914(5)$ to $0.953(6)$. At a bare quark mass of $m_q a = 0.80$ the fourth Binder cumulant and the M-E-like distribution lead to the impression that the universality class is indeed the Ising one. This is predicted for QCD from a simulation of the three states Potts model with external field which might be regarded as an effective model for QCD with heavy quarks. For a final conclusive result probably larger lattices and higher statistics are needed.
The chiral transition which occurs at small quark masses has been analysed in a mass range where no clear sign of a first order transition shows up. Thus the universality class of the transition could not be analysed in this study. Indeed the crossover region expands down to bare quark masses of m_q= 14MeV or 25MeV for improved and unimproved staggered fermions, respectively. This finding combined with results obtained with two light and one heavier flavour suggest that the physical transition is a smooth crossover.

Chapter 4

QCD thermodynamics with improved staggered fermions

The final aim of QCD thermodynamic calculations is a lattice determination of the equation of state and the transition temperature at the physical point where the bare parameters are chosen such that the correct mass spectrum is realized. In such a simulation the contribution of strange quarks can no longer be neglected as it has been done in previous studies of two flavour QCD [28]. In this chapter a first attempt to incorporate the strange quark sector in a non-perturbative way in a complete thermodynamic calculation will be described. The following section is dedicated to the determination of the critical temperature with two and three light flavours and additionally two light and one heavy flavour using improved staggered fermions. The results will be compared to standard staggered, Wilson and domain wall fermion simulations and the effect of the strange quark will be analysed. In the second section the pressure and energy density for two, two plus one and three flavours will be discussed. The relative contribution of the strange quark to the equation of state can be extracted from this calculation at least for temperatures a few times the critical temperature. A correct determination of the situation close to the finite temperature phase transition cannot be expected since the correct chiral properties of QCD are not realized for the quark masses considered. Finally in both sections the finite cut-off effects in thermodynamic quantities are discussed. The comparison with unimproved staggered fermions shows a drastic reduction of cut-off distortions for the p4 action in the equation of state and the transition temperature.

4.1 The critical temperature

The critical temperature $T_c = 1/N_\tau a(\beta_c)$ is calculated by determining the pseudo critical couplings from the approximate order parameters of QCD, the chiral condensate and the Polyakov loop. Possible criteria to fix a value for β_c are the peak position of the susceptibilities or the vanishing of the third cumulant as discussed in chapter 3. The lattice spacing at the critical coupling has to be calculated from physical quantities. In this work the transition temperature is expressed in terms of the string tension σa^2 and the vector meson mass $m_V a$. For three quark flavours the critical couplings have been determined for the bare quark masses discussed in chapter 3. Additional simulations with the p4 fat action at bare quark masses of $m_{u,d}a = 0.05$, 0.10 and 0.20 for two and $m_{u,d}a = 0.10$, $m_s a = 0.25$ for two plus one flavours have been performed on zero and finite

$N_f = 2$							
	$T \neq 0$				$T = 0,\ N_\sigma^4 = 16^4$		
$m_{u,d}a$	$N_\sigma^3 \times N_\tau$	# β	# iter.	β_c	β	# iter.	period
0.05	$8^3 \times 4$	4	3700	3.585 (11)	3.585	340	2
0.10	$16^3 \times 4$	10	36300	3.646 (4)	3.60, 3.663, 3.70	2180	5
0.20	$8^3 \times 4$	6	6300	3.778 (12)	3.778	750	5
$N_f = 2+1$							
	$T \neq 0$				$T = 0,\ N_\sigma^4 = 16^4$		
$m_{u,d}a/m_s a$	$N_\sigma^3 \times N_\tau$	# β	# iter.	β_c	β	# iter.	period
0.10/0.25	$16^3 \times 4$	10	31550	3.543 (2)	3.55, 3.60	750	5
$N_f = 3$							
	$T \neq 0$				$T = 0,\ N_\sigma^4 = 16^4$		
$m_{u,d}a$	$N_\sigma^3 \times N_\tau$	# β	# iter.	β_c	β	# iter.	period
0.05	$16^3 \times 4$	6	6890	3.395 (15)	3.395	400	2
0.10	$16^3 \times 4$	16	21750	3.475 (2)	3.475	1000	5
0.20	$16^3 \times 4$	8	29650	3.602 (3)	3.602	980	5
0.40	$16^3 \times 4$	9	36600	3.772 (4)	3.771	750	5
0.60	$16^3 \times 4$	6	41750	3.877 (2)	3.876	1000	5
1.00	$16^3 \times 4$	8	101300	3.978 (2)	3.978	850	5

Table 4.1: The simulation parameters for the determination of the critical temperature. For the $T \neq 0$ lattice the largest lattice size simulated, the number of β values and iterations and the pseudo critical couplings are given. The β values, the number of iterations and the periodicity of the Wilson loop and meson correlation measurements are presented for the zero temperature simulation.

temperature lattices of size $8^3 \times 4$, $16^3 \times 4$ and 16^4, respectively. The string tensions are extracted from smeared Wilson loops as discussed in the appendix C and the pseudo scalar and vector meson masses have been determined from wall source correlation functions at couplings close to the critical one. The parameters of the finite and zero temperature simulations are collected in table 4.1. There the number of β values and iterations are given. In general the zero temperature simulations have been performed at the pseudo critical couplings. For some masses this is not realized and results from two or three couplings given in column 6 have been linearly interpolated to the critical β value. The Wilson loops and meson correlation functions have been measured on every fifth configuration for larger and on every second configuration for smaller quark masses. This periodicity is given in column 8.
The resulting string tension, pseudo scalar and vector meson masses are collected in table 4.2 together with $T_c/\sqrt{\sigma}$ and $T_c/m_{\rm V}$. In addition to the statistical error also the error due to the uncertainty in the pseudo critical coupling is taken into account in these quantities. This has been achieved by analysing the effect of a shift in β on the string tension and meson masses for $m_q a = 0.10$, where simulations at several values of the coupling have been performed. It has then been assumed that the relative effect is the same for other quark masses. Down to $m_q a = 0.10$ the additional error due to the uncertainty in β_c is negligibly small. This is no longer true for the mass $m_q a = 0.05$.

$N_f = 2$						
$m_{u,d}a$	β_c	σa^2	$m_{\rm PS}a$	$m_{\rm V}a$	$T_c/\sqrt{\sigma}$	$T_c/m_{\rm V}$
0.05	3.585 (11)	0.286 (14)	0.697 (6)	1.260 (35)	0.467 (11)	0.198 (6)
0.10	3.646 (4)	0.271 (10)	0.958 (2)	1.377 (25)	0.480 (10)	0.182 (4)
0.20	3.778 (12)	0.205 (12)	1.295 (15)	1.530 (35)	0.552 (16)	0.163 (4))
$N_f = 2+1$						
$m_{u,d}a/m_sa$	β_c	σa^2	$m_{\rm PS}a$	$m_{\rm V}a$	$T_c/\sqrt{\sigma}$	$T_c/m_{\rm V}$
0.10/0.25	3.543 (2)	0.271 (11)	0.962 (3)	1.343 (20)	0.480 (10)	0.186 (3)
$N_f = 3$						
$m_{u,d}a$	β_c	σa^2	$m_{\rm PS}a$	$m_{\rm V}a$	$T_c/\sqrt{\sigma}$	$T_c/m_{\rm V}$
0.05	3.395 (15)	0.303 (13)	0.706 (6)	1.320 (35)	0.454 (10)	0.189 (6)
0.10	3.475 (2)	0.283 (11)	0.967 (1)	1.415 (15)	0.470 (9)	0.177 (2)
0.20	3.602 (3)	0.248 (4)	1.322 (2)	1.608 (9)	0.502 (4)	0.155 (1)
0.40	3.772 (4)	0.189 (4)	1.814 (4)	1.985 (10)	0.575 (6)	0.126 (1)
0.60	3.877 (2)	0.176 (3)	2.210 (4)	2.347 (12)	0.596 (5)	0.107 (1)
1.00	3.978 (2)	0.154 (2)	2.838 (6)	2.979 (15)	0.637 (4)	0.084 (1)

Table 4.2: The critical temperature in terms of the string tension and rho meson mass. Additionally the critical couplings, the string tension and the rho meson and pion masses are given.

The two flavour transition temperature for p4 fat improved staggered fermions is compared to unimproved staggered, Wilson, Clover and domain wall fermions in figure 4.1(a) and 4.1(b) for $T_c/\sqrt{\sigma}$ and $T_c/m_{\rm V}$, respectively. For the transition temperature in units of the vector meson mass the discrepancy between unimproved staggered and Wilson fermions is largely reduced when improved fermion discretisations are used. Clover (green points), domain wall (turquoise points) and p4 improved staggered (blue points) results agree within 10%. This observation shows that standard staggered and Wilson fermions suffer from severe finite cut-off distortions different from pure gauge theory, where the cut-off effects are already small for the Wilson gauge action and consistent results can be obtained for different discretisations. The critical temperature $T_c/m_{\rm V}$ for improved actions turns out to be systematically larger than the standard staggered data at least for values of $m_{\rm PS}/m_{\rm V} > 0.5$. If this trend continues towards smaller quark masses then the transition temperature can be estimated to $T_c/m_{\rm V} = 0.23(1)$ ($T_c = 177(8)$ MeV) in the chiral limit.
The transition temperature in units of the string tension $\sqrt{\sigma}$ unfortunately does not agree for improved staggered and Clover data. One finds critical temperatures for the Clover action at $N_\tau = 4$ which are up to 20 % smaller than the standard staggered data whereas the p4 improved staggered results predict a critical temperature which is a few percent larger. On the other hand at smaller lattice spacing corresponding to the $N_\tau = 6$ critical point, a calculation using the non-perturbative Clover action [85] remarkably coincides with the improved staggered fermion result at $m_{\rm PS}/m_{\rm V} \approx 0.85$. This suggests that at $N_\tau = 4$ the lattice spacing even for improved Wilson fermions is still too large to reliably determine the scale from the string tension. The estimate for the critical coupling in the limit $m \to 0$ from $T_c/\sqrt{\sigma}$ is thus based on the quite linear trend for standard staggered fermions for smaller quark masses and the fact that for $m_{\rm PS}/m_{\rm V} > 0.5$ the p4 improved actions leads to a slightly larger $T_c/\sqrt{\sigma}$ compared to the standard action. As for $T_c/m_{\rm V}$ this suggests a critical temperature of about $T_c/\sqrt{\sigma} = 0.42(2)$ corresponding to 176(9) MeV.

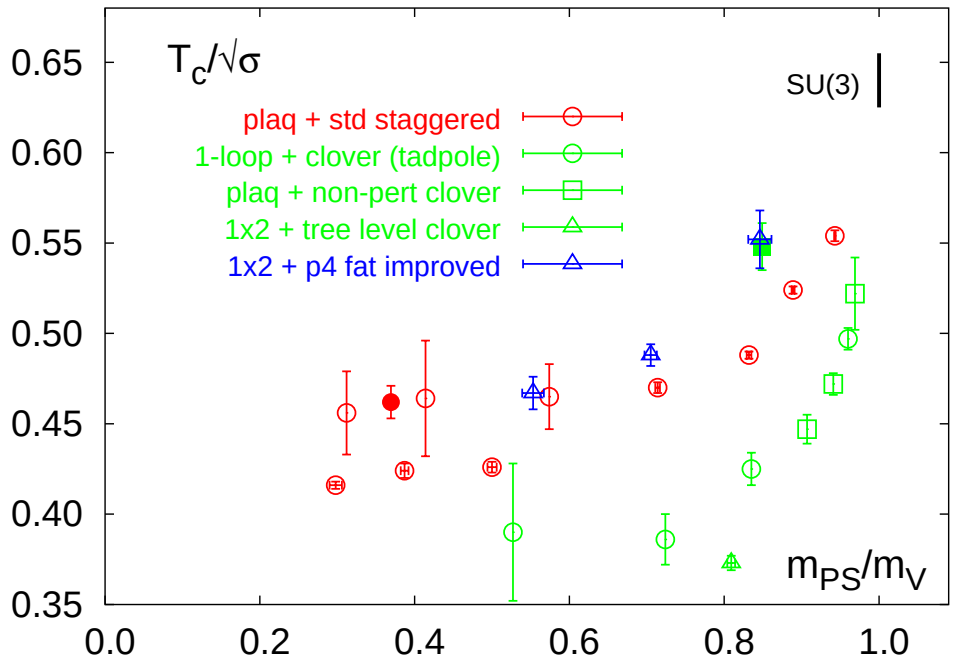

(a) $T_c/\sqrt{\sigma}$

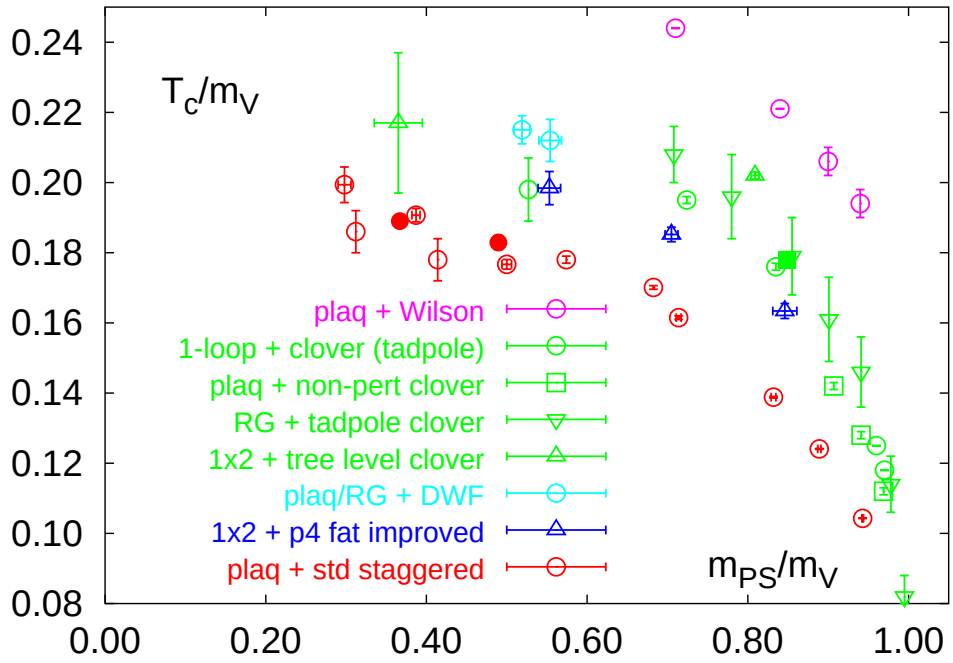

(b) T_c/m_V

Figure 4.1: The transition temperature for two flavour QCD in units of the string tension and the vector meson mass. Open/filled symbols correspond to $N_\tau = 4$ and 6. All standard staggered data [57, 86] are plotted in red, the standard Wilson data [87] in pink and results for domain wall fermions [88] in turquois. The p4 improved staggered data are in blue, the different Clover results [85, 89, 86] in combination with several gluon actions are all plotted in green.

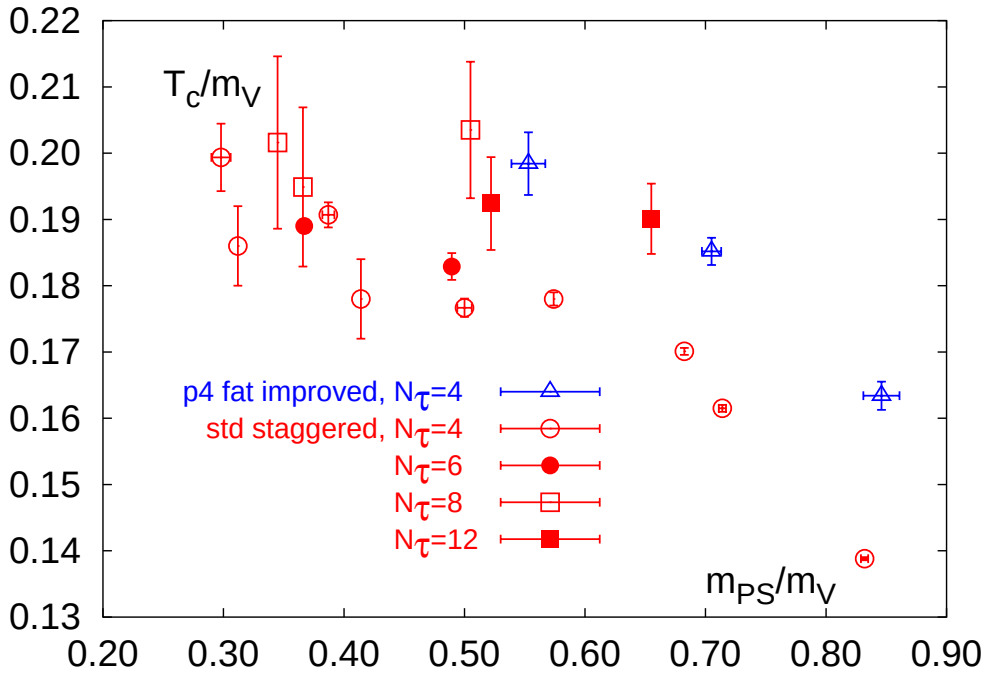

Figure 4.2: T_c/m_V for standard [57, 90] and p4 fat improved staggered fermions versus m_{PS}/m_V.

The cut-off effects for staggered fermions can be analysed by comparing the results from the p4 fat improved action with standard staggered data for T_c/m_V with N_τ up to 12. From figure 4.2 one can read off the tendency that with increasing N_τ the transition temperature in units of the vector meson mass becomes larger. For $N_\tau = 8$ and even more 12 the results agree with the calculation using improved staggered fermions at $N_\tau = 4$. There is thus clear evidence that the sizable cut-off effects in T_c/m_V for standard staggered fermions can be reduced with the p4 action.
One of the main goals of this work is to investigate the flavour dependence of thermodynamic quantities. The results for two, two plus one and three flavours which are collected in table 4.1 are plotted in figures 4.3(a) and 4.3(b). The qualitative behaviour is quite the same for two and three flavours. A rapid drop or strong increase for $T_c/\sqrt{\sigma}$ and T_c/m_V, respectively, is apparent for quite large quark masses. The comparison of results with the p4 improved action shows that the dependence on the number of quark flavours is a small but systematic effect. As one would expect when increasing the number of degrees of freedom of the system, the critical temperatures for three flavours is smaller than the two flavour one at the same meson mass ratio. The four flavour Naik results do also support this observation. The one data point from the two plus one flavour simulation does agree within errors with $T_c/\sqrt{\sigma}$ and T_c/m_V for two flavours. Thus the heavier strange quark seems to be irrelevant for the transition temperature and the dynamics at the transition seems to be dominated by the lightest particle state, the pseudo scalar corresponding to the pion. The pseudo scalar masses extracted from the up/down - up/down and strange - up/down quark propagators, the pion and the kaon, have been determined to be 0.962 (3) and 1.255 (5), respectively. This gives a pion to kaon mass ratio of m_π/m_K =0.77(1). Since at the physical point this ratio is about 0.30 one might expect that the dominance of the pion for the dynamics of the transition is even enhanced and the two plus one and two flavour critical temperatures also agree in the chiral limit for a fixed strange quark mass of $m_s/T = 1$.
In the figures 4.4(a) and 4.4(b) the same results for the critical temperature are plotted against

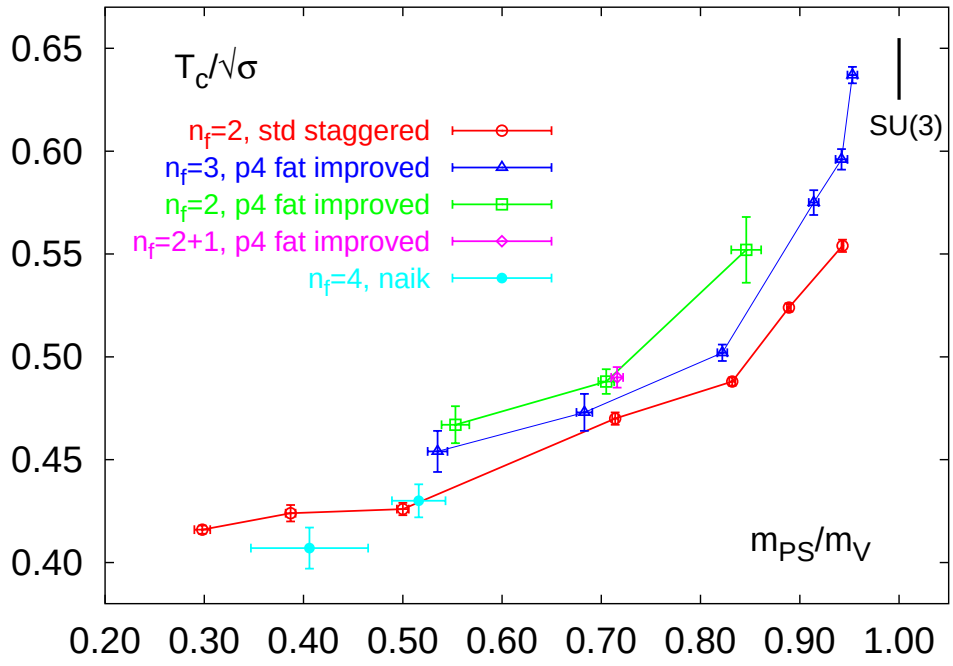

(a) $T_c/\sqrt{\sigma}$

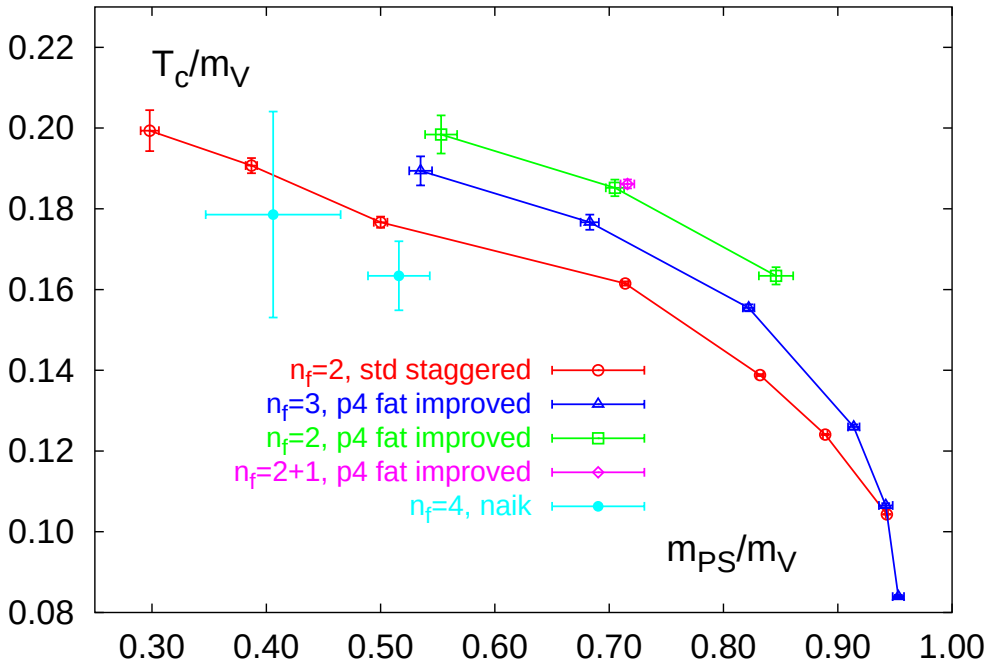

(b) $T_c/m_{\rm V}$

Figure 4.3: The critical temperature versus $m_{\rm PS}/m_{\rm V}$ for different number of flavours using standard [57], Naik [56] and p4 fat improved staggered fermions.

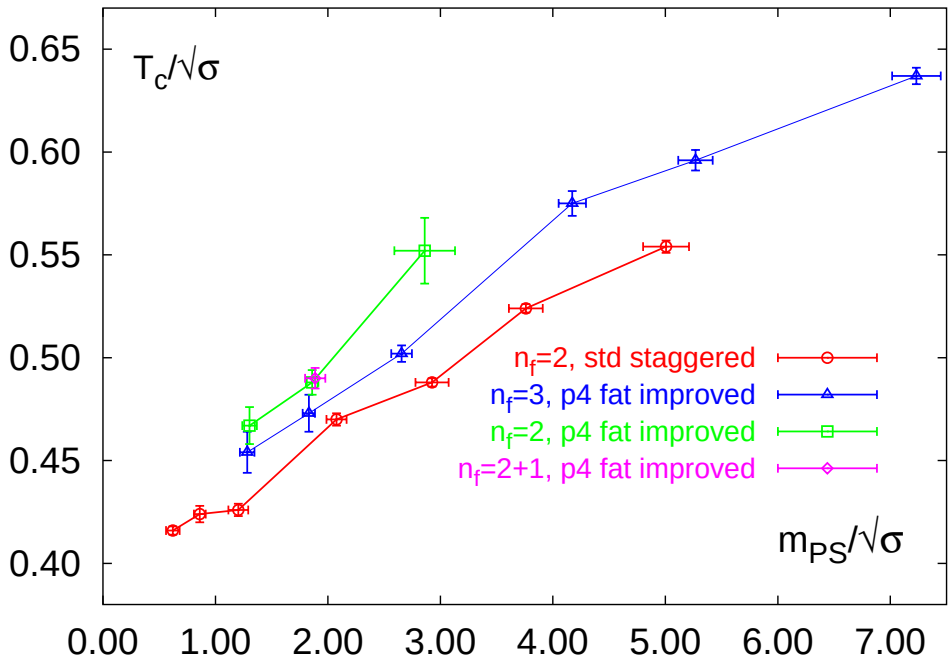

(a) $T_c/\sqrt{\sigma}$

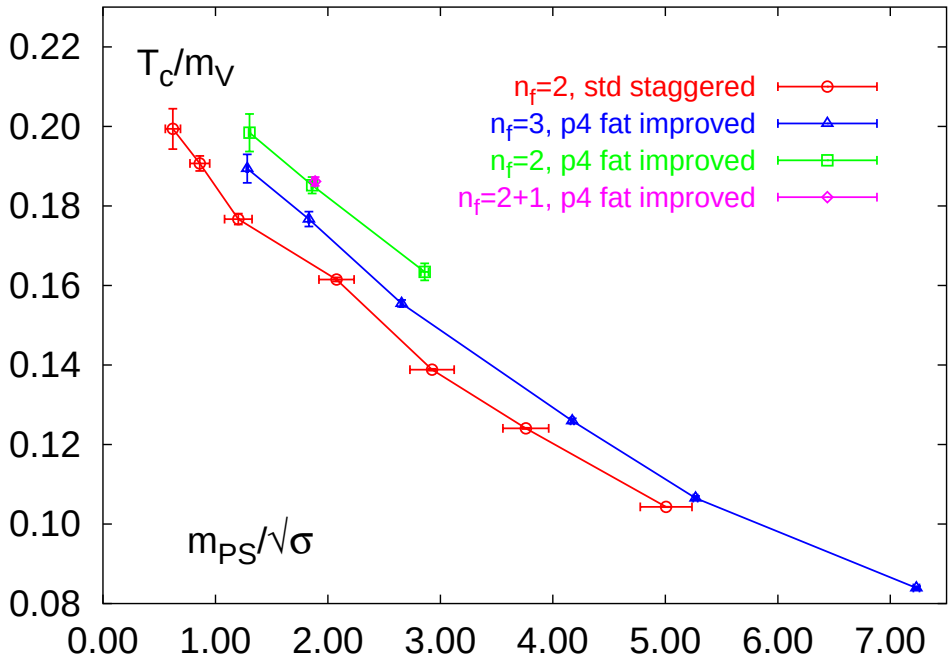

(b) T_c/m_{V}

Figure 4.4: The transition temperature for two, two plus one and three flavour QCD in units of the string tension and the vector meson mass versus $m_{\mathrm{PS}}/\sqrt{\sigma}$ with standard [57] and p4 fat improved staggered fermions.

$m_{PS}/\sqrt{\sigma}$. They show quite a linear trend over the whole range of mass values. For two flavour QCD an extrapolation linearly in $m_{PS}/\sqrt{\sigma}$ leads to approximately the same critical temperature of about 180 MeV as for the extrapolation in m_{PS}/m_V. In the case of three flavours T_c is about 5 to 10 MeV lower.

4.2 The equation of state

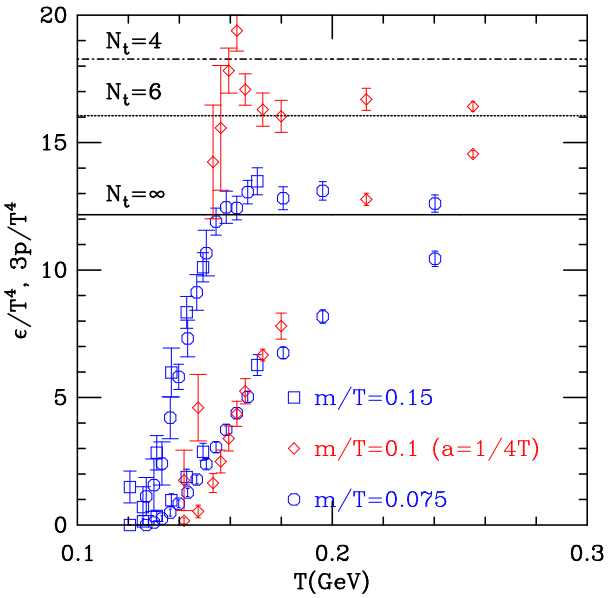

Figure 4.5: The equation of state along lines of constant m_q/T. The blue symbols correspond to $N_\tau = 6$ results for two mass values. The blue symbols are results on an $N_t = 4$ lattice. Horizontal lines correspond to Stefan-Boltzmann value for $N_t = 4$, 6, and the continuum.

In this section the equation of state for two, two plus one and three quark flavours using the 1×2 improved gauge action and the p4 fat improved staggered fermion action will be analysed. One point of interest is the reduction of the large cut-off effects present for the standard Wilson gauge and staggered fermion action. There the results for the pressure and the energy density from $N_\tau = 4$ and $N_\tau = 6$ simulations differ significantly [28]. In figure 4.2 they are plotted for points of constant m_q/T. The energy density increases rapidly near the transition while the pressure only rises smoothly. For both N_τ=4 and 6 lattices the energy density is much smaller than the infinite temperature Stefan-Boltzmann value.
A second interesting question is connected to the influence of strange quarks on the equation of state. In the context of heavy ion collision the enhancement of strange particles is discussed as a signature for the formation of a quark-gluon plasma [91]. Since the relative production rate of strange anti-strange quark pairs is higher in a quark gluon plasma than the production of bound states containing a strange quark in a hadron gas it is expected that the relative abundance of strange particles after the freeze out is an appropriate signal to test whether the system has been in the plasma state of matter or not. This simple picture has to be refined by taking into account the detailed dynamics of the heavy ion experiment to really have predictive power.
On the lattice a first analysis of the contribution of the strange quark sector to the energy density has been performed by Kogut *et al.* [92] already in 1987 with a temporal extent $N_\tau = 4$. They calculated the fermionic part of the energy density by separately taking into account the contributions from the light and heavy quarks,

$$\begin{aligned}
\frac{\epsilon_{u,d}}{T^4} &= \left(\frac{N_\tau}{N_\sigma}\right)^3 \frac{n_{u,d}}{4}\left(\left.\frac{d\gamma_F}{d\xi}\right|_{\xi=1} \overline{\langle \mathrm{Tr}\ D_4\ M^{-1}\rangle}_{u,d} + \left.\frac{dm_{u,d}a}{d\xi}\right|_{\xi=1} \overline{\langle \mathrm{Tr}\ M^{-1}\rangle}_{u,d}\right) \\
\frac{\epsilon_{s}}{T^4} &= \left(\frac{N_\tau}{N_\sigma}\right)^3 \frac{n_{s}}{4}\left(\left.\frac{d\gamma_F}{d\xi}\right|_{\xi=1} \overline{\langle \mathrm{Tr}\ D_4\ M^{-1}\rangle}_{s} + \left.\frac{dm_{s}a}{d\xi}\right|_{\xi=1} \overline{\langle \mathrm{Tr}\ M^{-1}\rangle}_{s}\right) \quad , \qquad (4.1)
\end{aligned}$$

where in the quantity $\overline{\langle \mathcal{O} \rangle}$ the zero temperature contributions are already subtracted. Such a separation of ϵ/T^4 in a gluonic, light and heavy quark sector is only correct for non-interacting systems. Especially in the temperature regime a few times T_c pure gauge results for the equation of state have turned out to be of non-perturbative nature. Perturbative descriptions failed to give the correct behaviour. Additionally the derivative $d\gamma_F/d\xi\big|_{\xi=1}$ has only been approximated by its lowest order perturbative value

$$\left.\frac{d\gamma_F}{d\xi}\right|_{\xi=1} = 1 + \mathcal{O}(g^2) \quad .$$

The total derivative of the masses with respect to the anisotropy vanishes in the chiral limit, therefore this part in ϵ_F has been neglected.

$$\left.\frac{dm_q a}{d\xi}\right|_{\xi=1} \to 0 \quad \text{as} \quad m_q a \to 0 \quad .$$

For the strange quark this is however a crude approximation since m_s/T should be of the order of one at T_c.
The final result of reference [92] is plotted in figure 4.6 where the contribution to ϵ_F from the two light and one heavy quarks are normalized to one flavour. At temperatures $T \gg T_c$ the energy density for the light isodoublett shows ideal gas behaviour. In the strange quark sector even at temperatures a few times the critical temperature the strange quark contribution is strongly suppressed. Close to the transition point the energy density in the strange quark sector reaches only half the value of a non-interacting Fermi gas. These results, however, have to be interpreted with care, since the assumptions and approximations discussed above are in no way justified. Furthermore as already pointed out, do staggered fermions at $N_\tau = 4$ suffer from severe cut-off effects. In this work a simulation is performed which uses methods which in principle allow a complete non-perturbative calculation of the pressure and the energy density and is designed to reduce the cut-off distortions.

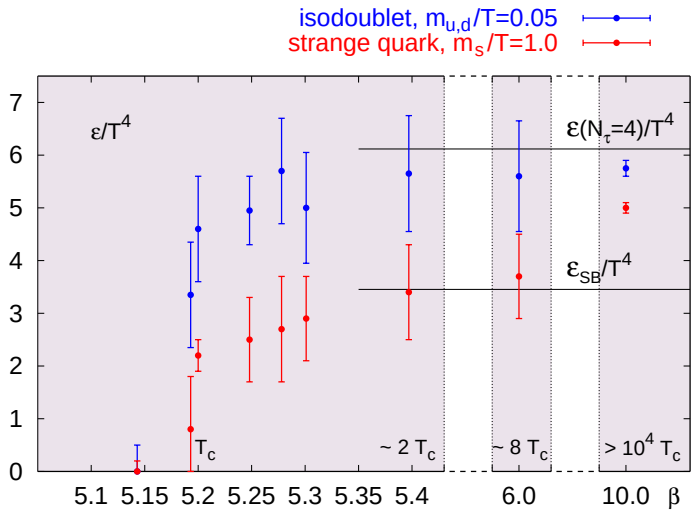

Figure 4.6: The fermionic part of the energy density calculated for two light flavours with $m_{u,d}/T = 0.1$ and one heavier flavour with $m_s/T = 1.00$.

4.2.1 The numerical simulation

Numerical simulations on finite and zero temperature lattices of size $16^3 \times 4$ and 16^4 have been performed at several values of the gauge coupling for two, two plus one and three flavours. The light bare quark masses are $m_{u,d}a = 0.10$ and the heavier strange quark mass is $m_s a = 0.25$ corresponding to $m_s/T = 1.00$. On the $16^3 \times 4$ lattice 15 to 20 β values have been calculated with

a statistics of up to 3000 trajectories close to the critical point and 1000 trajectories away from it. In the zero temperature simulations up to 800 trajectories were generated to obtain a statistical error comparable to the finite temperature calculations.
On the $T \neq 0$ lattices the pseudo critical couplings have been extracted from the peak position of the chiral susceptibility (table 4.3). Results consistent with these values can also be found when analysing the Polyakov loop susceptibility or the third Binder cumulant. The scale has been set by either calculating the string tension σa^2 or the pseudo scalar and vector meson masses $m_{\rm V}$ and $m_{\rm PS}$, respectively. In the two plus one flavour case in addition to the pseudo scalar corresponding to the pion also the kaon has been analysed. These masses are also given in table 4.3. The ratio of pseudo scalar and vector meson masses is in all three cases, $m_{\rm PS}/m_{\rm V} \simeq 0.7$ indicating that the quark masses used in this analysis are certainly too large to investigate in more detail the temperature interval close to T_c, where the correct chiral properties of QCD have to be realized. In the high temperature phase, however, the dependence on the bare quark masses has been found

n_f	β_c	σa^2	$T_c/\sqrt{\sigma}$	$T_c/m_{\rm V}$	$m_{\rm PS}a$		$m_{\rm V}a$
					$m_\pi a$	$m_{\rm K}a$	
2	3.646 (4)	0.271 (10)	0.480 (10)	0.182 (4)	0.958 (2)	-	1.377 (25)
2+1	3.543 (2)	0.271 (11)	0.480 (10)	0.186 (3)	0.962 (3)	1.255(5)	1.343 (20)
3	3.475 (2)	0.283 (11)	0.470 (9)	0.177 (2)	0.967 (1)	-	1.415 (15)

Table 4.3: Pseudo-critical couplings, string tensions calculated at these couplings and the resulting pseudo-critical temperatures for $n_f = 2$ and 3 as well as QCD with two light and a heavier strange quark. In addition results for the pseudo scalar and vector meson masses are given.

to be strongly reduced [56, 28] and reliable conclusions may be expected.
The temperature scale T/T_c is fixed by string tension measurements for several couplings on zero temperature lattices,

$$\frac{T}{T_c}(\beta) = \frac{1/N_\tau a(\beta)}{1/N_\tau a(\beta_c)} = \frac{\sqrt{\sigma}a(\beta_c)}{\sqrt{\sigma}a(\beta)} \quad .$$

The details of these calculations can be found in the appendix C. A parametrisation of $\sqrt{\sigma}a$ as a function of β will be used to calculate T/T_c also at intermediate couplings where there are no measurements performed. The ansatz is motivated by renormalisation group arguments [93]

$$\sqrt{\sigma}a(\beta) = R(\beta)(1 + c_2\hat{a}^2(\beta) + c_4\hat{a}^4(\beta))/c_0 \tag{4.2}$$

with $\hat{a} \equiv R(\beta)/R(\bar{\beta})$. From the discussion in the appendix one knows that it is only suitable for an interpolation and can in this form not be used to extrapolate to the continuum limit.

4.2.2 The pressure p/T^4

The pressure has been calculated using the integral method [94] which makes use of the fact that for homogeneous systems it is directly related to the free energy density by $p = -f = TV^{-1}\ln Z$. The derivative of this equation with respect to β and finally the integration of the resulting gauge action yields the pressure

$$\frac{p}{T^4}\Big|_{\beta_0}^{\beta} = \left(\frac{N_\tau}{N_\sigma}\right)^3 \int_{\beta_0}^{\beta} d\beta' \left(\langle S_G\rangle_0 - \langle S_G\rangle_T\right) \quad . \tag{4.3}$$

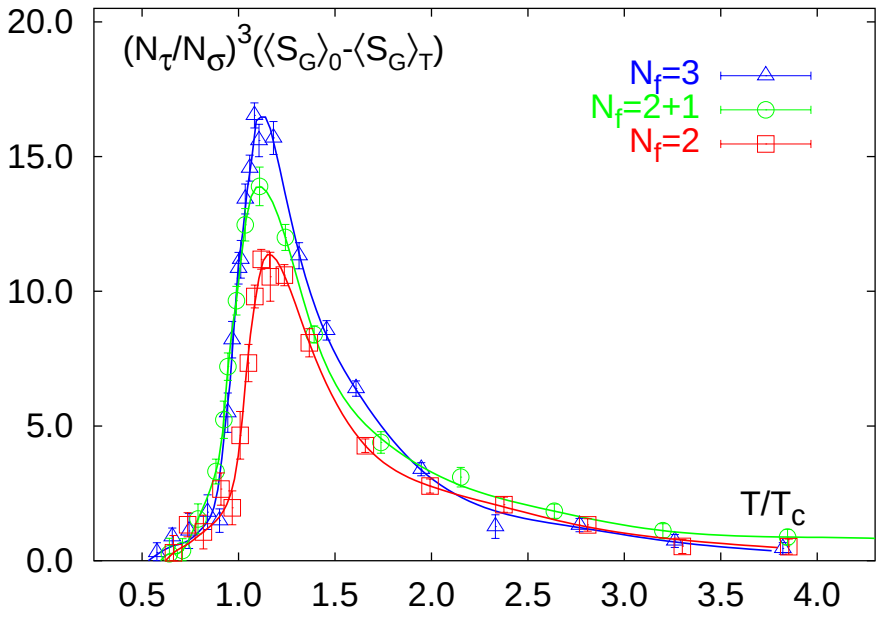

Figure 4.7: The action differences from 16^4 and $16^3 \times 4$ lattices for $n_f = 2$, 3 and 2+1.

The zero temperature contribution $\langle S_G \rangle_0$ calculated on the 16^4 lattice is subtracted to normalize the pressure to zero at $T = 0$. The action difference for the two, two plus one and three flavour simulations are plotted in figure 4.7 for values of the coupling corresponding to a temperature range of $0.6\ T_c \leq T \leq 4\ T_c$. At around $T_0 \simeq 0.6 T_c$ the action difference is zero within errors which defines the lower border for the integration. For the peak in the action difference a systematic increase with increasing number of flavours is visible in figure 4.7, which after integration leads to the increase of the pressure with increasing number of the degrees of freedom. This is apparent from figure 4.8a, where the pressure for $n_f = 2$ and 3 as well as the 2+1-flavour case is shown.
To test whether the flavour dependence for the QCD pressure is the same as for a non-interacting system of quarks and gluons, the pressure is normalised to an ideal quark gluon gas,

$$\frac{p_{\mathrm{SB}}}{T^4} = \left(16 + \frac{21}{2} g_f\right) \frac{\pi^2}{90} \quad . \tag{4.4}$$

Here g_f counts the effective number of degrees of freedom of a massive Fermi gas which contribute to the free energy or pressure. For a massless gas $g_f = n_f$, in general it is defined as

$$g_f = \sum_{f=u,d,..} g(m_f/T) \quad , \tag{4.5}$$

with

$$g(m/T) = \frac{360}{7\pi^4} \int_{m/T}^{\infty} \mathrm{d}x x \sqrt{x^2 - (m/T)^2} \ln\left(1 + \mathrm{e}^{-x}\right) \quad . \tag{4.6}$$

For the quark mass values used in this analysis one gets $g(0.4) = 0.9672$ and $g(1) = 0.8275$, respectively. The correspondingly normalized curves are given in figure 4.8b. They indicate that for two and three flavours the dependence on n_f is at least for $T \gtrsim 2T_c$ governed by the ideal gas

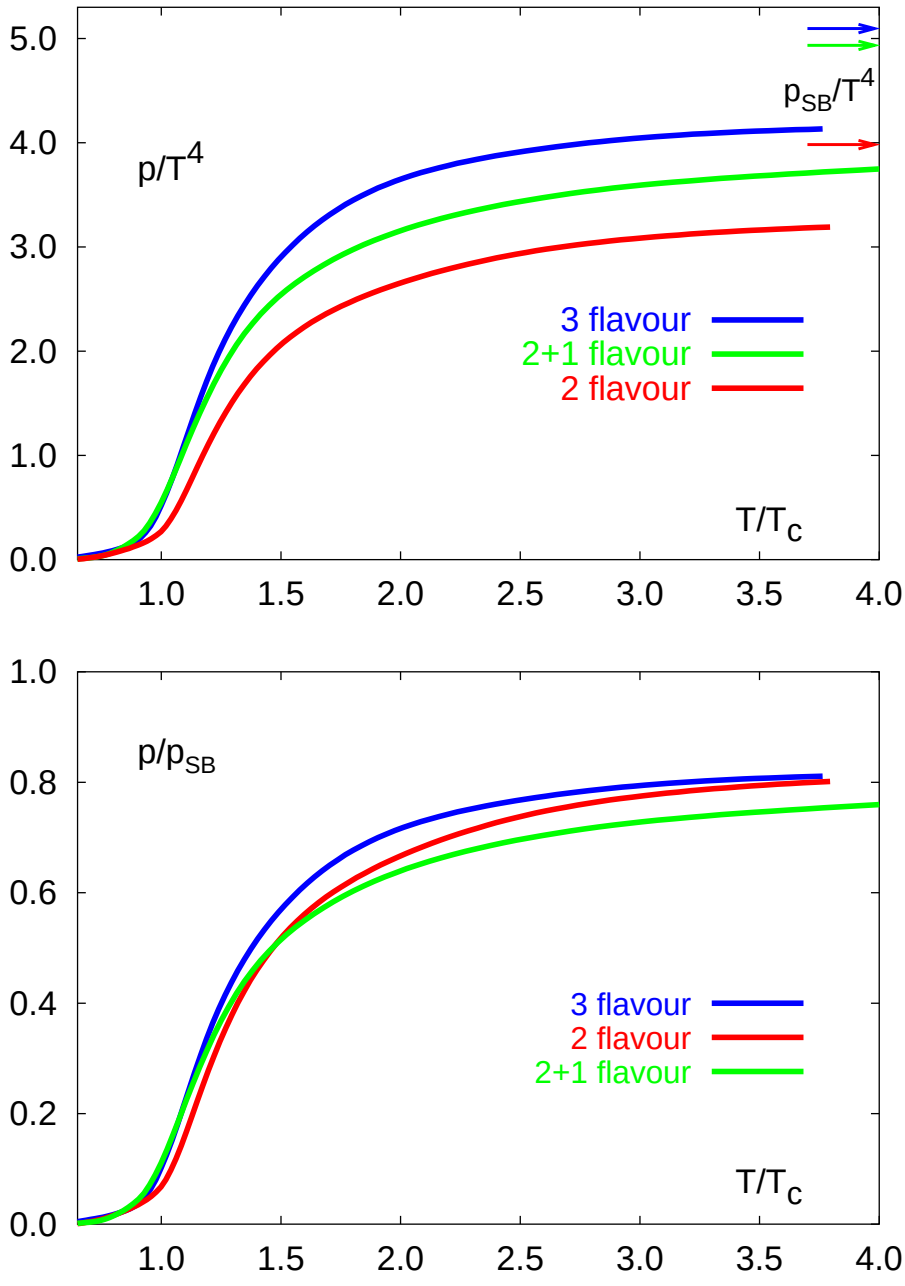

Figure 4.8: The pressure for $n_f = 2$, 2+1 and 3 calculated with the p4-action (a) and the normalized values $p/p_{\rm SB}$ (b).The arrows indicate the continuum ideal gas limits for two and three flavour QCD with quarks of mass $m_{u,d}/T = 0.4$ as well as the case of two flavour QCD with $m_{u,d}/T = 0.4$ and an additional heavier quark of mass $m_s/T = 1$.

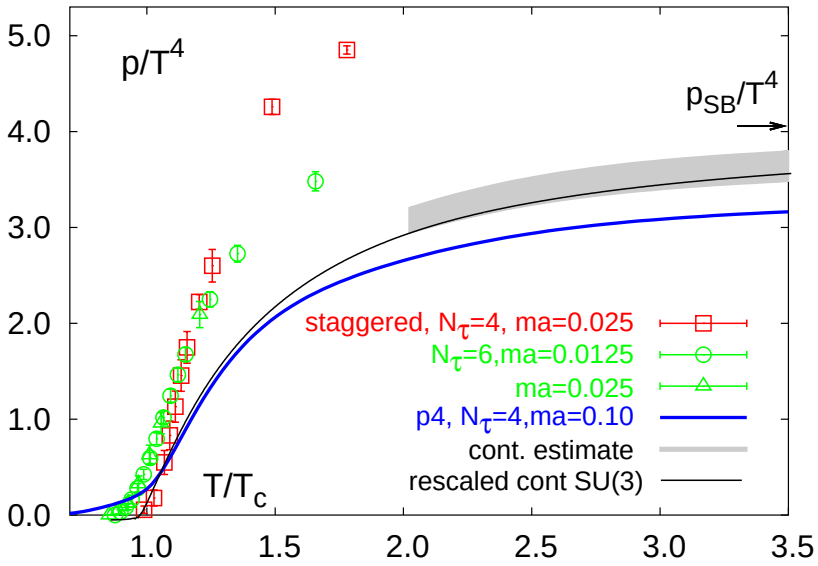

Figure 4.9: The pressure for $n_f = 2$. Shown are results obtained with the p4-action on lattices with temporal extent $N_\tau = 4$ (line) as well as with the standard staggered fermion action on $N_\tau = 4$ (squares) and 6 (circles, triangles) lattices. Also shown is an estimate of the continuum equation of state for massless QCD (grey band), based on the assumption that the systematic error of the current analysis is $(15 \pm 5)\%$ and the continuum extrapolation of pure gauge theory rescaled by the appropriate number of degrees of freedom.

behaviour. In the presence of a heavier quark the deviations of the pressure from the ideal gas value is larger than in the massless limit . This is in qualitative agreement with the observations made by Kogut *et al.* [92].

Cut-off effects

The cut-off distortions for different combinations of gluon and fermion actions are plotted in figure 4.10 for the free energy. The $N_\tau = 4$ values of these perturbative calculations can be compared to actual simulations performed with these actions for different number of quark flavours. Obviously the numerical results normalized by the corresponding Stefan Boltzmann values qualitatively follow the same pattern as the ideal gas ratio f/f_{SB} (figure 4.11). This clearly shows that also in full QCD simulations the perturbative calculation of the high temperature limit gives useful hints for the quality of the action in thermodynamic studies as it is the case for quenched simulations. Although this analysis is restricted to a single temporal lattice size, i.e. $N_\tau = 4$, one may try to estimate the continuum limit. Since a complete extrapolation to $a = 0$ would demand calculations at larger N_τ, the remaining cut-off effects have to be estimated on the basis of what has been found in pure gauge simulations. There the analyses of finite cut-off effects have shown that at temperatures $T \simeq (2-4)\ T_c$ the ideal gas calculations correctly describe qualitative features of the cut-off dependent terms. However, they overestimate their influence by roughly a factor 2. If this carries over to calculations with light quarks, which also have a thermal mass of $\mathcal{O}(g(T)T)$ one may expect that the finite cut-off distortion in this numerical calculations is also reduced by

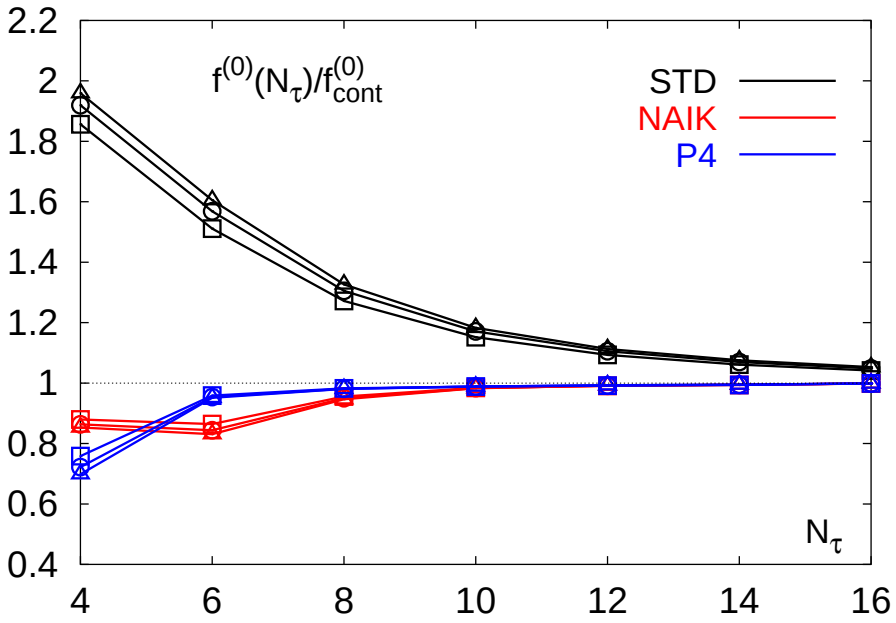

Figure 4.10: The ideal gas value of the pressure for the standard staggered and Wilson gauge action, the p4 and Naik improved staggered with 1×2 gauge action. To distinguish the number of quark flavours different plotting symbols have been used. The triangle for four, the circle for three and the square for two flavours.

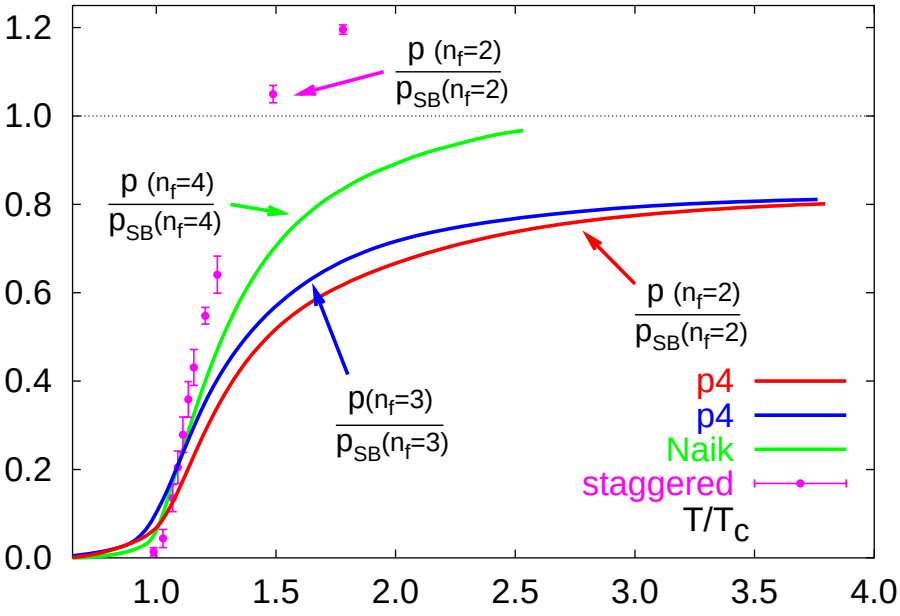

Figure 4.11: The pressure at $N_\tau = 4$ normalized by the appropriate Stefan Boltzmann value for the Naik action ($n_f = 4$), the p4 fat action ($n_f = 2,\ 3$) and the standard staggered action ($n_f = 2$).

a similar factor. The ideal gas limit for the p4 improved action leads to results which are 26% and 29% below the continuum value for $n_f = 2$ and 3, respectively. Combined with the small systematic errors resulting from the use of non-zero quark masses in this calculation one may thus expect that the continuum equation of state for massless QCD at temperatures $T \gtrsim 2T_c$ is about 15% above the values obtained in the simulation. This estimate for the continuum limit is shown for two-flavour QCD in figure 4.9 together with results from a calculation with the standard Wilson gauge and staggered fermion action on lattices with temporal extent $N_\tau = 4$ and 6 [28]. These latter data lie substantially higher which is in accordance with the larger cut-off effects for the unimproved actions.
An alternative estimate for the continuum limit comes from the observation that at high temperatures the flavour dependence agrees with that of an ideal gas. One thus may try to rescale the continuum extrapolation of the pressure in pure gauge theory with the appropriate number of degrees of freedom. The resulting curve which is also shown in figure 4.9 is in good agreement to the continuum estimate based on the correction of cut-off effects.

4.2.3 The interaction measure $(\epsilon - 3p)/T^4$ and the energy density ϵ/T^4

The calculation of $(\epsilon - 3p)/T^4$ is much more involved than for the pressure since one additionally needs the β-functions for the gauge coupling and the quark mass. In the case of two plus one quark flavours the following expression has to be evaluated

$$\begin{aligned}
\frac{\epsilon - 3p}{T^4} &= \left(\frac{\epsilon - 3p}{T^4}\right)_{\text{gluon}} + \left(\frac{\epsilon - 3p}{T^4}\right)_{\text{up,down}} + \left(\frac{\epsilon - 3p}{T^4}\right)_{\text{strange}} \\
\left(\frac{\epsilon - 3p}{T^4}\right)_{\text{gluon}} &= \left(\frac{N_\tau}{N_\sigma}\right)^3 R_\beta \left(\langle S^{1\times 2}\rangle_0 - \langle S^{1\times 2}\rangle_T \right) \\
\left(\frac{\epsilon - 3p}{T^4}\right)_{\text{up,down}} &= \left(\frac{N_\tau}{N_\sigma}\right)^3 \frac{n_{u,d}}{4} R_{m_{u,d}} \left(\langle \text{Tr } M^{-1}\rangle_0 - \langle \text{Tr } M^{-1}\rangle_T \right)_{m_{u,d}} \\
\left(\frac{\epsilon - 3p}{T^4}\right)_{\text{strange}} &= \left(\frac{N_\tau}{N_\sigma}\right)^3 \frac{n_s}{4} R_{m_s} \left(\langle \text{Tr } M^{-1}\rangle_0 - \langle \text{Tr } M^{-1}\rangle_T \right)_{m_s} \quad , \qquad (4.7)
\end{aligned}$$

with $R_\beta = a(d\beta/da)|_{(am_{u,d};am_s)}$ and $R_{m_{u,d/s}} = a(dam_{u,d/s}/da)|_{(\beta,am_{s/u,d})}$. One thus has to analyse in addition to the action differences also the difference of the operator $\langle \text{Tr } M^{-1}\rangle$ on zero and finite temperature lattices. The results are plotted in figure 4.12 for the light and in the $n_f = 2+1$ case also for the heavier quark.
From the interpolation of the string tension measurements presented in appendix C the β-function R_β can be determined non-perturbatively via the expression

$$a\frac{d\beta}{da}\bigg|_{(am_{u,d};am_s)} = \sqrt{\sigma}a\left(\frac{da\sqrt{\sigma}}{d\beta}\right)^{-1}\bigg|_{(am_{u,d},am_s)} \quad .$$

From the calculations performed in this work the β-function for the quark masses can only be approximated. In principle they can be determined from hadron masses using

$$\begin{aligned}
a\frac{dam_\pi}{da} &= am_\pi \\
a\frac{dam_\rho}{da} &= am_\rho \\
a\frac{dam_{\text{K}}}{da} &= am_{\text{K}} \quad . \qquad (4.8)
\end{aligned}$$

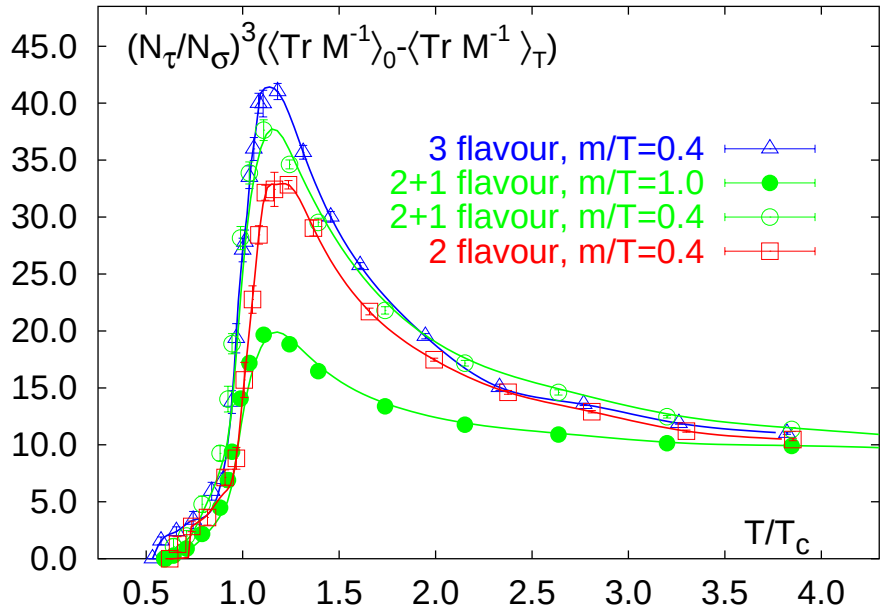

Figure 4.12: The difference of $\langle TrM^{-1}\rangle$ on zero and finite temperature lattices for $n_f = 2$, 2+1 and 3 calculated with the p4-action. Given are the results for the light quarks with $m/T = 0.4$ and the heavier quark of the two plus one flavour simulation with $m/T = 1.00$.

Since the meson masses are functions of β, $am_{u,d}$ and am_s these expressions can be rewritten

$$\begin{aligned} R_\beta \frac{\partial \ln am_\pi}{\partial \beta} + R_{m_{u,d}} \frac{\partial \ln am_\pi}{\partial am_{u,d}} + R_{m_s} \frac{\partial \ln am_\pi}{\partial am_s} &= 1 \\ R_\beta \frac{\partial \ln am_\rho}{\partial \beta} + R_{m_{u,d}} \frac{\partial \ln am_\rho}{\partial am_{u,d}} + R_{m_s} \frac{\partial \ln am_\rho}{\partial am_s} &= 1 \\ R_\beta \frac{\partial \ln am_{\mathrm{K}}}{\partial \beta} + R_{m_{u,d}} \frac{\partial \ln am_{\mathrm{K}}}{\partial am_{u,d}} + R_{m_s} \frac{\partial \ln am_{\mathrm{K}}}{\partial am_s} &= 1 \quad . \end{aligned} \tag{4.9}$$

One now assumes that the mesons containing no strange quark are independent of the strange quark mass. This seems to be justified by the small difference in the spectrum calculation of am_{PS} and am_{V} for 2, 2+1 and 3 flavours. Then the partial derivative of the pion and rho mass with respect to m_s vanishes and the system of linear equations simplifies. Furthermore one has to choose an explicit ansatz for the quark mass dependence of the meson masses since a direct measurement has not been carried out. In this work the following expressions have been used

$$\begin{aligned} am_\pi^2 &= h(\beta)\ am_{u,d} \\ am_\rho &= f(\beta) + g(\beta)\ am_{u,d} \\ am_{\mathrm{K}}^2 &= l(\beta) \frac{am_{u,d} + am_s}{2} \quad , \end{aligned} \tag{4.10}$$

where the quadratic dependence of the pseudo scalar mesons on the quark mass is motivated by their Goldstone character for the flavour $SU(2)$ or $SU(3)$, respectively.

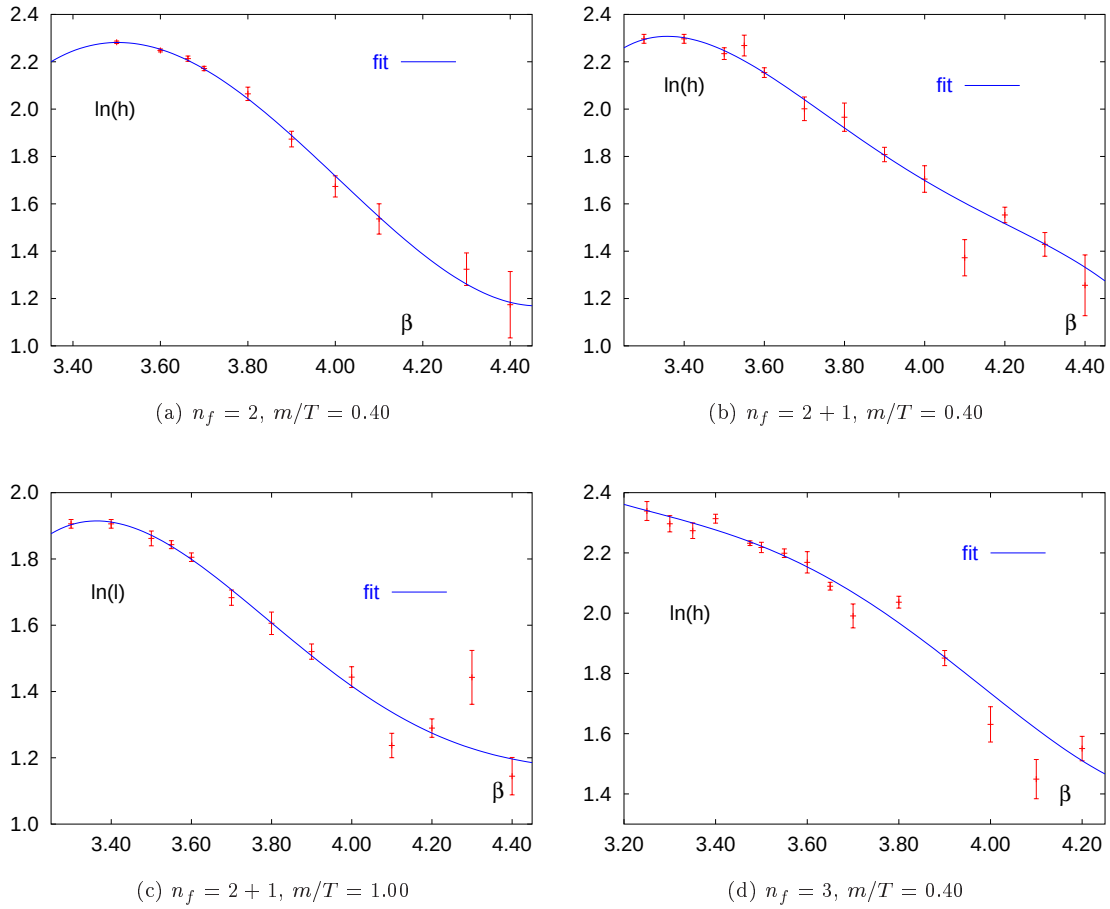

(a) $n_f = 2$, $m/T = 0.40$

(b) $n_f = 2+1$, $m/T = 0.40$

(c) $n_f = 2+1$, $m/T = 1.00$

(d) $n_f = 3$, $m/T = 0.40$

Figure 4.13: The functions $\ln h(\beta)$ and $\ln l(\beta)$ extracted from the pion and kaon mass measurements together with a fourth order polynomial fit to the data points.

The equations 4.9 can now be solved with the result

$$R_\beta = \frac{f}{f'} + \mathcal{O}(am_{u,d}) \tag{4.11}$$

$$R_{m_{u,d}} = 2m_{u,d}\left(1 - \frac{1}{2}\frac{h'}{h}\frac{f}{f'}\right) + \mathcal{O}\left((am_{u,d})^2\right) \tag{4.12}$$

$$R_{m_s} = 2m_s\left(1 - \frac{m_{u,d}+m_s}{m_s}\frac{1}{2}\frac{l'}{l}\frac{f}{f'} + \frac{m_{u,d}}{m_s}\frac{1}{2}\frac{h'}{h}\frac{f}{f'}\right) + \mathcal{O}\left(am_{u,d}\, am_s, (am_{u,d})^2\right) \tag{4.13}$$

where f', h' and l' denote the derivative of these functions with respect to β.
Now since R_β has been determined quite precisely from the string tension measurements it will be used to define f/f' neglecting the correction in $am_{u,d}$. The derivatives of the functions $\ln h(\beta)$ and $\ln l(\beta)$ with respect to β yield h'/h and l'/l. From the measurements of the pion and kaon masses the values of h and l can be calculated using the above formula 4.10. The logarithm of these data together with fits using fourth order polynomials are plotted in figure 4.13. Since the meson masses for β values away from the critical point have only been calculated on 20 to 40 configurations separated by five Hybrid R trajectories, the determination of $R_{m_{u,d}}$ and R_{m_s} is not thought of as a very precise measurement but merely as a rough estimate. In this sense also

the interaction measure and the energy density taking into account fermionic contributions are calculated to get an idea how large the effect of finite quark masses on these quantities might be. Now one is in the position to calculate $(\epsilon - 3p)/T^4$ and the energy density ϵ/T^4. As already mentioned before, in the chiral limit $m_{u,d} \to 0$ the β-function for the light quark mass vanishes, $R_{m_{u,d}} \to 0$. Thus neglecting the part from the light quark sector might be interpreted as taking the chiral limit. In figure 4.14 the interaction measure is plotted for the gluonic, the gluonic plus fermionic contributions from the strange quark sector $\overline{\langle TrM^{-1}\rangle}_{m_s}$ and finally the complete contributions from the gluonic, light and heavy quark sector. The peak in the quantity $\left((\epsilon - 3p)/T^4\right)_{\text{gluon}}$ increases with increasing number of flavours and for temperatures $T \gtrsim 2T_c$ all curves agree within errors. Additionally the continuum extrapolation for pure gauge theory has been included in this plot which is substantially lower within the complete temperature range than the full QCD results. This shows that, although only the gluonic action difference is included in $\left((\epsilon - 3p)/T^4\right)_{\text{gluon}}$, the quark degrees of freedom lead to a larger interaction measure.
When the fermionic contributions are taken into account the expected systematic increase in the maximum of $(\epsilon - 3p)/T^4$ with the number of flavours is lost for $\left((\epsilon - 3p)/T^4\right)_{\text{gluon+strange}}$ and the agreement at high temperatures does not show up. From this one analysis it is however not possible to definitely understand these peculiarities, but one might speculate that finite quark mass effects are responsible for it. In earlier studies [28, 56] it turned out that the interaction measure at larger temperatures decreases with the quark mass. Since the light masses $m_{u,d}/T = 0.4$ in this simulation are relatively heavy it is reasonable to assume that for smaller quark masses the large contributions from the light quark sector are substantially reduced. The situation is different for the strange quark where at T_c the physical mass of about $m_s/T = 1.0$ is realised in this simulation. On the other hand do the spectrum calculations at the critical point show that the kaon to vector meson mass ratio of $m_{\text{K}}/m_{\text{V}} = 0.93$ is still much larger than the physical value of 0.65. In the three flavour simulation this ratio is approximately realized for $m_{\text{PS}}/m_{\text{V}}$=0.68(1). There the third flavour had a mass of $m_s a = 0.10$ instead of $m_s a = 0.25$ in the $n_f = 2 + 1$ case. It is thus reasonable to assume that the quark masses used here are still too large. This would explain the large contribution from the heavy quark sector to $(\epsilon - 3p)/T^4$.
The energy density has been calculated by adding three times the pressure to $(\epsilon - 3p)/T^4$ (see figure 4.15). For $n_f = 2$ and 3 the energy density shows the same flavour dependence as the pressure. When normalized to the corresponding Stefan Boltzmann value, both curves in figure 4.16 more or less agree for temperatures larger than 2.5 T_c. The energy density for a massive ideal Fermi gas is calculated as follows

$$\frac{\epsilon_{\text{SB}}}{T^4} = \left(8 + \frac{21}{4} h_f\right) \frac{\pi^2}{15} \quad . \tag{4.14}$$

Similar to the case of the pressure, h_f counts the effective number of degrees of freedom of a massive Fermi gas relevant for the energy density. When $m/T = 0$ this factor is n_f, in general it is

$$h_f = \sum_{f=u,d,..} h(m_f/T) \quad , \tag{4.15}$$

with

$$h(m/T) = \frac{120}{7\pi^4} \int_{m/T}^{\infty} \mathrm{d}x \; x^2 \sqrt{x^2 - (m/T)^2} \frac{1}{1 + \mathrm{e}^x} \quad . \tag{4.16}$$

For a single quark flavour the corresponding values are $h(0.4) = 0.9881$ and $h(1) = 0.9230$, respectively. The overall Stefan Boltzmann values for three and two plus one flavours are $\epsilon_{\text{SB}}/T^4 = 15.504$ and 15.279, thus the effect of the heavier quark flavour is quite small for the energy density of an ideal gas. For the $n_f = 2+1$ simulation depending on whether taking into account only the gluonic or additionally the fermionic contributions different conclusions on the suppression in the strange

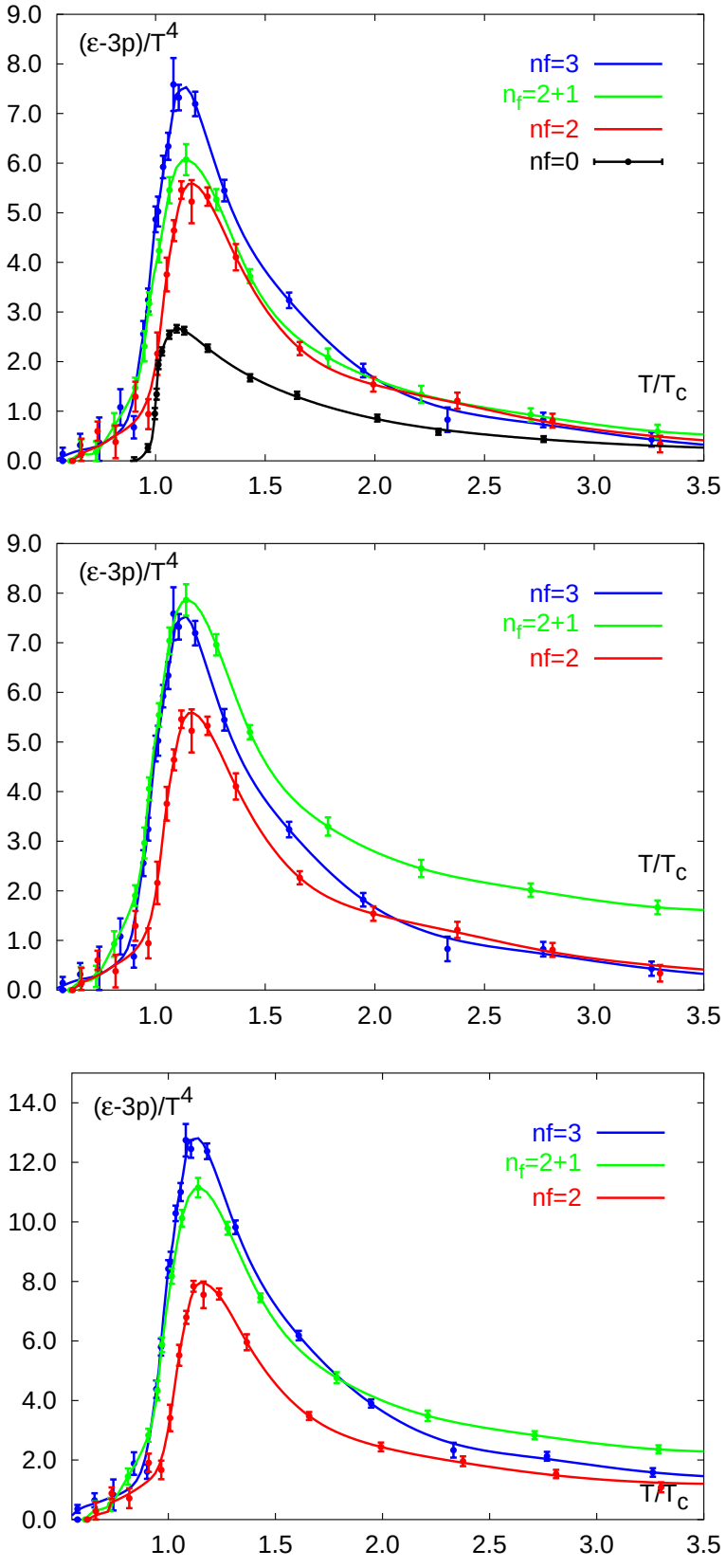

Figure 4.14: The quantities $\left((\epsilon - 3p)/T^4\right)_{\text{gluon}}$, $\left((\epsilon - 3p)/T^4\right)_{\text{gluon+strange}}$ *and* $\left((\epsilon - 3p)/T^4\right)_{\text{gluon+up,down+strange}}$ *for* $n_f = 2$, *2+1 and 3 calculated with the p4-action (from the top to the bottom).*

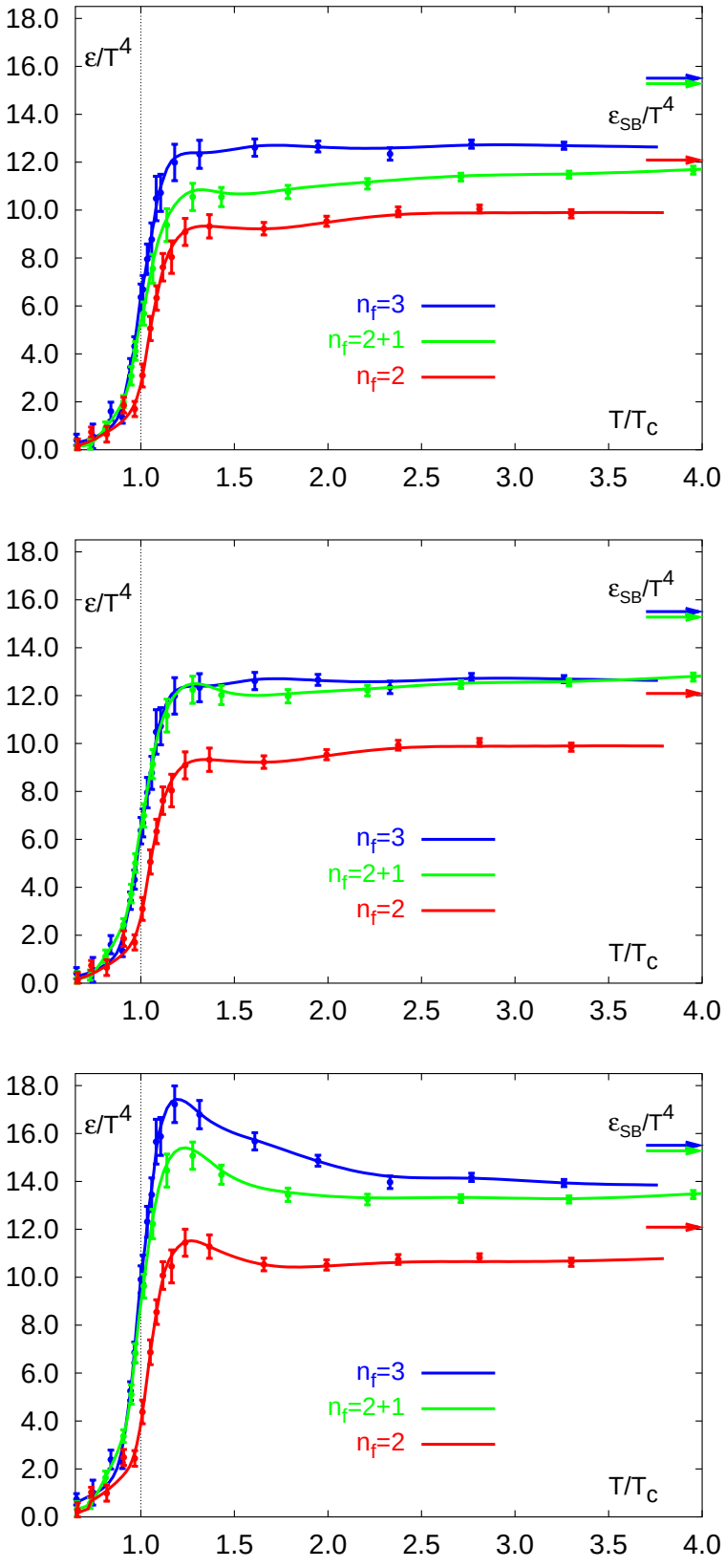

Figure 4.15: The energy density ϵ/T^4 for $n_f = 2$, 2+1 and 3 calculated with the p4-action taking into account the different gluonic and fermionic contributions (the details are given in the text and in the previous figure)

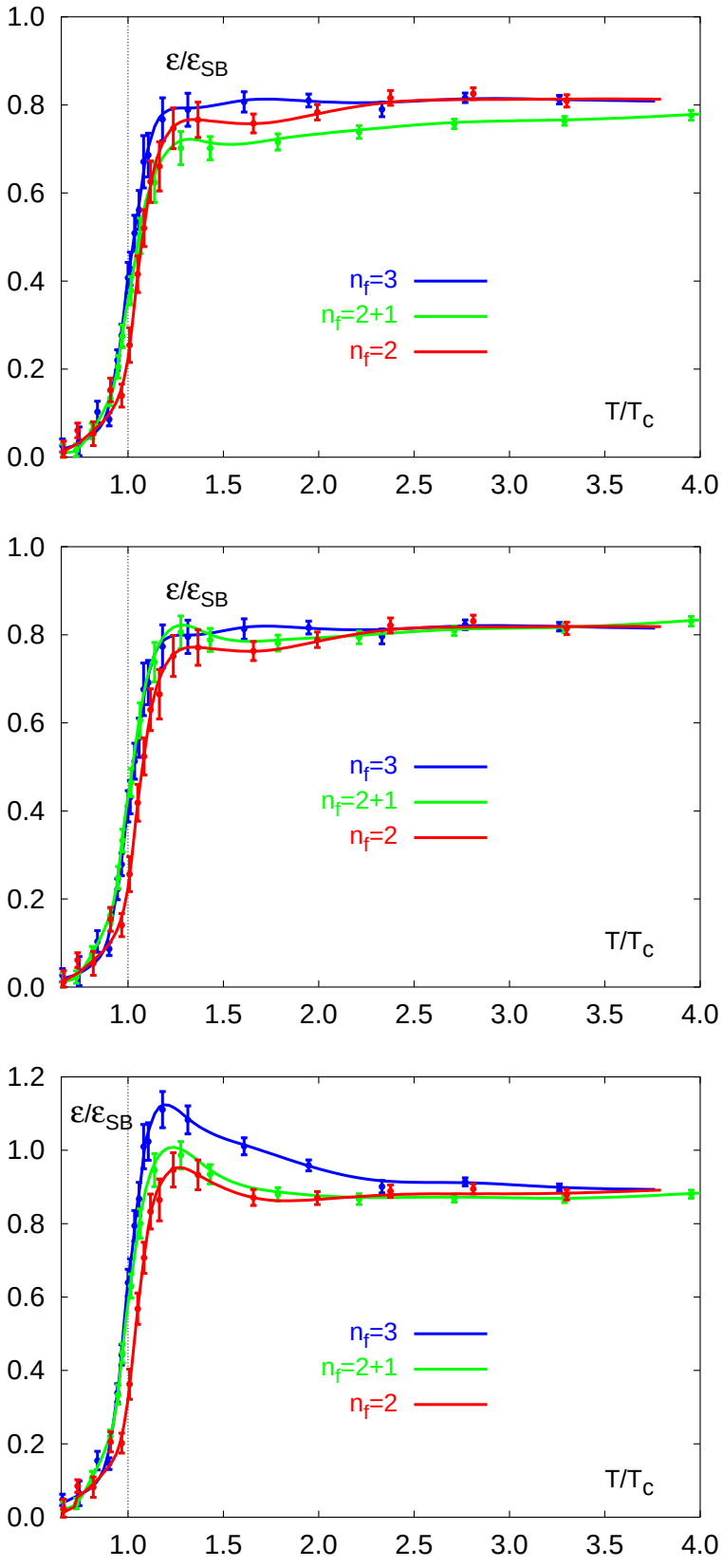

Figure 4.16: The energy density $\epsilon/\epsilon_{\rm SB}$ for $n_f = 2$, 2+1 and 3 which is normalized by the corresponding Stefan Boltzmann value. (the details are given in the text)

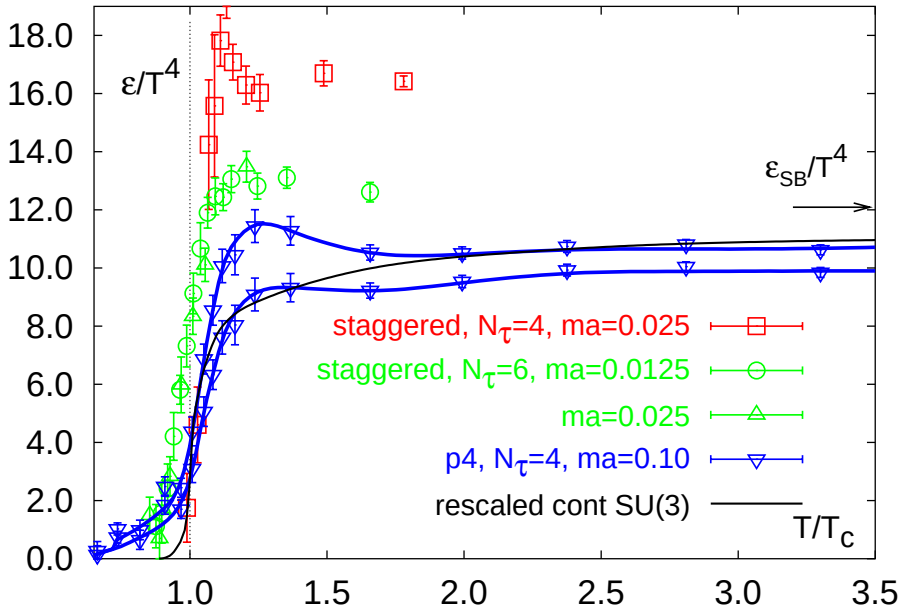

Figure 4.17: The energy density ϵ/T^4 for $n_f = 2$ with the standard staggered action ($N_\tau = 4$ and 6), the p4 fat action ($N_\tau = 4$) and the continuum extrapolation of pure gauge theory rescaled by the appropriate number of degrees of freedom. For the p4 action the energy density with only gluonic contributions is given in the lower curve.

quark sector can be drawn. For the gluonic case a clear suppression for large temperatures as for the pressure has been found. When the heavy quark sector or the complete contributions are taken into account all normalised curves show nearly the same behaviour for $T \gtrsim 2.5 T_c$. From the above discussion it is however reasonable to assume that the physical situation is best described by $(\epsilon/T^4)_{\text{gluon}}$. Then the results of Kogut *et al.* are confirmed by this simulation.

Cut-off effects

Finally the cut-off effects in two flavour QCD for the energy density will be analysed. In figure 4.18 the perturbative ideal gas value for the energy density for different fermion and gluon actions for $n_f = 2$, 3 and 4 are plotted. The staggered action in combination with the Wilson gauge action has cut-off distortions of nearly 70% at $N_\tau = 4$ and approaches the continuum ideal gas value only for quite large temporal lattice sizes. The Naik and p4 action together with the tree-level 1×2 gluon action show much smaller deviation from the Stefan Boltzmann value, about 20% for the Naik action at $N_\tau = 4$ and 7% for the p4 action at $N_\tau = 6$. In the lattice simulations a similar pattern can be found as for the $N_\tau = 4$ perturbative calculation. This is especially true when only the gluonic sector is included in ϵ/T^4 for the improved actions. The complete contributions for the Naik action show a quite strong overshooting close to T_c. Only at temperatures $T \gtrsim 2T_c$ the ordering between Naik and standard staggered fermions are according to the ideal gas. Thus again as in the case of the pressure the high temperature limit qualitatively reflects the cut-off distortions present in lattice simulations at high temperatures.

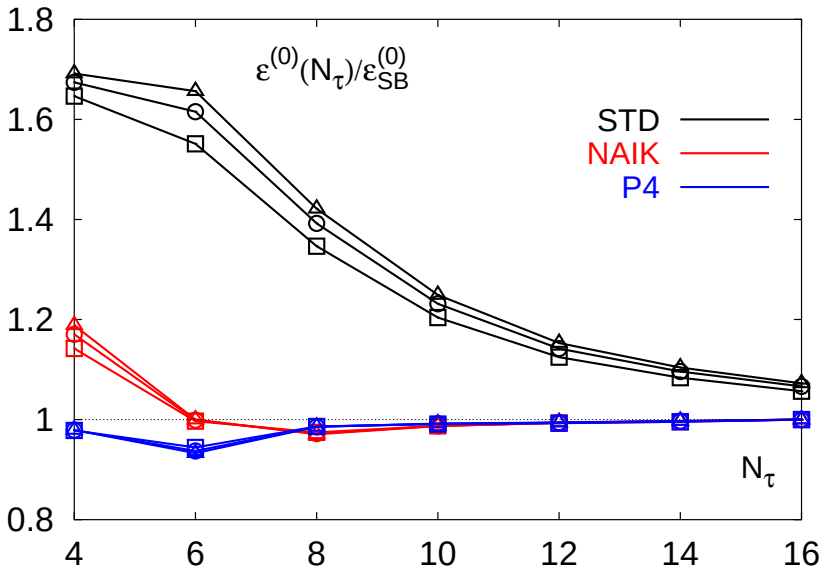

Figure 4.18: The ideal gas value of the energy density for the standard staggered and Wilson gauge action, the p4 and Naik improved staggered with 1×2 gauge action. To distinguish the number of quark flavours different plotting symbols have been used. The triangle for four, the circle for three and the square for two flavours.

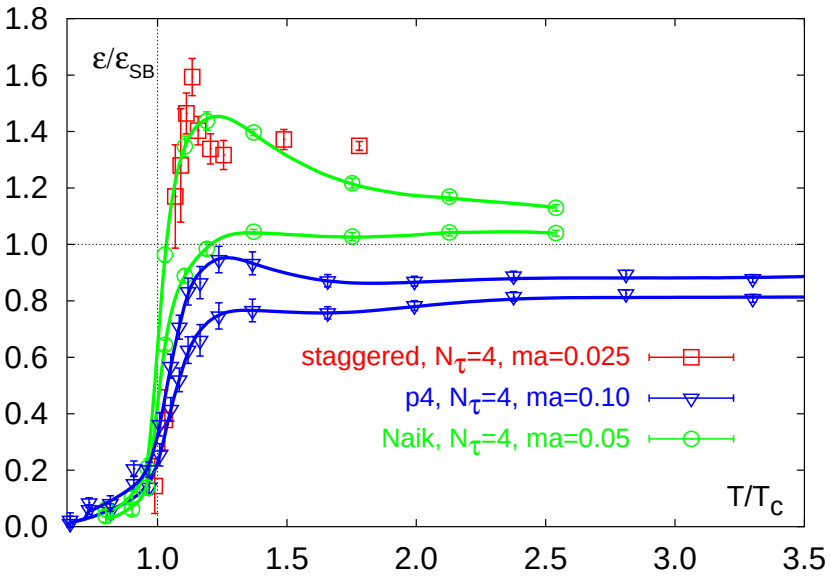

Figure 4.19: The energy density normalized by the appropriate Stefan Boltzmann value for the Naik action ($n_f = 4$), the p4 fat action ($n_f = 2$) and the standard staggered action ($n_f = 2$) at $N_\tau = 4$. The lower curves for the Naik and p4 action take into account only the gluonic contributions. The upper curve contains the complete gluonic and fermionic contributions.

For two flavours all lattice data available are collected in figure 4.17. The results obtained with the standard staggered action show strong cut-off effects and even at $N_\tau = 6$ the energy density is larger than the Stefan-Boltzmann value. Such a behaviour is not expected since in pure gauge theory at temperatures of 1.5 T_c the continuum extrapolation lies substantially below $\epsilon_{\rm SB}/T^4$. Therefore it is reasonable to assume that for the $N_\tau = 6$ results with the standard staggered action there are still finite lattice spacing effects present. Since also for the energy density results from two and three flavour simulations with the p4 action agree when rescaled by the corresponding Stefan Boltzmann value, the continuum extrapolated pure gauge result has been rescaled by a factor of 2.3125 accounting for the fermion degrees of freedom and is included in figure 4.17. As in the case of the pressure it seems to be a reasonable estimate for the continuum result of the energy density in the temperature range $(2-4)T_c$. Then the energy density calculated with the p4 action definitely shows strongly reduced cut-off effects. Whatever contribution to the energy density is taken into account, only the gluonic or the complete, the agreement is within 15%.

4.2.4 Finite step size effects on the equation of state

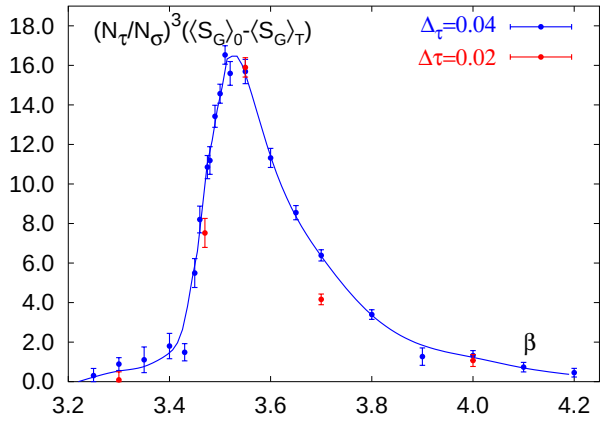

Figure 4.20: The step size dependence of the action difference with $\Delta\tau = 0.04$ and 0.02.

The simulation of QCD with n_f flavours different from four has to be performed with an algorithm which is not exact. The results discussed in this chapter have been obtained using the Hybrid R algorithm with a step size of $\Delta\tau = am_q/2.5$. In the calculation of the pressure with light quarks of $am_q = 0.10$ a step size of $\Delta\tau = 0.04$ has thus been used. To quantify the error induced by this choice additional simulations with $\Delta\tau = 0.02$ have been performed on $16^3 \times 4$ and 16^4 lattices at five coupling values. The action difference on zero and finite temperature lattices, which is the main input for a pressure calculation is plotted in figure 4.20. There one observes the trend that the difference calculated with the smaller step-size is systematically smaller. This leads to a smaller pressure after integration if the temperature scale would not change significantly. Therefore, if in the future calculations of the pressure proceed to a higher accuracy, the step size should be extrapolated to zero. In [50] it is reported that this problem becomes worse for smaller quark masses.

4.3 Conclusions

In this work the critical temperature of the QCD phase transition and the equation of state have been investigated with improved staggered fermions. The reduction of finite lattice spacing effects and the analysis of the flavour dependence of thermodynamic quantities have been the main points

of interest. For the transition temperature in units of the vector meson mass T_c/m_{V} two flavour results from different discretisations using improved actions converge towards a unique result. When the transition temperature is expressed in terms of the string tension more simulations at $N_\tau = 6$ are needed for improved Wilson fermions to confirm the agreement of $T_c/\sqrt{\sigma}$ with improved staggered data at $N_\tau = 4$. A present estimate for the two flavour critical temperature is 180(10) MeV for $m = 0$. In general simulations at smaller quark masses are needed to reliably extrapolate to the chiral limit using improved discretisation schemes. The same is true for the flavour dependence which up to now only has been investigated at relatively large quark masses. For am_q corresponding to $m_{\mathrm{PS}}/m_{\mathrm{V}} > 0.5$ a small but systematic increase of the critical temperature has been observed when changing the number of flavours from three to two.
The equation of state for the pressure and the energy density have been calculated with two and three light and additionally two light and one heavier quark flavour. The use of the p4 fat improved staggered fermion action leads to the expected reduction of cut-off effects and a first continuum estimate for the pressure has been obtained for $T = (2-4)T_c$ on the basis of the analysis of the remaining cut-off effects predicted by the high-temperature limit. For the energy density it is a subtle task to correctly incorporate the contributions from the fermionic sector and a reliable continuum estimate was not possible with the present lattice data. The situation close to the transition has to be investigated using smaller quark masses such that the correct physical mass spectrum is realised.
For both, the pressure and the energy density, the quark mass dependence in the case of two and three flavours closely follow the pattern expected from the analysis of an ideal Fermi gas. The strange quark contributions are however significantly suppressed relative to an ideal gas. For the energy density this observation is made, when only the gluonic contributions are taken into account. In the future one would like to perform simulations with fixed strange quark mass and not, as in this work, with fixed m_s/T. Additionally calculations at smaller N_τ are needed to be able to perform the continuum extrapolation $a \to 0$.
As for the critical temperature it would be nice to see that other discretisation schemes predict the same equation of state in the continuum than staggered fermions. The only calculation up to now has been performed with Wilson fermions [103], which unfortunately suffer from severe cut-off effects for thermodynamic quantities.

Acknowledgements

Mit dieser Arbeit geht ein zehnjähriges Kapitel meines Lebens zu Ende, in dem sich sehr viel um Physik gedreht hat. Ich möchte allen danken, die mich dabei unterstützt haben und mit denen ich vieles gemeinsam im Studium erlebt habe. Es hat mir viel Freude und Spass bereitet.

Für die Zeit als Diplomand und Doktorand gilt mein besonderer Dank meinem Betreuer Prof. Dr. Frithjof Karsch. Ich danke ihm für seine ständige Diskussionsbereitschaft und seine Anregungen, die sehr zum Gelingen der Arbeit beigetragen haben. Die vielen Möglichkeit, auf Konferenzen in aller Welt über die Arbeit vorzutragen sowie bei einem Forschungsaufenthalt zwei Monate in Japan zu leben, habe ich sehr geschätzt.

Darüber hinaus möchte ich Dr. Edwin Laermann für seine Ausdauer, Fragen zu beantworten, sehr herzlich danken.

Bei allen anderen Mitgliedern der Arbeitsgruppe bedanke ich mich für die freundschaftliche Unterstützung, den anregenden Gedankenaustausch und das gute, offene Arbeitsklima, zu dem nicht zuletzt die Sekretärinnen Gudrun Eickmeyer, Karin Lacey und Susi von Reder viel beigetragen haben. Ein besonderes Dankeschön geht an Peter Schmidt, mit dem ich seit dem Grundstudium viel physikalisches und nicht-physikalisches erlebt habe und der es über vier Jahre lang mit mir in einem Büro ausgehalten hat.

Zuletzt der Dank an alle die, die mit theoretischer Physik nichts so recht anzufangen wissen, mich aber trotzdem darin bestärkt haben, genau daran zu arbeiten. Dafür danke ich meinen Eltern, die mich während des gesamten Studiums unterstützt haben. Und last but not least ein besonderer Dank an Anja.

Andreas Peikert

Appendix A

The Euclidean Dirac γ matrices and the $SU(N)$ generators λ

A.1 Dirac matrices

In Euclidean metric the γ matrices are defined in terms of the Pauli matrices σ as

$$\gamma_i = \begin{pmatrix} 0 & -i\sigma_i \\ i\sigma_i & 0 \end{pmatrix} \quad i = 1,2,3 \qquad \gamma_i = \begin{pmatrix} 0 & 1 \\ 1 & 0 \end{pmatrix} \tag{A.1}$$

where the Pauli matrices are given by

$$\sigma_1 = \begin{pmatrix} 0 & 1 \\ 1 & 0 \end{pmatrix} \qquad \sigma_2 = \begin{pmatrix} 0 & -i \\ i & 0 \end{pmatrix} \qquad \sigma_3 = \begin{pmatrix} 1 & 0 \\ 0 & -1 \end{pmatrix} \tag{A.2}$$

The followiing relations hold

$$\gamma_\mu = \gamma_\mu^\dagger \tag{A.3}$$

$$\{\gamma_\mu, \gamma_\nu\} = 2\delta_{\mu\nu} \quad . \tag{A.4}$$

A.2 $SU(N)$ generators

Elements Λ of the group $SU(N)$ can be written as

$$\Lambda = \exp\left(\sum_{a=1}^{N^2-1} iT_a\omega^a\right) \quad , \tag{A.5}$$

where $\omega^a \in \mathbb{R}$. T_a are the traceless, hermitian generators, which are normalized as follows

$$\mathrm{Tr}\ (T_a T_b) = \frac{1}{2}\delta_{ab} \tag{A.6}$$

The generators are defined through the commutation relations and the corresponding total anti-symmetric structure constants $f_{abc} \in \mathbb{R}$ of $SU(N)$

$$[T_a, T_b] = i f_{abc} T_c \quad a, b, c = 1, .., N^2 - 1 \quad . \tag{A.7}$$

For $SU(3)$ the generators are in general expressed in terms of the Gellmann matrices $T_a = 1/2\lambda^a$, which have the following representation

$$\begin{aligned}
\lambda^1 &= \begin{pmatrix} 0 & 1 & 0 \\ 1 & 0 & 0 \\ 0 & 0 & 0 \end{pmatrix} \qquad \lambda^2 = \begin{pmatrix} 0 & -i & 0 \\ i & 0 & 0 \\ 0 & 0 & 0 \end{pmatrix} \qquad \lambda^3 = \begin{pmatrix} 1 & 0 & 0 \\ 0 & -1 & 0 \\ 0 & 0 & 0 \end{pmatrix} \\
\lambda^4 &= \begin{pmatrix} 0 & 0 & 1 \\ 0 & 0 & 0 \\ 1 & 0 & 0 \end{pmatrix} \qquad \lambda^5 = \begin{pmatrix} 0 & 0 & -i \\ 0 & 0 & 0 \\ i & 0 & 0 \end{pmatrix} \qquad \lambda^6 = \begin{pmatrix} 0 & 0 & 0 \\ 0 & 0 & 1 \\ 0 & 1 & 0 \end{pmatrix} \\
\lambda^7 &= \begin{pmatrix} 0 & 0 & 0 \\ 0 & 0 & -i \\ 0 & i & 0 \end{pmatrix} \qquad \lambda^8 = \frac{1}{\sqrt{3}} \begin{pmatrix} 1 & 0 & 0 \\ 0 & 1 & 0 \\ 0 & 0 & -2 \end{pmatrix} \quad .
\end{aligned} \tag{A.8}$$

Appendix B

The force computation in the Hybrid R algorithm for the 1×2 gluon and the p4 fat link staggered fermion action.

The integration of the equations of motion in the Hybrid R algorithm requires the calculation of the time-derivative of the conjugate momentum $H_\mu(x)$, which is implicitely defined through the requirement $\dot{\mathcal{H}} = 0$,

$$0 = \sum_{x,\mu} \mathrm{tr}\, H_\mu(x)\dot{H}_\mu(x) + \frac{d}{d\tau}S_\mathrm{G} - \frac{n_f}{N_{W,KS}}\mathrm{tr}\, \chi^* \frac{d}{d\tau}\left(M^\dagger(U)M(U)\right)\chi \quad , \tag{B.1}$$

where $\chi = 1/(M^\dagger(U)M(U))\ M(U)\ R$ with the Gaussian noise vector R. Thus the derivative of the gauge action and the fermion matrix with respect to the mlecular dynamics time has to be calculated. In the following sections the corresponding expressions for the 1×2 gluon action, the p4 and fat link actions are presented.

B.1 The gauge action

The 1×2 gluon action expressed in terms of link variables reads

$$\begin{aligned} S_G^{2\times 1} &= \beta \sum_{x,\mu>\nu} \frac{5}{3}\left(1 - \frac{1}{2N_c}\left(U_{\mu,\nu}(x) + U^\dagger_{\mu,\nu}(x)\right)\right) \\ &\quad -\frac{1}{6}\left(1 - \frac{1}{4N_c}\left(U^{1\times 2}_{\mu,\nu}(x) + U^{1\times 2\dagger}_{\mu,\nu}(x) + U^{2\times 1}_{\mu,\nu}(x) + U^{2\times 1\dagger}_{\mu,\nu}(x)\right)\right) \end{aligned} \tag{B.2}$$

with

$$\begin{aligned} U_{\mu,\nu}(x) &\equiv U_\mu(x)U_\nu(x+\hat{\mu})U^\dagger_\mu(x+\hat{\nu})U^\dagger_\nu(x) \\ U^{1\times 2}_{\mu,\nu}(x) &\equiv U_\mu(x)U_\nu(x+\hat{\mu})U_\nu(x+\hat{\mu}+\hat{\nu})U^\dagger_\mu(x+2\hat{\nu})U^\dagger_\nu(x+\hat{\nu})U^\dagger_\nu(x) \\ U^{2\times 1}_{\mu,\nu}(x) &\equiv U_\mu(x)U_\mu(x+\hat{\mu})U_\nu(x+2\hat{\mu})U^\dagger_\mu(x+\hat{\mu}+\hat{\nu})U^\dagger_\mu(x+\hat{\nu})U^\dagger_\nu(x) \quad . \end{aligned} \tag{B.3}$$

The derivatives of the plaquette and the 1×2 loop is then given by

$$\begin{aligned}
\dot{U}_{\mu,\nu}(x) &= \dot{U}_\mu(x)U_\nu(x+\hat{\mu})U_\mu^\dagger(x+\hat{\nu})U_\nu^\dagger(x) \\
&+ U_\mu(x)\dot{U}_\nu(x+\hat{\mu})U_\mu^\dagger(x+\hat{\nu})U_\nu^\dagger(x) \\
&+ U_\mu(x)U_\nu(x+\hat{\mu})\dot{U}_\mu^\dagger(x+\hat{\nu})U_\nu^\dagger(x) \\
&+ U_\mu(x)U_\nu(x+\hat{\mu})U_\mu^\dagger(x+\hat{\nu})\dot{U}_\nu^\dagger(x)
\end{aligned} \tag{B.4}$$

$$\begin{aligned}
\dot{U}_{\mu,\nu}^{1\times 2}(x) &= \dot{U}_\mu(x)U_\nu(x+\hat{\mu})U_\nu(x+\hat{\mu}+\hat{\nu})U_\mu^\dagger(x+2\hat{\nu})U_\nu^\dagger(x+\hat{\nu})U_\nu^\dagger(x) \\
&+ U_\mu(x)\dot{U}_\nu(x+\hat{\mu})U_\nu(x+\hat{\mu}+\hat{\nu})U_\mu^\dagger(x+2\hat{\nu})U_\nu^\dagger(x+\hat{\nu})U_\nu^\dagger(x) \\
&+ U_\mu(x)U_\nu(x+\hat{\mu})\dot{U}_\nu(x+\hat{\mu}+\hat{\nu})U_\mu^\dagger(x+2\hat{\nu})U_\nu^\dagger(x+\hat{\nu})U_\nu^\dagger(x) \\
&+ U_\mu(x)U_\nu(x+\hat{\mu})U_\nu(x+\hat{\mu}+\hat{\nu})\dot{U}_\mu^\dagger(x+2\hat{\nu})U_\nu^\dagger(x+\hat{\nu})U_\nu^\dagger(x) \\
&+ U_\mu(x)U_\nu(x+\hat{\mu})U_\nu(x+\hat{\mu}+\hat{\nu})U_\mu^\dagger(x+2\hat{\nu})\dot{U}_\nu^\dagger(x+\hat{\nu})U_\nu^\dagger(x) \\
&+ U_\mu(x)U_\nu(x+\hat{\mu})U_\nu(x+\hat{\mu}+\hat{\nu})U_\mu^\dagger(x+2\hat{\nu})U_\nu^\dagger(x+\hat{\nu})\dot{U}_\nu^\dagger(x)
\end{aligned} \tag{B.5}$$

With these expressions at hand the time derivative of the gluonic action can be calculated. The indices are rearranged such that $\dot{U}_\mu(x)$ can be factored out and reexpressed by $\dot{U}_\mu(x) = iH_\mu(x)U_\mu(x)$

$$\begin{aligned}
\dot{S}_G^{2\times 1} &= -\frac{\beta}{2N_c}\sum_{x,\mu}\mathrm{tr}\; iH_\mu(x)\Big\{\sum_{\nu\neq\mu}U_\mu(x)\Big\{ \\
&\quad \frac{5}{3}\Big[U_\nu(x+\hat{\mu})U_\mu^\dagger(x+\hat{\nu})U_\nu^\dagger(x) \\
&\qquad +U_\nu^\dagger(x+\hat{\mu}-\hat{\nu})U_\mu^\dagger(x-\hat{\nu})U_\nu(x-\hat{\nu})\Big] \\
&\quad -\frac{1}{12}\Big[U_\mu(x+\hat{\mu})U_\nu(x+2\hat{\mu})U_\mu^\dagger(x+\hat{\mu}+\hat{\nu})U_\mu^\dagger(x+\hat{\nu})U_\nu^\dagger(x) \\
&\qquad +U_\nu(x+\hat{\mu})U_\mu^\dagger(x+\hat{\nu})U_\mu^\dagger(x-\hat{\mu}+\hat{\nu})U_\nu^\dagger(x-\hat{\mu})U_\mu^\dagger(x-\hat{\mu}) \\
&\qquad +U_\mu(x+\hat{\mu})U_\nu^\dagger(x+2\hat{\mu}-\hat{\nu})U_\mu^\dagger(x+\hat{\mu}-\hat{\nu})U_\mu^\dagger(x-\hat{\nu})U_\nu(x-\hat{\nu}) \\
&\qquad +U_\nu^\dagger(x+\hat{\mu}-\hat{\nu})U_\mu^\dagger(x-\hat{\nu})U_\mu^\dagger(x-\hat{\mu}-\hat{\nu})U_\nu^\dagger(x-\hat{\mu})U_\mu(x-\hat{\mu}) \\
&\qquad +U_\nu(x+\hat{\mu})U_\nu(x+\hat{\mu}+\hat{\nu})U_\mu^\dagger(x+2\hat{\nu})U_\nu^\dagger(x+\hat{\nu})U_\nu^\dagger(x) \\
&\qquad +U_\nu^\dagger(x+\hat{\mu}-\hat{\nu})U_\nu(x+\hat{\mu}-2\hat{\nu})U_\mu^\dagger(x-2\hat{\nu})U_\nu^(x-2\hat{\nu})U_\nu(x-\hat{\nu})\Big]\Big\} \\
&\quad -h.c.\Big\} \\
&\equiv \sum_{x,\mu}\mathrm{tr}\; iH_\mu(x)\left(P_\mu^{\mathrm{gauge}}(x) - h.c.\right)
\end{aligned} \tag{B.6}$$

B.2 The fermionic action

The derivative of the fermionic action is given by

$$\begin{aligned}
\frac{d}{d\tau}S^{\text{fermion}} &= -\frac{n_f}{N_M}\text{tr }\chi^*\frac{d}{d\tau}\left(M^\dagger[U]M[U]\right)\chi \\
&= -\frac{n_f}{N_M}\text{tr }\chi^*\frac{d}{d\tau}\left(D^\dagger[U]D[U]\right)\chi \\
&= -\frac{n_f}{N_M}\text{tr }\left(\chi^*\dot{D}^\dagger[U]D[U]\chi+\chi^*D^\dagger[U]\dot{D}[U]\chi\right) \\
&= \frac{n_f}{N_M}\text{tr }\left(\chi^*\dot{D}[U](D[U]\chi)+(D[U]\chi)^*\dot{D}[U]\chi\right) \\
&= \frac{n_f}{N_M}\text{Tr tr }\left(\dot{D}[U]\ (D[U]\chi)\otimes\chi^*+\dot{D}[U]\ \chi\ \otimes(D[U]\chi)^*\right)
\end{aligned} \tag{B.7}$$

where $M=m\mathbb{1}+D$ and the property $D^\dagger=-D$ has been used. Tr denotes the trace in space.

B.2.1 The fat link action

The matrix $D[U]$ for fat links is defined as

$$\begin{aligned}
D[U]_{xy} &= c_{1,0,0,0}\frac{1}{1+6\omega}\left(A[U]_{xy}+\omega F[U]_{xy}\right) \\
A[U]_{xy} &= \sum_\nu U_\nu(x)\delta_{x+\hat{\nu};y}-U_\nu^\dagger(x-\hat{\nu})\delta_{x-\hat{\nu};y} \\
F[U]_{xy} &= \sum_\nu\sum_{\rho\neq\nu}\Big(U_\rho(x)U_\nu(x+\hat{\rho})U_\rho^\dagger(x+\hat{\nu}) \\
&\qquad +U_\rho^\dagger(x-\hat{\rho})U_\nu(x-\hat{\rho})U_\rho(x+\hat{\nu}-\hat{\rho})\Big)\delta_{x+\hat{\nu};y} \\
&\quad -\Big(U_\rho(x)U_\nu^\dagger(x-\hat{\nu}+\hat{\rho})U_\rho^\dagger(x-\hat{\nu}) \\
&\qquad +U_\rho^\dagger(x-\hat{\rho})U_\nu^\dagger(x-\hat{\nu}-\hat{\rho})U_\rho(x-\hat{\nu}-\hat{\rho})\Big)\delta_{x-\hat{\nu};y}
\end{aligned} \tag{B.8}$$

Now the time derivatives and thus the expression Tr tr $\left(\dot{D}[U](D[U]\chi)\otimes\chi^*+\dot{D}[U]\ \chi\otimes(D[U]\chi)^*\right)$ can be calculated for the different parts of the action seperately. The cyclic property of the trace has been used to bring $\dot{U}_\mu(x)$ to the front.

$$\begin{aligned}
&\sum_x \text{tr }\chi^*\dot{A}[U](D[U]\chi)+\text{tr }(D[U]\chi)^*\dot{A}[U]\chi \\
&= \sum_x\sum_\mu \text{tr }\left(\dot{U}_\mu(x)(D\chi)_{x+\hat{\mu}}\otimes\chi_x^*\ -\ \dot{U}_\mu(x)\chi_{x+\hat{\mu}}\otimes(D\chi)_x^*+h.c.\right) \\
&= \sum_x\sum_\mu \text{tr }iH_\mu(x)\left(P_\mu^A(x)-h.c.+P_\mu^A(x)-h.c.\right)
\end{aligned} \tag{B.9}$$

$$
\begin{aligned}
&\sum_x \text{tr } \chi^* \dot{F}[U](D[U]\chi) + \text{tr } (D[U]\chi)^* \dot{F}[U]\chi \\
&= \sum_x \sum_\nu \text{tr } \sum_{\mu\neq\nu} \Big(\dot{U}_\mu(x) U_\nu(x+\hat{\mu}) U_\mu^\dagger(x+\hat{\nu}) (D\chi)_{x+\hat{\nu}} \otimes \chi_x^* \\
&\quad + \dot{U}_\mu(x) (D\chi)_{x+\hat{\mu}} \otimes \chi^*_{x+\hat{\mu}-\hat{\nu}} U_\mu^\dagger(x-\hat{\nu}) U_\nu(x-\hat{\nu}) \\
&\quad - \dot{U}_\mu(x) U_\nu^\dagger(x+\hat{\mu}-\hat{\nu}) U_\mu^\dagger(x-\hat{\nu}) (D\chi)_{x-\hat{\nu}} \otimes \chi_x^* \\
&\quad - \dot{U}_\mu(x) (D\chi)_{x+\hat{\mu}} \otimes \chi^*_{x+\hat{\nu}+\hat{\mu}} U_\mu^\dagger(x+\hat{\nu}) U_\nu^\dagger(x) \\
&\quad + \dot{U}_\mu(x) U_\nu^\dagger(x+\hat{\mu}-\hat{\nu}) \chi_{x-\hat{\nu}+\hat{\mu}} \otimes (D\chi)^*_{x-\hat{\nu}} U_\mu(x-\hat{\nu}) \\
&\quad + \dot{U}_\mu(x) U_\nu(x+\hat{\mu}) \chi_{x+\hat{\mu}+\hat{\nu}} \otimes (D\chi)^*_{x+\hat{\nu}} U_\mu^\dagger(x) \\
&\quad - \dot{U}_\mu(x) U_\nu(x+\hat{\mu}) U_\mu^\dagger(x+\hat{\nu}) \chi_{x+\hat{\nu}} \otimes (D\chi)^*_x \\
&\quad - \dot{U}_\mu(x) \chi_{x+\hat{\mu}} \otimes (D\chi)^*_{x+\hat{\mu}-\hat{\nu}} U_\mu^\dagger(x-\hat{\nu}) U_\nu(x-\hat{\nu}) \\
&\quad + \dot{U}_\mu(x) U_\nu(x+\hat{\mu}-\hat{\nu}) U_\mu^\dagger(x-\hat{\nu}) \chi_{x-\hat{\nu}} \otimes (D\chi)^*_x \\
&\quad + \dot{U}_\mu(x) \chi_{x+\hat{\mu}} \otimes (D\chi)^*_{x+\hat{\mu}+\hat{\nu}} U_\mu^\dagger(x+\hat{\nu}) U_\nu^\dagger(x) \\
&\quad + \dot{U}_\mu(x) U_\nu^\dagger(x+\hat{\mu}-\hat{\nu}) (D\chi)_{x+\hat{\mu}-\hat{\nu}} \otimes \chi^*_{x-\hat{\nu}} U_\nu(x-\hat{\nu}) \\
&\quad + \dot{U}_\mu(x) U_\nu(x+\hat{\mu}) (D\chi)_{x+\hat{\mu}+\hat{\nu}} \otimes \chi^*_{x+\hat{\nu}} U_\nu^\dagger(x) + h.c. \Big) \\
&= \sum_x \sum_\mu \text{tr } i H_\mu(x) \Big(P_\mu^F(x) - h.c. + P_\mu^F(x) - h.c. \Big)
\end{aligned}
\tag{B.10}
$$

Since the fields χ only live on even lattice sites one has to distinguish the even and the odd case. Printed in blue are the expressions which are valid for even sites in red the ones for odd sites.

B.2.2 The p4 action

The matrix $D[U]$ for the p4 action is defined as

$$
\begin{aligned}
D[U]_{xy} &= c_{1,0,0,0}\ A[U]_{xy} \ + \ c_{1,2,0,0}\ B_2[U]_{xy} \\
A[U]_{xy} &= \sum_\nu U_\nu(x)\delta_{x+\hat{\nu};y} - U_\nu^\dagger(x-\hat{\nu})\delta_{x-\hat{\nu};y} \\
B_2[U]_{xy} &= \sum_\nu \sum_{\rho\neq\nu} \Big(U_\nu(x) U_\rho(x+\hat{\nu}) U_\rho(x+\hat{\nu}+\hat{\rho}) \\
&\qquad + U_\rho(x) U_\rho(x+\hat{\rho}) U_\nu(x+2\hat{\rho}) \Big) \delta_{x+\hat{\nu}+2\hat{\rho};y} \\
&\quad + \Big(U_\nu(x) U_\rho^\dagger(x+\hat{\nu}-\hat{\rho}) U_\rho^\dagger(x+\hat{\nu}-2\hat{\rho}) \\
&\qquad + U_\rho^\dagger(x-\hat{\rho}) U_\rho^\dagger(x-2\hat{\rho}) U_\nu(x-2\hat{\rho}) \Big) \delta_{x+\hat{\nu}-2\hat{\rho};y} \\
&\quad - \Big(U_\rho^\dagger(x-\hat{\rho}) U_\rho^\dagger(x-2\hat{\rho}) U_\nu^\dagger(x-\hat{\nu}-2\hat{\rho}) \\
&\qquad + U_\nu^\dagger(x-\hat{\nu}) U_\rho^\dagger(x-\hat{\nu}-\hat{\rho}) U_\rho^\dagger(x-\hat{\nu}-2\hat{\rho}) \Big) \delta_{x-\hat{\nu}-2\hat{\rho};y} \\
&\quad - \Big(U_\rho(x) U_\rho(x+\hat{\rho}) U_\nu^\dagger(x-\hat{\nu}+2\hat{\rho}) \\
&\qquad + U_\nu^\dagger(x-\hat{\nu}) U_\rho(x-\hat{\nu}) U_\rho(x-\hat{\nu}+\hat{\rho}) \Big) \delta_{x-\hat{\nu}+2\hat{\rho};y}
\end{aligned}
\tag{B.11}
$$

The expression for $A[U]$ is given in the previous section, for $B_2[U]$ it is

$$\begin{aligned}
&\sum_x \mathrm{tr}\ \chi^* \dot{B}_2[U](D[U]\chi) + \mathrm{tr}\ (D[U]\chi)^* \dot{B}_2[U]\chi \\
&= \sum_x \sum_\mu \mathrm{tr} \sum_{\nu\neq\mu} \Big(-\dot{U}_\mu(x) U_\mu(x+\hat{\mu})(D\chi)_{x+2\hat{\mu}} \otimes \chi^*_{x+\hat{\nu}} U_\nu(x) \\
&\quad - \dot{U}_\mu(x) U^\dagger_\nu(x+\hat{\mu}-\hat{\nu})(D\chi)_{x+\hat{\mu}-\hat{\nu}} \otimes \chi^*_{x-\hat{\mu}} U_\mu(x-\hat{\mu}) \\
&\quad + \dot{U}_\mu(x) U_\mu(x+\hat{\mu})(D\chi)_{x+2\hat{\mu}} \otimes \chi^*_{x-\hat{\nu}} U_\nu(x-\hat{\nu}) \\
&\quad + \dot{U}_\mu(x) U_\nu(x+\hat{\mu})(D\chi)_{x+\hat{\mu}+\hat{\nu}} \otimes \chi^*_{x-\hat{\mu}} U_\mu(x-\hat{\mu}) \\
&\quad - \dot{U}_\mu(x)(D\chi)_{x+\hat{\mu}} \otimes \chi^*_{x-\hat{\mu}+\hat{\nu}} U^\dagger_\nu(x-\hat{\mu}) U_\mu(x-\hat{\mu}) \\
&\quad + \dot{U}_\mu(x)(D\chi)_{x+\hat{\mu}} \otimes \chi^*_{x+2\hat{\mu}} U^\dagger_\nu(x+\hat{\nu}) U^\dagger_\nu(x) \\
&\quad - \dot{U}_\mu(x) U_\mu(x+\hat{\mu}) U^\dagger_\nu(x+2\hat{\mu}-\hat{\nu})(D\chi)_{x+2\hat{\mu}-\hat{\nu}} \otimes \chi^*_x \\
&\quad - \dot{U}_\mu(x) U^\dagger_\nu(x+\hat{\mu}-\hat{\nu}) U^\dagger_\nu(x+\hat{\mu}-2\hat{\nu})(D\chi)_{x+\hat{\mu}-2\hat{\nu}} \otimes \chi^*_x \\
&\quad + \dot{U}_\mu(x) U_\nu(x+\hat{\mu}) U_\nu(x+\hat{\mu}+\hat{\nu})(D\chi)_{x+\hat{\mu}+2\hat{\nu}} \otimes \chi^*_x \\
&\quad + \dot{U}_\mu(x)(D\chi)_{x+\hat{\mu}} \otimes \chi^*_{x-\hat{\mu}-\hat{\nu}} U_\nu(x-\hat{\mu}-\hat{\nu}) U_\mu(x-\hat{\mu}) \\
&\quad + \dot{U}_\mu(x) U_\mu(x+\hat{\mu}) U_\nu(x+2\hat{\mu})(D\chi)_{x+\hat{\mu}+\hat{\nu}} \otimes \chi^*_x \\
&\quad + \dot{U}_\mu(x)(D\chi)_{x+\hat{\mu}} \otimes \chi^*_{x-2\hat{\nu}} U_\nu(x-2\hat{\nu}) U_\nu(x-\hat{\nu}) \\
&\quad - [\ (D\chi) \longleftrightarrow \chi\ ,\ even \longleftrightarrow odd\ ] + h.c. \Big) \\
&= \sum_x \sum_\mu \mathrm{tr}\ i H_\mu(x) \Big(P^{B_2}_\mu(x) - h.c. + P^{B_2}_\mu(x) - h.c. \Big)
\end{aligned} \tag{B.12}$$

Putting everything together the force term for the 1×2 gluonic and p4 fat improved fermion action is defined by

$$0 = \sum_x \sum_\mu \mathrm{tr}\ H_\mu(x) \Big(\dot{H}_\mu(x) + i F_\mu(x) \Big) \tag{B.13}$$

with

$$\begin{aligned}
F_\mu(x) &= P_\mu(x) - P^\dagger_\mu(x) \\
&= P^{\mathrm{gauge}}_\mu(x) + c_{1,0,0,0} \frac{1}{1+6\omega} \left(P^A_\mu(x) + \omega P^F_\mu(x) \right) + c_{1,2,0,0} P^{B_2}_\mu(x) \\
&+ c_{1,0,0,0} \frac{1}{1+6\omega} \left(P^A_\mu(x) + \omega P^F_\mu(x) \right) + c_{1,2,0,0} P^{B_2}_\mu(x) - h.c.
\end{aligned} \tag{B.14}$$

For the equation B.13 to be satisfied, $\dot{H}_\mu(x)$ has to be proportional to the unity matrix. $H_\mu(x)$ should remain traceless, therfore $\dot{H}_\mu(x)$ is chosen to be so.

$$i\dot{H}_\mu(x) = P_\mu(x) - P^\dagger_\mu(x) - \frac{1}{3}\mathrm{tr}\ \left[P_\mu(x) - P^\dagger_\mu(x) \right] \tag{B.15}$$

This last equation finally defines the force for the 1×2 gluonic and p4 fat improved fermion action in the Hybrid R algorithm.

Appendix C

The static quark potential at zero temperature

The determination of the heavy quark potential in full QCD will be presented. The string tension extracted from it is used to set the scale in finite temperature simulations. Finally the fit ansatz to describe the string tension as a function of the coupling β will be discussed.
The potential between a static quark anti-quark pair has been calculated from the temporal Wilson loop

$$W(R,L) \equiv \left\langle \mathrm{Tr} \prod_{l \in \mathcal{C}} U_l \right\rangle \quad , \tag{C.1}$$

along a path $\mathcal{C}$ with a space- and time-like extension R and L, respectively.
From it the local potential has been extracted

$$V(R,L) = \ln \frac{W(R,L+1)}{W(R,L)} \quad , \tag{C.2}$$

which for large temporal extension should approach a constant yielding $V_{q\bar{q}}(R)$. The potential has then been fitted to the ansatz

$$V_{q\bar{q}}(R) = V_0 + \frac{\alpha}{R} + \sigma R \quad , \tag{C.3}$$

with the parameter α in the Coulomb term and the string tension σ in the linear part.
As discussed in chapter 1 the signal-to-noise ratio can be improved by applying the smearing technique proposed by the APE group [22]. The procedure consists of iteratively adding a spatial staple to the link

$$U_\mu \rightarrow U_\mu + \gamma \sum_{\nu - \mu} (1 \times 1 - \mathrm{staples})_\nu \quad , \tag{C.4}$$

where the factor γ together with the number of smearing steps n are the parameters which are used for tuning.

C.1 The string tension from improved staggered fermion simulations

For full QCD the static quark potential has been calculated at several values of the coupling for two, two plus one and three quark flavours at the bare quark mass $m_{u,d} = 0.10$ for the light and $m_s = 0.25$ for the heavy flavour. On each configuration different smearing paramters γ and number of smear steps n have been tested. They are given in table C.1. In most cases consistent results could be extracted from two or more combinations of γ and n. Without smearing no stable results could be extracted for the potential.

n	0	5	5	10	10
γ	0.0	0.1	0.3	0.1	0.3

Table C.1: Smear parameters and number of smear steps for the Wilson loop measurement.

Finally the string tension has been determined through a fit of the form C.3 to the potential data. Although the p4 action has shown to improve the rotational symmetry of the heavy quark potential (see figure 2.10), the distortions are still too large to include the off axis data in the fit. In figure C.1 the resulting string tensions are plotted together with a fit to the data using the renormalization group inspired ansatz [93],

$$\sqrt{\sigma}a(\beta) = R(\beta)(1 + c_2\hat{a}^2(\beta) + c_4\hat{a}^4(\beta))/c_0 \tag{C.5}$$

with $\hat{a} \equiv R(\beta)/R(\bar{\beta})$. $\bar{\beta}$ is a normalisation constant.
The fit parameters are given in table C.2. In this work the fit will only be applied to interpolate the string tension data to define a temperature scale in thermodynamic calculations of chapter 4. In principle the fit has the correct asymptotic form and should allow an extrapolation to the

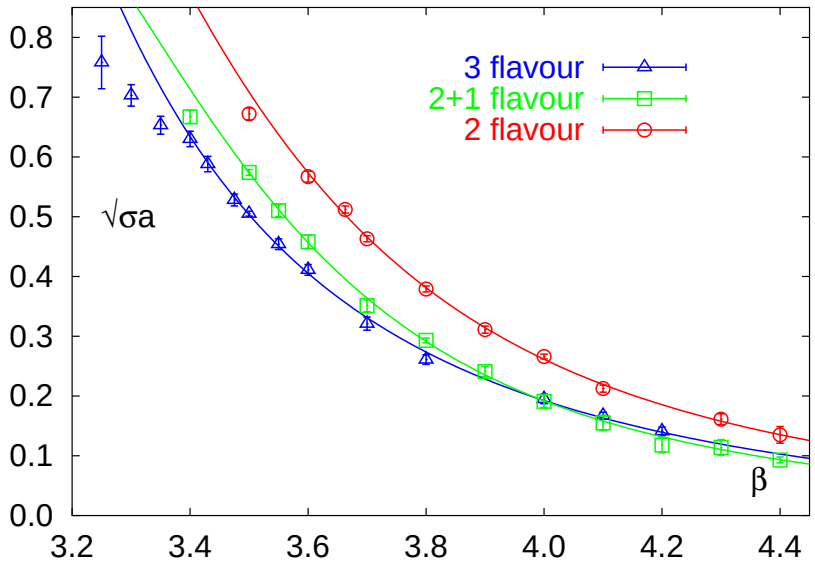

Figure C.1: The string tension $a\sqrt{\sigma}$ and a fit to the data using the ansatz C.5.

continuum limit. The constant c_0 in the fit should determine the λ parameter of lattice QCD, $\lambda_{\rm lat} = \sqrt{\sigma}\, c_0$. That this is for the bare coupling scheme in fact not the case will be discussed for the quenched theory.

flavour content	$[\beta_{min}, \beta_{max}]$	$\bar{\beta}$	c_0	c_2	c_4
2	[3.6,4.4]	3.70	0.0570 (35)	0.669 (208)	-0.0822 (1088)
2+1	[3.5,4.4]	3.60	0.0526 (32)	1.026 (224)	-0.1964 (1065)
3	[3.4,4.2]	3.50	0.0448 (15)	0.507 (115)	-0.0071 (677)

Table C.2: Fit parameter used for the interpolation of string tension data.

In pure gauge theory the heavy quark potential has been analysed for the Wilson gauge action [39] and different improved actions [41, 44]. Here the results of tree-level 1×2 improved actions will be reviewed since this action is also used in the full QCD study. The string tension data from [41] have been fitted to the ansatz given in equation C.5 and are plotted in figure C.2. The parameters of the fit have been collected in table C.3. From $\lambda_{\rm lat}^{1\times 2}$ the λ parameter in the $\overline{\rm MS}$-scheme has been calculated using the relation $\lambda_{\overline{\rm MS}}/\lambda_{\rm lat}^{1\times 2} = 5.442$ (collumns 7 and 8). The resulting $\lambda_{\overline{\rm MS}} = 158(2)$MeV is in good agreement with the one extracted for the Wilson gauge action, $\lambda_{\overline{\rm MS}} = 161(2)$MeV [39],* when the bare coupling scheme is used. It has on the other hand been shown [39], that effective coupling schemes, e.g. defined through the action, lead to much larger values of $\lambda_{\overline{MS}} \approx 223(15)$MeV. Unfortunately for the 1×2 action the λ paramter in an effective scheme cannot be calculated since the corresponding constants relating the $\overline{\rm MS}$- with effective schemes are not known. Nevertheless, the agreement between the Wilson and 1×2 improved gauge action within the bare coupling scheme suggests that also for the improved action the use of this scheme does not lead to a correct asymptotic result. From these considerations it is thus reasonable to assume, that the ansatz C.5 extrapolates properly to the asymptotic scaling region only when an effective coupling scheme is used. This statement should also be correct for full QCD with improved staggered fermions.

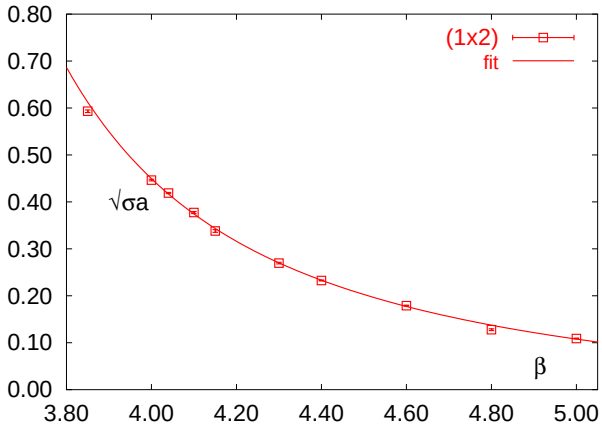

Figure C.2: The string tension $a\sqrt{\sigma}$ and a fit to the data using the ansatz C.5.

$[\beta_{min}, \beta_{max}]$	$\bar{\beta}$	c_0	c_2	c_4	$\lambda_{\rm lat}$	$\lambda_{\overline{\rm MS}}$
[4.00,5.00]	6.00	0.0693 (7)	0.00392 (51)	0.0000146 (45)	29.1 (3)MeV	158 (2)MeV

Table C.3: Fit parameters for the fit C.5 to the string tension data. In collumns 7 and 8 the resulting λ-parameters are given.

*To be consistent within this work a value of $\sqrt{\sigma} = 420$MeV has been used instead of 465MeV in [39]

Bibliography

[1] K.G. Wilson, Phys. Rev. **D11** (1974) 2445.

[2] Announcement at CERN, Feb. 2000,
http://cern.web.cern.ch/CERN/Announcements/2000/NewStateMatter.

[3] H. Rothe, *Lattice Gauge Theories* (World Scientific, Singapore), 1992.

[4] I. Montvay and G. Münster, *Quantum Fields on the Lattice* (Cambridge University Press, Cambridge), 1994.

[5] H. Meyer-Ortmanns, *Phase transitions in quantum chromodynamics* Reviews of Modern Physics, Vol.68, No.2 (1996) 473.

[6] M. Creutz, Phys. Rev. **D21** (1980) 2308.

[7] H.B. Nielsen and M. Ninomiya, Nucl. Phys. **B185** (1981) 20; Nucl. Phys. **B195** (1981) 541 (erratum).

[8] J. Kogut and L. Susskind, Phys. Rev. **D11**, 395 (1975); L. Susskind, Phys. Rev. **D16**, 3031 (1977).

[9] H. Kluberg-Stern, A. Morel, O. Napoly and B. Petersson, Nucl. Phys. **B220** (1983) 447.

[10] Y. Luo, Phys. Rev. **D55** (1997) 353 [hep-lat/9604025].

[11] M. F. Golterman, Nucl. Phys. **B273** (1986) 663; M. F. Golterman and J. Smit, Nucl. Phys. **B255** (1985) 328.

[12] B. Sheikholeslami and R. Wohlert, Nucl. Phys. **B259** (1985) 572.

[13] S. Aoki , Nucl. Phys. **B314** (1989) 79; S. Aoki *et al.* , Phys. Rev. Lett. **76** (1996) 873.

[14] P.H. Ginzparg, K.G. Wilson, Phys. Rev. **D25** (1982) 2649.

[15] S. Aoki (CP-Pacs collaboration), talk at *Lattice Field Theory on TFLOPS Supercomputers* (1999), (Kanazawa, Japan),
http://www.rccp.tsukuba.ac.jp/people/kanaya/JapanGerman.99/program.html.

[16] T. Blum, Nucl. Phys. **B73** (Proc. Suppl.)(1999) 167, [hep-lat/9809042].

[17] P.M. Vranas, contribution to "Lattice Fermions and Structure of the Vacuum" (Dubna, Russia), [hep-lat/0001006].

[18] H. Neuberger, Lattice99 proceedings, [hep-lat/9909042].

[19] F. Karsch, Nucl. Phys. **B205** (1982) 285; A. Hasenfratz and P. Hasenfratz, Nucl. Phys. **B193** (1981) 210; F. Karsch and I.O. Stamatescu, Phys. Lett. **B227** (1989) 153.

[20] R. Trinchero, Nucl. Phys. **B227** (1983) 61.

[21] E. Laermann, C. DeTar, O. Kaczmarek and F. Karsch, Nucl. Phys. Proc. Suppl. **73** (1999) 447 [hep-lat/9809105].

[22] M. Albanese *et al.* , Phys. Lett. **B192** (1987) 163

[23] R. Altmeyer *et al.* , Nucl. Phys. **B389** (1993) 445

[24] N. Cabibbo and E. Marinari, Phys. Lett. **B9** (1982) 387; M. Creutz, Phys. Rev. **D21** (1980) 2308; A.D. Kennedy and B.J. Pendleton, Phys. Lett. **B156** (1985) 393.

[25] S.L. Adler, Phys. Rev. **D23** (1981) 2901; M. Creutz, Phys. Rev. **D36** (1987) 515.

[26] S. Gottlieb *et al.* (JLQCD), Phys. Rev. **D35** (1987) 2531.

[27] S. Aoki *et al.* [JLQCD Collaboration], Phys. Rev. **D57** (1998) 3910 [hep-lat/9710048].

[28] C. Bernard, T. Blum, C. DeTar, S. Gottlieb, K. Rummukainen, U.M. Heller, J.E. Hetrick, D. Toussaint, L. Kärkkäinen, R.L. Sugar and M. Wingate, Phys. Rev. **D55** (1997) 6861.

[29] K. Symanzik, Nucl. Phys. **B226** (1983) 187 and Nucl. Phys. **B226** (1983) 205.

[30] G.P. Lepage, P.B. Mackenzie, Phys. Rev. **D48** (1993) 2250.

[31] P. Hasenfratz and F. Niedermayer, Nucl. Phys. **B414** (1994) 785 [hep-lat/9308004].

[32] U. M. Heller, F. Karsch and B. Sturm, Phys. Rev. **D60** (1999) 114502 [hep-lat/9901010].

[33] T. Blum, C. DeTar, S. Gottlieb, K. Rummukainen, U.H. Heller, J.E. Hetrick, D. Toussaint, R.L. Sugar and M. Wingate, Phys. Rev. **D55** (1997) 1133.

[34] P. Weisz, Nucl. Phys. **B212** (1983) 1; P. Weisz und R. Wohlert, Nucl. Phys. **B236** (1984) 397 and Nucl. Phys. **B247**(1984) 544.

[35] M. Lüscher und P. Weisz, Phys. Lett. **B158** (1985) 250.

[36] Y. Iwasaki, Nucl. Phys. **B258** (1985) 141; Y. Iwasaki, Univ. of Tsukuba report UTHEP-118 (1983) unpublished.

[37] T. Takaishi, Phys. Rev. **D54** (1996) 1050.

[38] G. Boyd, J. Engels, F. Karsch, E. Laermann, C. Legeland, M. Lutgemeier and B. Petersson, Nucl. Phys. **B469** (1996) 419 [hep-lat/9602007].

[39] R. G. Edwards, U. M. Heller and T. R. Klassen, Nucl. Phys. **B517**, 377 (1998) [hep-lat/9711003].

[40] A. Cella, G. Curci, A. Viceré und B. Vigna, Phys. Lett. **B333** (1994) 457.

[41] B. Beinlich, F. Karsch, E. Laermann and A. Peikert, Eur. Phys. J. **C6** (1999) 133 [hep-lat/9707023].

[42] J. Engels, F. Karsch and T. Scheideler, hep-lat/9905002.

[43] T. Umeda *et al.* [QCD-TARO Collaboration], Nucl. Phys. Proc. Suppl. **73**, 924 (1999) [hep-lat/9809086].

[44] M. Okamoto *et al.* [CP-PACS Collaboration], Phys. Rev. **D60** (1999) 094510 [hep-lat/9905005].

[45] B. Beinlich, F. Karsch and E. Laermann, Nucl. Phys. **B462** (1996) 415.

[46] A. Papa, Nucl. Phys. **B478**, 335 (1996) [hep-lat/9605004].

[47] B. Beinlich, F. Karsch and A. Peikert, Phys. Lett. **B390**, 268 (1997) [hep-lat/9608141].

[48] Y. Iwasaki, K. Kanaya, T. Yoshié, T. Hoshino, T. Shirakawa, Y. Oyanagi, S. Ichii und T. Kawai, Phys. Rev. **D46** (1992) 4657.

[49] Y. Iwasaki, K. Kanaya, L. Kärkkäinen, K. Rummukainen und T. Yoshie, Phys. Rev. **D49**, 3540 (1994).

[50] T. Blum, L. Kärkkäinen, D. Toussaint and S. Gottlieb, Phys. Rev. **D51** (1995) 5153.

[51] W. Bietenholz and H. Dilger, Nucl. Phys. **B549** (1999) 335 [hep-lat/9812016].

[52] W. Bietenholz, R. Brower, S. Chandrasekharan and U. J. Wiese, Nucl. Phys. **B495**, 285 (1997) [hep-lat/9612007].

[53] W. Bietenholz and H. Dilger, hep-lat/9803018.

[54] Y. Luo, Phys. Rev. **D57** (1998) 265 [hep-lat/9702013].

[55] S. Naik, Nucl. Phys. **B316** (1989) 238.

[56] J. Engels, R. Joswig, F. Karsch, E. Laermann, M. Lütgemeier and B. Petersson, Phys. Lett. B396 (1997) 210.

[57] M. Lütgemeier, *Phasenübergänge in der QCD mit fundamentalen und adjungierten Quarks*, Ph.D. thesis, Bielefeld, Nov. 1998.

[58] J. F. Lagaë and D. K. Sinclair, Phys. Rev. **D59** (1999) 014511 [hep-lat/9806014].

[59] A. Peikert, B. Beinlich, A. Bicker, F. Karsch and E. Laermann, Nucl. Phys. Proc. Suppl. **63**, 895 (1998) [hep-lat/9709157].

[60] C. Bernard *et al.* [MILC Collaboration], Phys. Rev. **D58**, 014503 (1998) [hep-lat/9712010].

[61] A. Bicker, *Gitteruntersuchungen zur Flavoursymmetrie von Staggered Quarks mit verbesserten Wirkungen*, Diploma thesis, Bielefeld, Mar. 1998.

[62] K. Orginos, D. Toussaint and R. L. Sugar [MILC Collaboration], Phys. Rev. **D60** (1999) 054503 [hep-lat/9903032].

[63] E. Fukugita *et al.* , Nucl. Phys. **B337** (1990) 457.

[64] R.D. Pisarski and F. Wilczek, Phys. Rev. **D29** (1984) 338.

[65] K. Rajagopal and F. Wilczek, Nucl. Phys. **B399** (1993) 395 hep-ph/9210253.

[66] S. Gavin, A. Gocksch and R.D. Pisarski, Phys. Rev. **D49** (1994) 3079 hep-ph/9311350.

[67] C. Alexandrou *et al.* , Phys. Rev. **D60** (1999) 034504.

[68] N. Attig, B. Petersson, M. Wolff and R.V. Gavai, Z. Phys. C **40** (1988) 471.

[69] C. Schmidt, diploma thesis, in preparation, Bielefeld, 2000.

[70] B. Svetitsky and L.G. Yaffe, Nucl. Phys. **B210** (1982) 423.

[71] T.A. DeGrand and C.E. DeTar, Nucl. Phys. **B225** (1983) 590.

[72] S. Stickan, *Skalenverhalten am Endpunkt einer Phasenübergangslinie erster Ordnung*, diploma thesis, Bielefeld, April 2000.

[73] F.Y.. Wu, Rev. Mod. Phys. **54** (1982) 235.

[74] P. Hasenfratz, F. Karsch and I.O. Stamatescu, Phys. Lett. **133B** (1983) 221.

[75] F. Green and F. Karsch, Nucl. Phys. **B238** (1984) 297.

[76] A.D. Bruce and N.B. Wilding, Phys. Rev. Lett. **68** (1992) 193.

[77] K. Rummukainen, M. Tsypin, K. Kajantie, M. Laine and M. Shaposhnikov, Nucl. Phys. **B532** (1998) 283 [hep-lat/9805013].

[78] H.W.J. Blöte, E. Luitjen and J.R. Heringa, J. Phys. A:Math. Gen. **28** (1995) 6289.

[79] K. Binder, Z. Phys. **B43** (1981) 119, K. Binder, Phys. Rev. **A25** (1982) 1699.

[80] Z. Frei and A. Patkos, Phys. Lett. **B247** (1990) 381.

[81] H. Meyer-Ortmanns, H.J. Pirner and A. Patkos, Phys. Lett. **B295** (1992) 255.

[82] H. Meyer-Ortmanns, H.J. Pirner and A. Patkos, "Chiral symmetry restoration in the linear sigma model," *Presented at Workshop on Dynamics of First Order Phase Transitions, Julich, Germany, 1-3 Jun 1992.*

[83] K. Kajantie and H. Kurki-Suonio, Phys. Rev. **D34**, 1719 (1986).

[84] T. Jolicoeur, H. Kluberg-Stern, M. Lev, A. Morel and B. Petersson, Nucl. Phys. **B235** (1984) 455.

[85] R. G. Edwards and U. M. Heller, Phys. Lett. **B462** (1999) 132 [hep-lat/9905008].

[86] C. Bernard *et al.* [MILC Collaboration], Phys. Rev. **D56**, 5584 (1997) and references therein.

[87] K.M. Bitar *et al.*, Phys. Rev. **D43**, 2396 (1991).

[88] P. Vranas *et al.*, contribution to Latticé99, hep-lat/9911002.

[89] A. Ali Khan *et al.* [CP-PACS Collaboration], hep-lat/9909075.

[90] C. Bernard *et al.*, Phys. Rev. **D54** (1996) 4585 [hep-lat/9605028] and references therein.

[91] for a recent review see: J. Rafelski and J. Letessier, *Diagnosis of QGP with Strange Hadrons*, hep-ph/9910300.

[92] J.B. Kogut and D.K. Sinclair, Phys. Rev. Lett. **60** (1988) 1250.

[93] C. Allton, Nucl. Phys. B [Proc. Suppl.] **53** (1997) 867 and hep-lat/9610016.

[94] J. Engels, J. Fingberg, F. Karsch, D. Miller and M. Weber, Phys. Lett. **B252** (1990) 625.

[95] U. Wolf, Phys. Rev. Lett. **62** (1989) 361.

[96] E. Laermann, Nucl. Phys. **B60** Proc. Suppl. (1998) 180.

[97] F. Brown et al., Phys. Rev. Lett. **65** (1990) 2491.

[98] S. Aoki et al. (JLQCD), Nucl. Phys. (Proc. Suppl.) **B73** (1999) 459.

[99] Y. Iwasaki et al., Phys. Rev. **D54** (1996) 7010.

[100] Y. Iwasaki et al., Phys. Rev. Lett. **78** (1997) 179.

[101] Y. Iwasaki, K. Kanaya, S. Kaya, S. Sakai and T. Yoshie, Nucl. Phys. Proc. Suppl. **47** (1996) 515 [hep-lat/9510005].

[102] C. Bernard *et al.*, Phys. Rev. **D61** (2000) 054503 [hep-lat/9908008].

[103] A. Ali Khan et al. (CP-PACS Collaboration), *Equation of State in Finite Temperature QCD with Improved Wilson Quarks*, hep-lat/9909075.

Hiemit erkläre ich, dass diese Arbeit von mir persönlich angefertigt wurde und nur die angegebenen Hilfsmittel verwendet wurden.

Andreas Peikert